THE UNIVERSITY OF CHICAGO

HIGH-ENERGY NEUTRINO FLUXES FROM SUPERMASSIVE DARK MATTER

A DISSERTATION SUBMITTED TO
THE FACULTY OF THE DIVISION OF THE PHYSICAL SCIENCES
IN CANDIDACY FOR THE DEGREE OF
DOCTOR OF PHILOSOPHY

DEPARTMENT OF PHYSICS

BY

PATRICK R. CROTTY

CHICAGO, ILLINOIS

JUNE 2002

Copyright © 2002 by Patrick R. Crotty

All rights reserved

ABSTRACT

We calculate the flux of high-energy ($E > 50$ GeV) neutrinos from the annihilations of supermassive (10^8 GeV $< M < 10^{16}$ GeV), strongly interacting dark matter particles in the core of the Sun. These particles, known as "simpzillas," could have been produced in large quantities towards the end of inflation and are a candidate for the non-baryonic dark matter. If they exist, they can be captured by the Sun, and their annihilations within will produce a distinctive neutrino signal observable by proposed Earth-based detectors such as IceCube. We therefore calculate the event rates in a hypothetical km^3 ice detector. We take all significant aspects of neutrino propagation through matter into account, including charged and neutral current scattering, oscillations, and charged lepton energy losses.

We find, in general, that the neutrino event rate from simpzilla annihilations is significant and detectable over a large range of simpzilla mass and interaction cross section, and can be as much as several hundred thousand per year.

ACKNOWLEDGMENTS

I would like to thank my Ph.D. thesis advisor, Dr. Edward W. "Rocky" Kolb, for his guidance and support. I would also like to thank the other members of my thesis committee for their constructive comments and suggestions: Drs. Michael Turner, Thomas Witten, James Truran, and Dietrich Müller. I thank Drs. David Rainwater and André de Gouvêa of Fermilab, Baha Balantekin of the University of Wisconsin, Donald E. Groom of LBL, and Tommy Ohlsson of the Technical University of Munich for useful discussions. I am grateful for the support of Dr. Donald G. York of the University of Chicago as well.

I have benefitted enormously from collaborating with Dr. John Beacom of Fermilab, and most of what I know about neutrino astrophysics I learned from him. He was of great assistance to me in undertaking this project, and was always willing and able to give me guidance and good suggestions. I thank him for helping and mentoring me in too many ways to count.

This work was completed on a DOE grant using the facilities of the Department of Astronomy and Astrophysics at the University of Chicago and the Theoretical Astrophysics Group at Fermilab. I thank the members and staff of both places for their hospitality, particularly Liz Duty (Fermilab) and Sandy Heinz, Jennifer Smith, Dana Nassau, and Melissa Gorman (all of U. Chicago).

TABLE OF CONTENTS

ABSTRACT iii

ACKNOWLEDGMENTS iv

LIST OF FIGURES vii

1 INTRODUCTION 1

2 SUPERMASSIVE DARK MATTER 5
- 2.1 Origin . . . 5
  - 2.1.1 Inflation . . . 5
  - 2.1.2 Wimpzilla production . . . 7
- 2.2 Capture by the Sun . . . 8
- 2.3 Annihilation . . . 11
  - 2.3.1 Annihilation rate . . . 11
  - 2.3.2 Initial neutrino spectrum . . . 13

3 HIGH-ENERGY NEUTRINOS: WEAK INTERACTIONS 16
- 3.1 Weak interactions with nucleons . . . 16
- 3.2 Weak interactions with electrons . . . 21
- 3.3 "Punch-through" neutrinos . . . 32

4 HIGH-ENERGY NEUTRINOS: OSCILLATIONS 33
- 4.1 Two-flavor oscillations . . . 34
  - 4.1.1 In vacuum . . . 34
  - 4.1.2 In matter . . . 39
- 4.2 Three-flavor oscillations . . . 42
- 4.3 Numerical simulation of neutrino oscillations . . . 44
  - 4.3.1 Analytical approximation . . . 44
  - 4.3.2 Other oscillation parameter choices . . . 45

5 CHARGED LEPTON INTERACTIONS 49
- 5.1 Electromagnetic energy losses . . . 50
  - 5.1.1 Electronic . . . 50
  - 5.1.2 Photonuclear scattering . . . 51
  - 5.1.3 Brehmsstrahlung . . . 52
  - 5.1.4 Pair production . . . 53
  - 5.1.5 Total energy losses . . . 54
- 5.2 Weak energy losses . . . 56
- 5.3 Decays . . . 56
  - 5.3.1 e . . . 56

5.3.2 μ 56
5.3.3 τ 57
5.4 Secondary neutrinos from τ decays 58

6 CALCULATION OF THE EMERGENT NEUTRINO FLUX 61
6.1 Monte Carlo code 61
6.1.1 Without oscillations 61
6.1.2 With oscillations 66
6.2 Numerical results 67
6.3 Analytical approximation 68

7 DETECTION OF SIMPZILLA NEUTRINOS 79

8 CONCLUSION 90

REFERENCES 91

LIST OF FIGURES

2.1 Supermassive dark matter density fraction 9
2.2 Simpzilla capture rate in the Sun 12
2.3 Initial simpzilla neutrino spectrum 15

3.1 Charged current cross sections for ν_e, ν_μ, $\bar{\nu}_e$, $\bar{\nu}_\mu$ 22
3.2 Neutral current cross sections for all flavors of ν, $\bar{\nu}$ 23
3.3 Charged current cross sections for ν_τ and $\bar{\nu}_\tau$ 24
3.4 ν_e, ν_μ charged current differential cross sections 25
3.5 ν_τ charged current differential cross sections 26
3.6 ν_e, ν_μ, ν_τ neutral current differential cross sections 27
3.7 $\bar{\nu}_e, \bar{\nu}_\mu$ charged current differential cross sections 28
3.8 $\bar{\nu}_\tau$ charged current differential cross sections 29
3.9 $\bar{\nu}_e, \bar{\nu}_\mu, \bar{\nu}_\tau$ neutral current differential cross sections 30
3.10 Proton-neutron ratio in the Sun 31

4.1 Oscillation probabilities of 50 GeV neutrinos in the Sun 46
4.2 Oscillation probabilities of 100 GeV neutrinos in the Sun 47

5.1 Decay distributions for τ 59

6.1 Simpzilla neutrino fluxes at Earth, without secondaries or oscillations 69
6.2 Simpzilla neutrino fluxes at Earth, with secondaries 70
6.3 Simpzilla neutrino fluxes at Earth, with oscillations 71
6.4 Simpzilla neutrino fluxes at Earth, with secondaries and oscillations . 72
6.5 Distribution of emergent ν_τ energies 76
6.6 Distribution of emergent $\bar{\nu}_\tau$ energies 77
6.7 Analytical approximation for neutrino fluxes, without secondaries or oscillations 78

7.1 Event rate spectrum, without secondaries or oscillations 81
7.2 Event rate spectrum, with secondaries 82
7.3 Event rate spectrum, with oscillations 83
7.4 Event rate spectrum, with secondaries and oscillations 84
7.5 Total event rate, without secondaries or oscillations 85
7.6 Total event rate, with secondaries 86
7.7 Total event rate, with oscillations 87
7.8 Total event rate, with secondaries and oscillations 88

CHAPTER 1

INTRODUCTION

Neutrinos with energies much larger than a GeV are potentially of great utility for studying the Universe. They are believed to be copiously produced by powerful astrophysical sources such as active galactic nuclei (AGNs) and gamma ray bursts (GRBs), and may also result from exotic phenomena such as topological defect decays and dark matter decays or annihilations. Because neutrinos do not have electromagnetic interactions, they are able to probe ranges of energy and redshift which are inaccessible to photon astronomy due to interactions of gamma rays with the cosmic microwave background[1]. Accurate high-energy neutrino flux measurements could significantly advance our understanding of astrophysics, and possibly of particle physics beyond the Standard Model.

High-energy neutrinos may generally be categorized by whether their production is "top-down" or "bottom-up." In the bottom-up case, they result from the interactions of particles which have been accelerated to very high energies. For instance, AGN cores and jets and GRBs could be the sources of cosmic rays with energies above 10^{20} eV, which have been observed but which no known object in the neighborhood of our galaxy is capable of producing. Protons in AGNs and GRBs can be excited to energies of this scale by mechanisms such as first-order diffusive shock acceleration, and their photopionic interactions with the dense radiation fields typical of these objects will produce a high-energy neutrino flux. While there are some unresolved theoretical issues with AGNs and/or GRBs being the sources of the highest energy cosmic ray primaries[2], it would nonetheless be very interesting to observe them with

[1] At 10^6 GeV, which is roughly the GUT scale, the gamma ray horizon is less than the radius of our own galaxy.

[2] See Halzen (2001) for a good discussion.

a sufficiently powerful neutrino telescope.

In the top-down case, the neutrinos come from the decays or annihilations of massive non-Standard Model particles. These may include extremely massive GUT particles produced by the decays of topological defects, which themselves will immediately decay to produce prompt neutrinos at very high energies.

Another top-down possibility is the non-baryonic matter which is believed to account for approximately one third of the Universe's total density. There are myriad proposals for what this could be, although the two suggestions which have gotten the most attention recently are weakly-interacting massive particles known as "wimps" and a heavier variant called "wimpzillas." Wimps may be the lightest supersymmetric particle, which would be stable and have a mass on the order of the electroweak symmetry breaking scale (~ 250 GeV).

Wimpzillas[3], to be discussed in greater detail in the next chapter, can be produced towards the end of inflation by quantum interactions with the inflating space-time (Chung et al. 1998, 1999). Unlike wimps, they are never in thermal equilibrium, and hence there are no thermodynamic constraints on their masses, which tend to be on the order of 10^{10} GeV or more. If they have strong interactions, they can be captured by the Sun, and their annihilations within will produce a characteristic flux of high-energy neutrinos.

It is this flux which we have calculated, taking into account all relevant effects of the neutrinos' subsequent propagation to the Sun's surface and the Earth. This includes neutrino interactions with nucleons, the energy losses of the leptons produced by charged-current interactions, matter and vacuum flavor oscillations, and secondary

[3]We will use "wimpzillas" as a generic term for all supermassive dark matter particles regardless of their interactions, and "simpzillas" for that subset which have strong interactions. A simpzilla is thus a strongly interacting wimpzilla.

neutrinos produced by τ decays. We have found that the flux is well above background for a large region of parameter space, and should generally be fairly easy to detect if supermassive, strongly interacting particles comprise a significant fraction of the dark matter. When neutrino oscillations are included, the flavor composition of the flux at the Earth is roughly $1:1:1$.

With the advent of kilometer-scale neutrino telescopes such as the proposed IceCube detector in Antarctica, we stand on the threshold of a new era of high-energy neutrino astronomy. Most models for the diffuse neutrino fluxes from AGNs, GRBs, and topological defects predict that the signal emerges from the atmospheric background only above about 100 TeV; point sources may be observable at lower energies, but which are still outside the capabilities of past and current detectors. IceCube should be able to extend this range up to that of the highest-energy cosmic rays, and will also have the ability to distinguish among different neutrino flavors. We will therefore analyze our calculated fluxes from the point of view of their detectability by an idealized 1 km^3 ice Čerenkov detector.

Note on terminology and notation

Much of the discussion in this paper applies equally to neutrinos and antineutrinos. In order to avoid unnecessary and potentially confusing duplication, we adopt the following conventions.

Unless it is specifically stated or clear from the context that we are distinguishing between neutrinos and antineutrinos, we use the word *neutrino* and the symbols ν_e, ν_μ, ν_τ to refer to both neutrinos and antineutrinos. We also use the lepton symbols e, μ, τ without signs to refer to both leptons and antileptons, as well as the words *muon* and *tau* (though we avoid using *electron* to refer to a positron).

When a result is given using this "generic" notation and terminology, it should be taken as holding for *both* physically meaningful charge-conjugate expressions. For example, "$W \to e\nu_e$" should be read as "$W^- \to e^-\nu_e$ *and* $W^+ \to e^+\bar{\nu}_e$"; "The flux of ν_τ is x" = "The flux of ν_τ is x *and* the flux of $\bar{\nu}_\tau$ is x". (The latter should *not* be read as "The flux of $\nu_\tau + \bar{\nu}_\tau$ is x".)

CHAPTER 2

SUPERMASSIVE DARK MATTER

2.1 Origin

We briefly review the production of supermassive dark matter at the end of inflation. We follow the discussion in Peacock (1999).

2.1.1 Inflation

Inflation is characterized by an exponential time dependence of the scale factor,

$$a(t) \propto e^{Ht} \tag{2.1}$$

which arises naturally from the presence of a scalar field ϕ (the "inflaton") with the Lagrangian

$$\mathcal{L} = \frac{1}{2}\,\partial_\mu\phi\,\partial^\mu\phi - V(\phi) \tag{2.2}$$

The corresponding action is $S = \int d^4x\sqrt{-g}\,\mathcal{L}$. If we assume an isotropic, homogenous cosmology, then $\sqrt{-g} = a^3$. By setting $\delta S = 0$, we obtain the classical equation of motion for ϕ:

$$\ddot{\phi} + 3H\dot{\phi} - \nabla^2\phi + \frac{dV}{d\phi} = 0 \tag{2.3}$$

The equation of motion for $a(t)$ is the Friedmann equation,

$$H = \frac{\dot{a}}{a} = \sqrt{\frac{8\pi}{3M_{Pl}^2}}\sqrt{\rho_\phi} \tag{2.4}$$

where $\rho_\phi \equiv \sqrt{\frac{1}{2}\dot{\phi}^2 + V(\phi)}$, and we are assuming flatness.

Although it is not explicit in (2.3), the ϕ field is generally assumed to be coupled to other matter fields, which are produced during the post-inflation oscillatory phase ("reheating").

Not all inflaton potentials $V(\phi)$ lead to inflation. To produce an exponentially increasing scale factor of the form (2.1), we must impose the "slow-roll" condition

$$|\ddot{\phi}| \ll |3H\dot{\phi}|, \left|\frac{dV}{d\phi}\right| \tag{2.5}$$

This is equivalent to the conditions

$$\begin{aligned} \epsilon, \eta &\ll 1 \\ \epsilon &\equiv \frac{M_{Pl}^2}{16\pi}\left(\frac{V'}{V}\right)^2 \\ \eta &\equiv \frac{M_{Pl}^2}{8\pi}\left(\frac{V''}{V}\right) \end{aligned} \tag{2.6}$$

If the conditions for inflation are met in a particular region, then spatial inhomogeneities in ϕ are rapidly redshifted away. Hence, we can in practice ignore the spatial derivatives in (2.3). Inflation typically ends with ϕ executing damped oscillations about a minimum of the potential, assuming that $V = 0$ there (if not, the Universe inflates forever).

Although inflation solves many problems of standard cosmology including flatness and homogeneity, there is no consensus on what the potential $V(\phi)$ is, or even how to motivate the existence of the inflaton. The simplest form for $V(\phi)$ is that of a massive real Klein-Gordon field, $V(\phi) = \frac{1}{2}m_\phi^2\phi^2$. From the observed density perturbation spectrum of the Universe, it can be shown that $m_\phi \approx 10^{12}$ GeV.

However, this "chaotic" inflaton potential, so called because the initial value of the field ϕ is assumed to be randomly distributed before inflation, has the drawback that ϕ must begin at values well above the Planck scale for sufficient inflation[1] to take place. Various modifications have been proposed to get around this, for example "hybrid" inflation potentials with two inflatons, in which the quantum fluctuations of one cause both of them to roll to a global minimum after the slow-roll period (Linde 1994). The large-field problem can also be avoided on inflating branes, which causes the Friedmann equation to be modified by a term quadratic in ρ_ϕ (Maartens et al. 2000).

2.1.2 Wimpzilla production

Although the identity of the inflaton and the form of its potential remain a subject of debate, it has recently been shown that an inflationary phase in the early Universe can very conveniently resolve the dark-matter problem, through the gravitational creation of very massive particles (Chung et al. 1999, 1998; Kuzmin & Tkachev 1999).

The fundamental mechanism is the interaction of the quantum modes of the X-particle or wimpzilla field, generally considered to be a massive scalar, with the background space-time. No coupling to the inflaton is necessary, although that case has been studied and wimpzilla production still found to be robust (Chung 1998).

We assume the wimpzilla to be a real scalar particle. The equation of motion for its field is (Chung et al. 2001)

$$\ddot{X} + 3H\dot{X} - \frac{1}{a^2}\nabla^2 X + m_X^2 X = 0 \tag{2.7}$$

[1] To produce a present-day $\Omega \approx 1$ to the accuracy that has been measured, the scale factor needs to have expanded by a factor of roughly e^{60} during inflation.

The interaction with the background spacetime enters through a and H. Note that there is no direct coupling of X to the inflaton.

By simultaneously solving the equations of motion for ϕ (2.3), a (2.4), and X (2.7, although generally the equivalent differential equation for the Fourier modes of X is solved instead), it can be shown that wimpzillas are abundantly produced for m_X in the vicinity of m_ϕ. We refer the reader to the papers cited for more details.

Figure 2.1 shows wimpzilla production for chaotic inflation. It has been shown that wimpzilla production is robust in hybrid and natural inflation as well (Chung et al. 2001). For the rest of this paper, we will assume that wimpzillas (in particular, strongly-interacting wimpzillas) constitute the entirety of the $\sim 30\%$ of the Universe's density that is thought to be in the form of non-baryonic matter.

Since wimpzillas are never in thermal equilibrium, their production and present-day density are not influenced by whether they have strong, weak, or only gravitational interactions. There are, however, astrophysical arguments against their being electrically charged[2] (Goldman & Nussinov 1989; Gould et al. 1990; Nardi & Roulet 1990).

2.2 Capture by the Sun

Albuquerque et al. (Albuquerque et al. 2001a), whom we follow in this section and the next, derived the simpzilla capture rate in the Sun as a function of simpzilla mass m_X and interaction cross section σ. They assumed that the local dark matter density of $\rho_X \approx 0.3$ GeV/cm^3 consists entirely of simpzillas in a Maxwell-Boltzmann

[2]Charged wimpzillas would collect in neutron stars, form black holes in their cores, and consume them on a timescale of a few years. The observation of pulsars with ages much greater than this excludes charged massive particles from being a significant component of the dark matter.

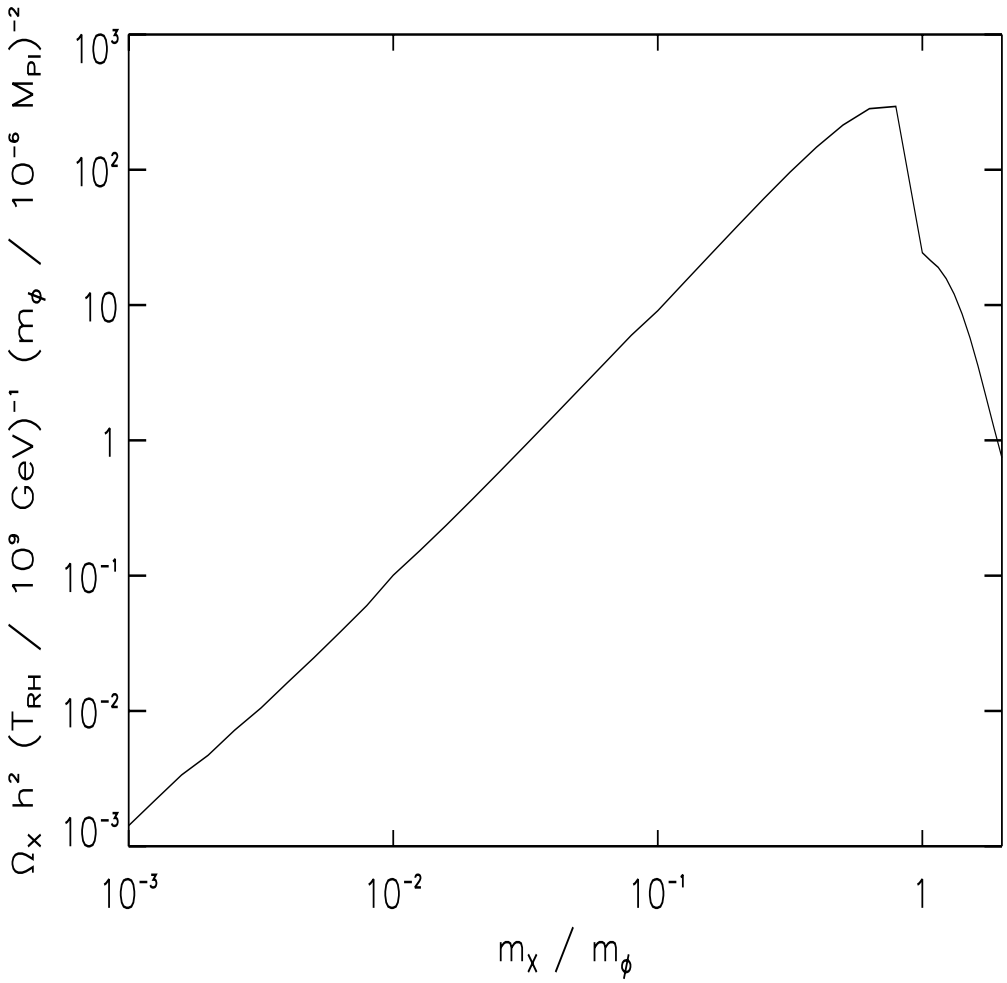

Figure 2.1 The present-day density fraction of supermassive dark matter as a function of the dark matter mass m_X (which is expressed in units of the inflaton mass). The inflaton is assumed to be a massive Klein-Gordon field with potential $V(\phi) = \frac{1}{2}m_\phi^2\phi^2$. Note the peak at $m_X \approx m_\phi$. The factors multiplying Ω_X are: the Hubble parameter "fudge factor" $h \approx 0.65$; the temperature at reheating $T_{RH} \approx 10^9$ GeV; the inflaton mass m_ϕ and Planck mass M_{Pl}, where $m_\phi \approx 10^{-6}M_{Pl}$ for chaotic inflation. The factors in parentheses are thus of order 1.

velocity distribution, and that the Sun was many interaction lengths thick (implying a simpzilla interaction cross section characteristic of the strong force). Extending the work of Press & Spergel (1985), Gould (1987), and Griest & Seckel (1987), they calculated the simpzilla capture rate in the Sun. With the definitions

$$\begin{aligned} q &\equiv 20\left(\frac{m_X}{10^{12}\ \mathrm{GeV}}\right)\left(\frac{10^{-24}\ \mathrm{cm}^2}{\sigma}\right)\left(\frac{R_\odot}{7\times 10^{10}\ \mathrm{cm}}\right)^2\left(\frac{2\times 10^{33}\ \mathrm{g}}{M_\odot}\right) \\ y &\equiv 2.5\left(\frac{v_\odot}{600\ \mathrm{km/s}}\right)\left(\frac{u_{th}}{240\ \mathrm{km/s}}\right) \\ x &\equiv \frac{y}{\sqrt{q-1}}\quad (q>1) \end{aligned} \tag{2.8}$$

the capture rate is

$$\begin{aligned} q &\leq 1: \\ \Gamma_C &= 10^{17}\left(1+y^2\right)\left(\frac{10^{12}\ \mathrm{GeV}}{m_X}\right)\left(\frac{u_{th}}{240\ \mathrm{km/s}}\right)\left(\frac{R_\odot}{7\times 10^{10}\ \mathrm{cm}}\right)^2\ [\mathrm{s}^{-1}] \\ q &> 1: \\ \Gamma_C &= 10^{17}\left[1+y^2-e^{-x^2}\left(1+y^2+x^2\right)\right]\left(\frac{10^{12}\ \mathrm{GeV}}{m_X}\right)\left(\frac{u_{th}}{240\ \mathrm{km/s}}\right) \\ &\times \left(\frac{R_\odot}{7\times 10^{10}\ \mathrm{cm}}\right)^2\ [\mathrm{s}^{-1}] \end{aligned} \tag{2.9}$$

Here, u_{th} is the velocity dispersion in the Maxwell-Boltzmann distribution, which for a spherical dark matter halo is generally taken to be in the range of 300 km/s (Press & Spergel 1985), and $v_\odot$ is the escape velocity from the Sun, which is roughly 600 km/s. The factors in parentheses in the above equations, apart from the ones with m_X and σ (which we vary), are therefore all of order 1.

The two different forms for Γ_C come from the efficiency of the simpzilla energy

loss in the Sun. For $q \leq 1$, most of the simpzillas are captured. For $q > 1$, however, only the lower-velocity portion of the simpzilla distribution is captured.

We show the simpzilla capture rate in Figure 2.2.

2.3 Annihilation

2.3.1 Annihilation rate

The simpzillas captured by the Sun rapidly (i.e. over a time period much shorter than the age of the Sun) reach equilibrium, where the number annihilated per unit time equals the number captured. This occurs even for values of σ_A, the simpzilla annihilation cross section, as small as what is typical of weak interactions. Albuquerque et al. showed that the resulting simpzilla configuration at the core of the Sun is stable and avoids collapse to a black hole. The size of the configuration is less than $10^{-5} R_\odot$.

We take $\Gamma_A = \frac{1}{2}\Gamma_C$, where Γ_A is the number of annihilations per unit time (each of which destroys two simpzillas). Note that this has the effect of making the *equilibrium* value of Γ_A independent of σ_A.

We neglect simpzilla decays, which are possible too. Simpzillas are at present an entirely hypothetical, non-Standard Model particle about which we have already made several simplifying assumptions (e.g. they are a real scalar field, and they account for the entirety of the $\sim 30\%$ of the Universe's energy density due to non-baryonic matter), and so in order to avoid overcomplication we also assume them to be stable. We leave open the possibility that experimental or theoretical advances could change some of these assumptions.

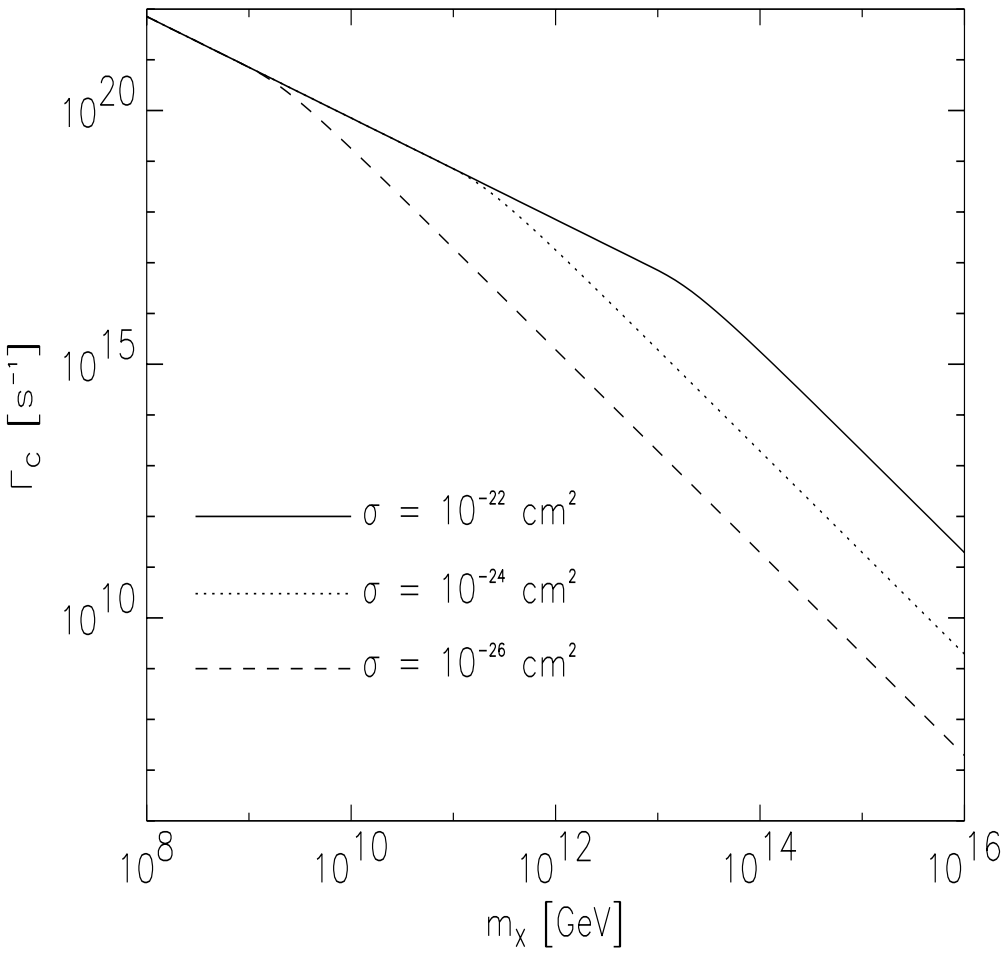

Figure 2.2 The rate of simpzilla capture by the Sun, for three different choices of the simpzilla interaction cross section. The steeper parts of the curves are where only the low-velocity tail of the simpzilla distribution is being captured. In the less steep part, most of them are captured.

2.3.2 Initial neutrino spectrum

Albuquerque et al. assumed that the simpzillas annihilate in the core of the Sun, with each annihilation producing two quarks or two gluons which then fragment into hadronic showers. The total number of hadrons produced per annihilation is $1.2 \times 10^7 \sqrt{M_{12}}$, where $M_{12} \equiv m_X/10^{12}$ GeV. Of these, $2.8 \times 10^5 \sqrt{M_{12}}$ are hadrons containing top quarks, with an energy distribution (Hill 1983)

$$\frac{dN}{dE} \approx \frac{2.8 \times 10^5 \sqrt{M_{12}}}{2m_t} \left(\frac{E}{m_t}\right)^{-\frac{3}{2}} \quad (E \geq m_t) \tag{2.10}$$

where $m_t \approx 175$ GeV is the top quark mass.

In the dense ($\rho \approx 200$ g/cm^3) solar core, hadrons composed of light and charmed quarks tend to lose most of their energy before decaying. Top hadrons, however, decay before significant energy loss. The top almost always decays in the channel $t \to Wb$, and the W also has a short enough lifetime to decay before losing much energy. It decays with equal branching ratios (each about 10.5%) into $e\nu_e$, $\mu\nu_\mu$, and $\tau\nu_\tau$. In the latter case, the τ, like the top quark and the W, decays at high energies, with a second ν_τ among the products. 18% of the τ decays result in a second ν_e and another 18% in a second ν_μ.

We only consider neutrinos with energies ≥ 50 GeV. This value is in the range of the expected ~ 100 GeV threshold for muon detection at IceCube (Ahrens et al. 2001), and also close to $\frac{1}{2}m_W$, the energy of the neutrino produced in the (two-body) decay of a W at rest. At these energies, the top quark[3] and the W generally decay

[3]Hadrons containing bottom quarks may be another source of high-energy neutrinos, because they also have very short lifetimes. However, B mesons have a large number of decay modes, and it is highly nontrivial to determine the flux of high-energy neutrinos produced when the B decay products interact significantly with the medium. We neglect high-energy simpzilla neutrinos from

on-shell. The total neutrino production rate above 50 GeV from t and W decays is

$$\frac{d\Phi_0^\ell}{dt} \approx \kappa_\ell 10^4 \sqrt{M_{12}} \Gamma_A \tag{2.11}$$

where $\kappa_\ell = \frac{1}{2}, \frac{1}{2}, 1$ for $\ell = e, \mu, \tau$ respectively.

The initial simpzilla neutrino energy spectrum has been analytically fitted by Albuqerque et al, giving (in our notation)

$$\begin{aligned} \frac{d\Phi_0^\ell}{dEdt} &= \kappa_\ell 10^4 \sqrt{M_{12}} \Gamma_A \sqrt{E_{min}} \times 0.939 \\ &\times \frac{E + m_W}{\sqrt{[E + m_t]\left[(E + m_t)^2 - m_t^2\right]\left[(E + m_W)^2 - m_W^2\right]}} \\ &\times \Theta\left(E - E_{min}\right) \end{aligned} \tag{2.12}$$

Here, $E_{min} = 50$ GeV. $\Theta(x)$ is the standard step function. The numerical factor 0.939 is a normalization constant.

We take (2.12) as the initial simpzilla neutrino (and antineutrino) distribution. We plot it in Figure 2.3. Note that the typical neutrino energy is $\ll m_X$, since there are $\sim 10^4\sqrt{M_{12}}$ produced per annihilation.

bottom hadrons in this paper, although they are certainly deserving of future study and could add significantly to the total neutrino flux.

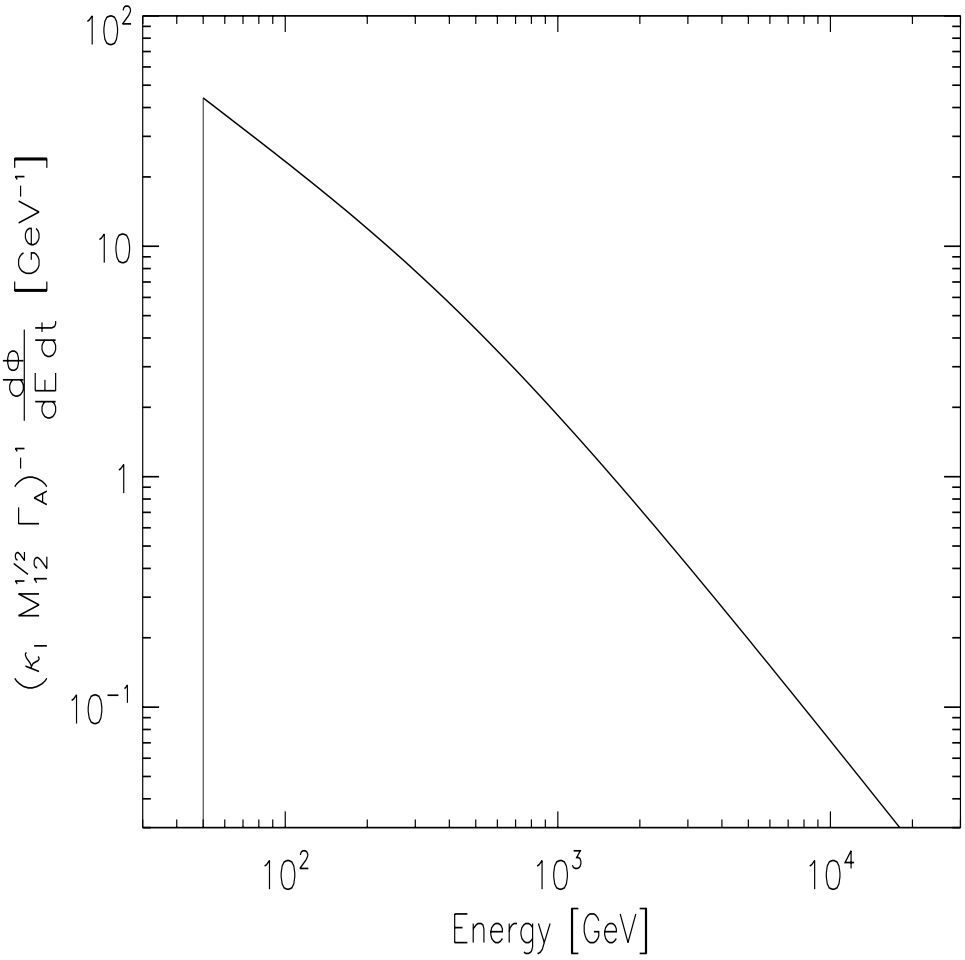

Figure 2.3 The initial energy distribution of neutrinos created in simpzilla annihilations. The factors multiplying $d\Phi/dEdt$ are explained in the text.

CHAPTER 3

HIGH-ENERGY NEUTRINOS: WEAK INTERACTIONS

In this chapter, we discuss the propagation of high-energy neutrinos through matter, in particular through the Sun. Neutrinos with energies $\lesssim 100$ GeV are likely to pass through the Sun without interacting. At higher energies, though, neutrino interactions are significant, and the initial flux of neutrinos from simpzilla annihilations at the core is greatly modified by the time it reaches the surface.

The neutrinos created in simpzilla annihilations at the Sun's core propagate outward through a plasma of protons, ^{4}He nuclei, and electrons. (Other isotopes are not sufficiently abundant to have a significant effect on our calculations.) The composition of the Sun, including the abundances of hydrogen and helium as a function of radial distance, is fairly well established, and must be taken into account due to the different cross sections of neutrinos on protons and neutrons.

The only physical phenomena affecting neutrino propagation are weak scatterings and flavor oscillations. We discuss the weak scatterings in this chapter and oscillations in Chapter 4.

3.1 Weak interactions with nucleons

Neutrinos at sufficiently high energies have significant interactions with nucleons, via either charged current (CC) (mediated by W) or neutral current (NC) (mediated by Z) scattering. In charged current interactions, the neutrino is absorbed and the corresponding charged lepton is produced. The subsequent energy losses of the lepton, discussed in Chapter 5, are of critical importance.

To determine the relative importances of the weak interactions, it is necessary to calculate the charged and neutral current cross sections on nucleons. Previous calcu-

lations of the neutrino-nucleon scattering cross sections at high energies (Gandhi et al. 1996, 1998) have assumed an isoscalar nucleon; that is, that its parton distributions are the average of those for the proton and neutron. This is a good assumption for a medium such as the interior of the Earth, which was the motivation for Gandhi et al.'s cross sections, but in the Sun protons substantially outnumber neutrons. As such, it is necessary to recalculate the cross sections separately for protons and neutrons, which we have done. We describe this below, using the formalism of Paschos & Yu (2002) for deep inelastic scattering (DIS) of a neutrino by a nucleon, which includes lepton mass effects in charged current scattering.

We work in terms of the Bjorken scaling variable x and inelasticity parameter y, defined as

$$\begin{aligned} x &\equiv \frac{Q^2}{2m_A(E_\nu - E')} \\ y &\equiv \frac{E_\nu - E'}{E_\nu} \end{aligned} \tag{3.1}$$

where Q^2 is the absolute value of the square of the invariant momentum transfer carried by the virtual W or Z, m_A is the mass of the nucleon[1], E_ν is the initial neutrino energy, and E' is the final neutrino (charged lepton) energy in NC (CC) scattering.

The double differential cross section is

$$\frac{d^2\sigma}{dxdy} = \frac{G_F^2 y}{16\pi}\kappa^2 L^{\mu\nu} W_{\mu\nu} \tag{3.2}$$

[1]We will use A in this chapter to refer to a generic nucleon, and N to refer specifically to an isoscalar nucleon.

where G_F is the Fermi constant, $L^{\mu\nu}$ and $W_{\mu\nu}$ are respectively the leptonic and hadronic tensors[2] and

$$\begin{aligned} \kappa &\equiv \text{(CC)}\ \frac{m_W^2}{Q^2+m_W^2} \\ &\equiv \text{(NC)}\ \frac{m_Z^2}{Q^2+m_Z^2} \end{aligned} \tag{3.3}$$

where m_W and m_Z are the masses of the gauge bosons. κ in (3.3) should not be confused with the κ_ℓ coefficient in (2.11).

The differential cross section may be put in the form (as before we follow Paschos & Yu (2002))

$$\begin{aligned} \frac{d^2\sigma}{dxdy} &= \frac{G_F^2 m_A E_\nu}{\pi}\kappa^2 \left[\frac{y}{2x}\left(xy+\frac{m_\ell^2}{2E_\nu m_A}\right)F_2(x,Q^2)\right. \\ &+ \left(1-y-\frac{m_A xy}{2E_\nu}-\frac{m_\ell^2}{4E_\nu^2}\right)F_2(x,Q^2) \\ &\pm \left(xy\left(1-\frac{y}{2}\right)-y\frac{m_\ell^2}{4m_A E_\nu}\right)F_3(x,Q^2) \\ &- \left.\frac{1}{x}\frac{m_\ell^2}{2m_A E_\nu}F_2(x,Q^2)\right] \end{aligned} \tag{3.4}$$

Here, F_2 and F_3 are the deep inelastic structure functions, which depend on whether the incident particle is a neutrino or antineutrino, and whether the reaction is charged or neutral current. The sign of the third term is + for neutrinos and − for antineutrinos. Neutrinos undergoing charged current scattering only interact with d, s, $\bar{u}$, and $\bar{c}$ quarks (in protons and neutrons the latter three are, of course, sea

[2]The leptonic and hadronic tensors are factors coming from the Feynman diagrams for charged and neutral current scattering – see e.g. chapters 6 and 8 of Halzen & Martin (1984).

quarks), and antineutrinos interact with the respective antiquarks. In neutral current scattering, all quarks and antiquarks contribute to the cross section.

Paschos & Yu (2002) give F_2 and F_3 for the different processes. For brevity, we only reproduce the ones for neutrino-proton charged and neutral current scattering here, and refer the reader to their paper for the others.

The structure functions for neutrino-proton charged current scattering are

$$\begin{aligned} F_2^{cc}(\nu p) &= 2x[d + s + \bar{u} + \bar{c}] \\ F_3^{cc}(\nu p) &= 2[d + s - \bar{u} - \bar{c}] \end{aligned} \tag{3.5}$$

and for neutral current scattering are

$$\begin{aligned} F_2^{nc}(\nu p) &= 2x[(g_L^2 + g_R^2)(u + c + \bar{u} + \bar{c}) + ({g'}_L^2 + {g'}_R^2)(d + s + \bar{d} + \bar{s})] \\ F_3^{nc}(\nu p) &= 2[(g_L^2 - g_R^2)(u + c - \bar{u} - \bar{c}) + ({g'}_L^2 - {g'}_R^2)(d + s - \bar{d} - \bar{s})] \end{aligned} \tag{3.6}$$

where g_L, etc. are defined in terms of the Weinberg angle θ_W as $g_L = \frac{1}{2} - \frac{2}{3}\sin^2\theta_W$, $g_R = -\frac{2}{3}\sin^2\theta_W$, ${g'}_L = -\frac{1}{2} + \frac{1}{3}\sin^2\theta_W$, and ${g'}_R = \frac{1}{3}\sin^2\theta_W$. As with Paschos and Yu, we take $\sin^2\theta_W = 0.23117$.

The quark distribution functions u, d, etc. are functions of x and Q^2. Note that we are neglecting top and bottom quarks, both of which contribute negligibly to the cross section in our energy range of interest (Gandhi et al. 1996, 1998). We assume all the other quarks to be massless.

Finally, m_ℓ in (3.4) is the mass of the charged lepton produced (if any). In neutral current scatterings, we obviously set $m_\ell = 0$. In charged current scatterings,

the electron and muon masses are too small to have a significant effect in our energy range of interest, and so we may ignore them (which means that the calculated charged current cross sections for ν_e and ν_μ are identical). We do not neglect the mass of the τ lepton, however, which is approximately 2 GeV and kinematically suppresses the cross section up to $E_\nu \approx 10^2$ GeV. Thus, the ν_τ charged current cross sections are calculated separately. (We should note here that the suppression of the tau neutrino charged current cross sections turns out to not be very significant for the particular problem we are studying, because neutrinos in the Sun rarely interact at energies where the difference in cross sections is significant.)

We have calculated the cross sections for 1 GeV $\leq E_\nu \leq 10^9$ GeV, using the CTEQ6-L leading-order parton distributions (Pumplin et al. 2002), and numerically integrating (3.4) over x and y. For all processes except charged current scatterings of ν_τ and $\bar{\nu}_\tau$, the range of integration is $0 \leq x, y \leq 1$. When the τ lepton mass must be taken into account, it modifies the integration range as shown in equation (2.14) of Paschos & Yu. Our results are shown in Figures 3.1 through 3.3. Note that the cross sections are approximately proportional to energy for $E < 10^5$ GeV, which is the regime in which the dominant contributions to the cross section come from the valence quarks (Gandhi et al. 1996). Above this, though, the dominant contributions come from the sea quarks, and the momentum transfer Q^2 in (3.3) is restricted to a small interval around the gauge boson mass, thus decreasing the value of κ. The effect of this is suppress the growth rate of the cross sections at higher energies.

By integrating (3.4) over only x, we may derive inelasticity parameter distributions $d\sigma/dy$. This is equivalent (up to a normalization and change of variable) to a probability distribution of the final neutrino or charged lepton energy E', which is of use for our Monte Carlo code to simulate the propagation of neutrinos through the

Sun. We show our calculations of $d\sigma/dy$ for some different energies in Figures 3.4 through 3.9.

We note that we are neglecting quasielastic ($\nu_\ell A \to \nu_\ell A'$, $\nu_\ell A \to \ell A'$) and resonant ($\nu_\ell A \to \ell A'\pi$, $\nu_\ell A \to \nu_\ell A'\pi^0$) scatterings. At 50 GeV, the lowest energy considered in our Monte Carlo, the cross sections for these processes are less than 5% of the DIS cross sections.

We also note the finding of Paschos & Yu that corrections to DIS cross sections due to nuclear effects are negligible. We neglect them too, treating the nucleons as free in our code.

The ratio of the proton and neutron densities in the Sun, which we calculate using the standard solar model given by Bahcall (1989), is shown in Figure 3.10. For our purposes, isotopes other than ^{1}H and ^{4}He may be neglected.

3.2 Weak interactions with electrons

We neglect neutrino-electron interactions in our calculations. Neutrinos have both charged and neutral current interactions with electrons, but in general the cross sections at a given energy are considerably smaller than they are for weak interactions with nucleons. Gandhi et al. have calculated neutrino-electron scattering cross sections between 10^2 and 10^{12} GeV for ν_e and ν_μ and their antineutrinos (the ones for tau neutrinos are similar). Their νe and $\bar{\nu} e$ cross sections are generally $20-200$ times smaller than our νA and $\bar{\nu} A$ cross sections at equivalent energies. As electrons are roughly as abundant as nucleons in the Sun, this means that there would be at most a $\sim 5\%$ correction to the interaction length.

There is one exception: the $\bar{\nu}_e e^- \to W^-$ Glashow resonance at 6.3 PeV. In a small region (of width a few PeV) on either side of the resonance, the $\bar{\nu}_e$-e^- scattering cross

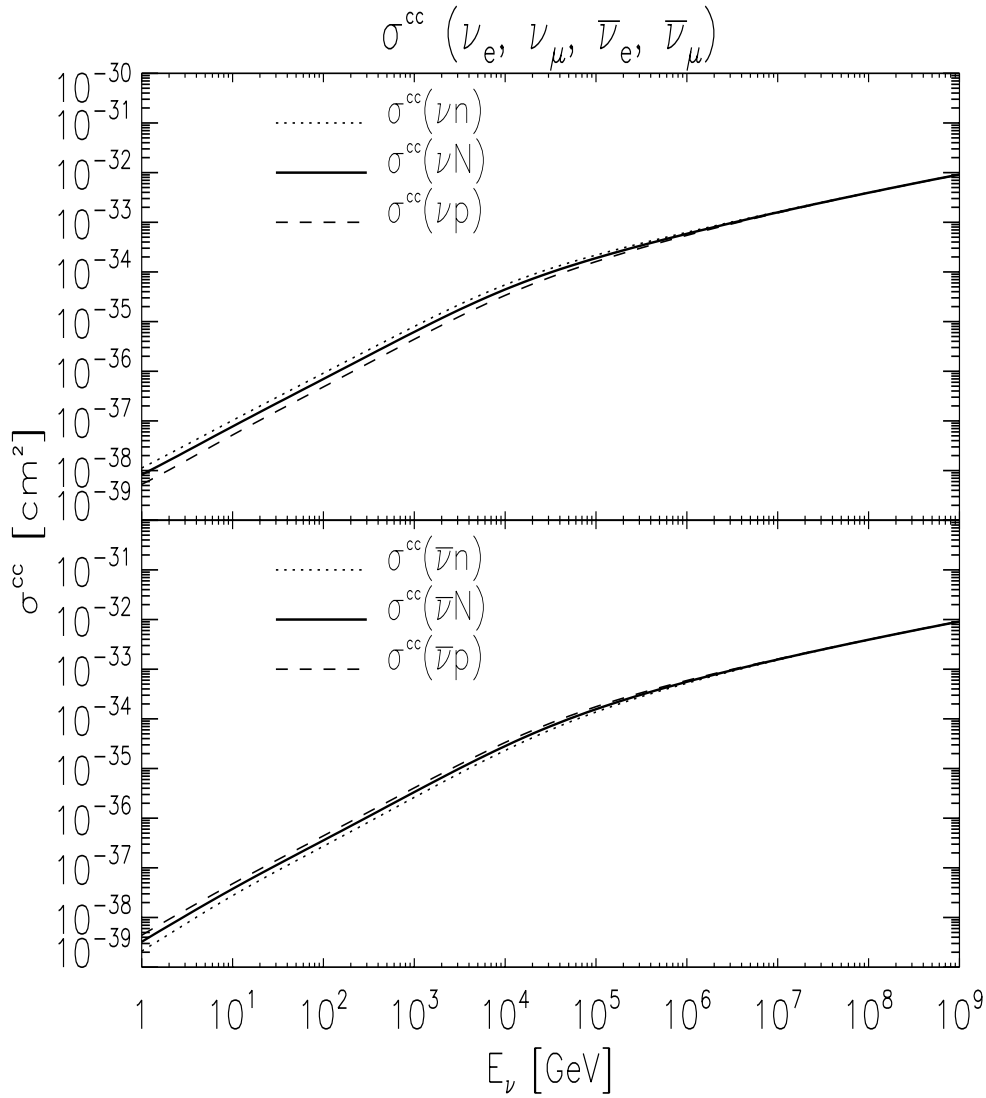

Figure 3.1 The charged current cross sections for ν_e, ν_μ, and their antineutrinos interacting with a neutron (n), a proton (p), and an isoscalar nucleon (N). The calculation was done using the CTEQ6-L parton distributions.

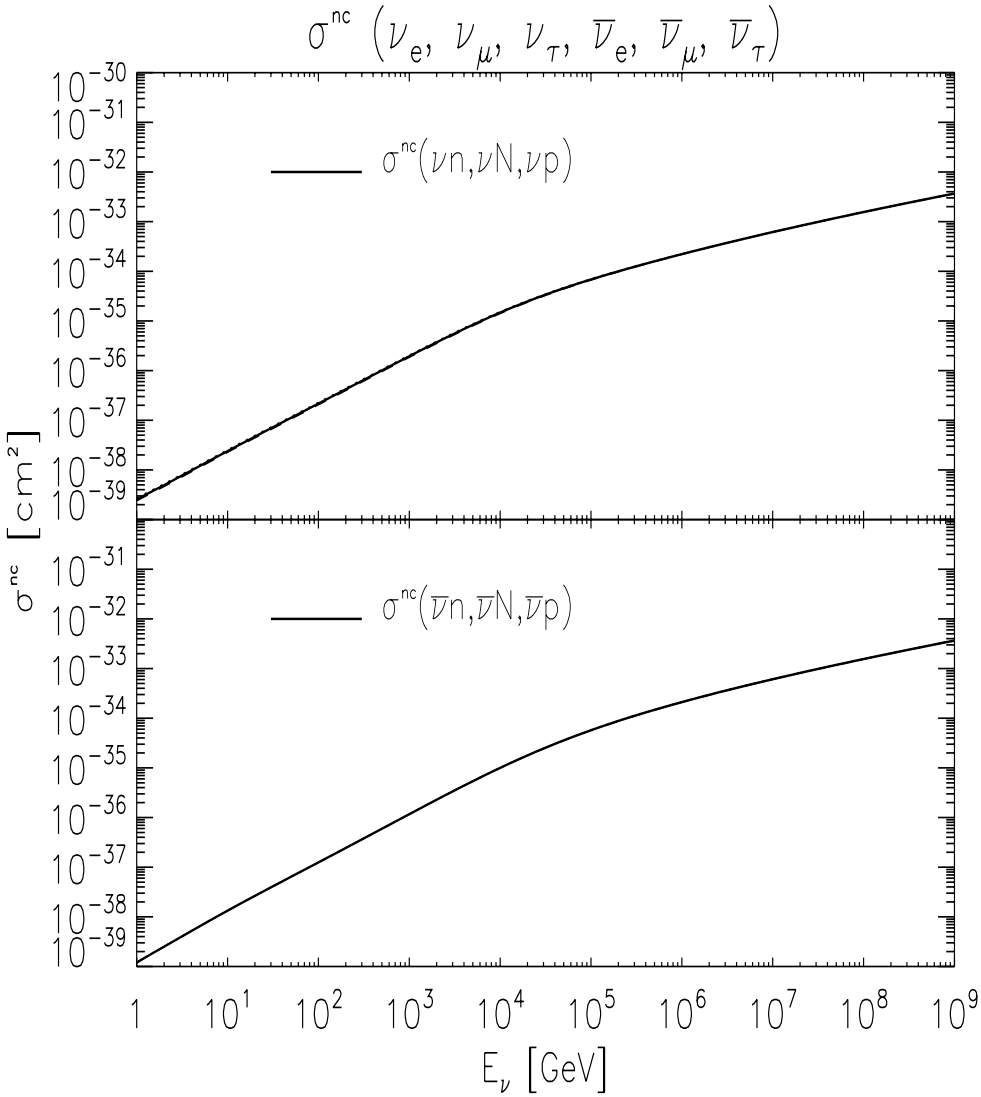

Figure 3.2 The neutral current cross sections for all neutrino and antineutrino flavors. The differences between the cross sections for scattering off protons, neutrons, and isoscalar nucleons are too small to see on this scale (although they are not zero).

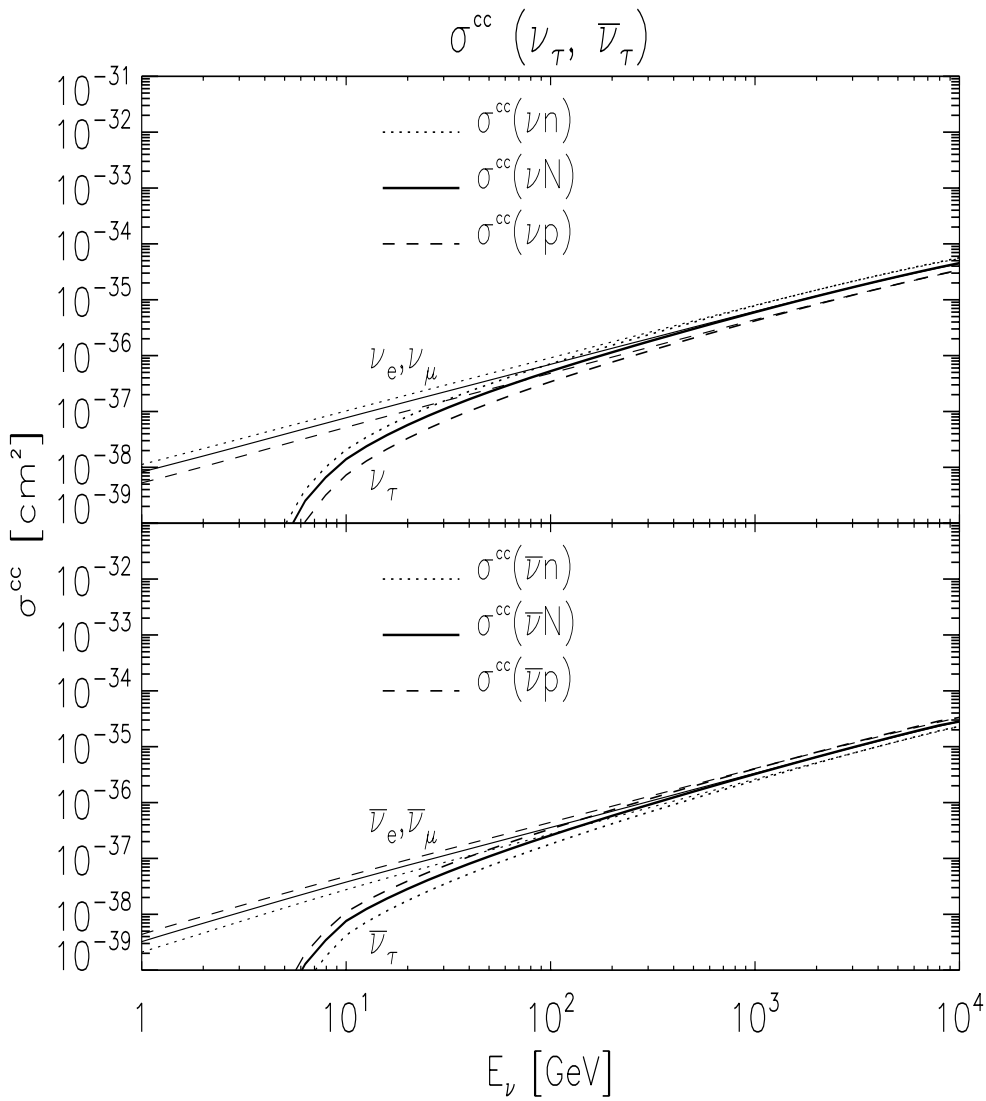

Figure 3.3 The charged current cross sections for ν_τ and $\bar{\nu}_\tau$ interacting with a neutron (n), a proton (p), and an isoscalar nucleon (N). The cross sections for ν_e, ν_μ and their antineutrinos are also plotted to show the kinematic suppression due to the τ mass.

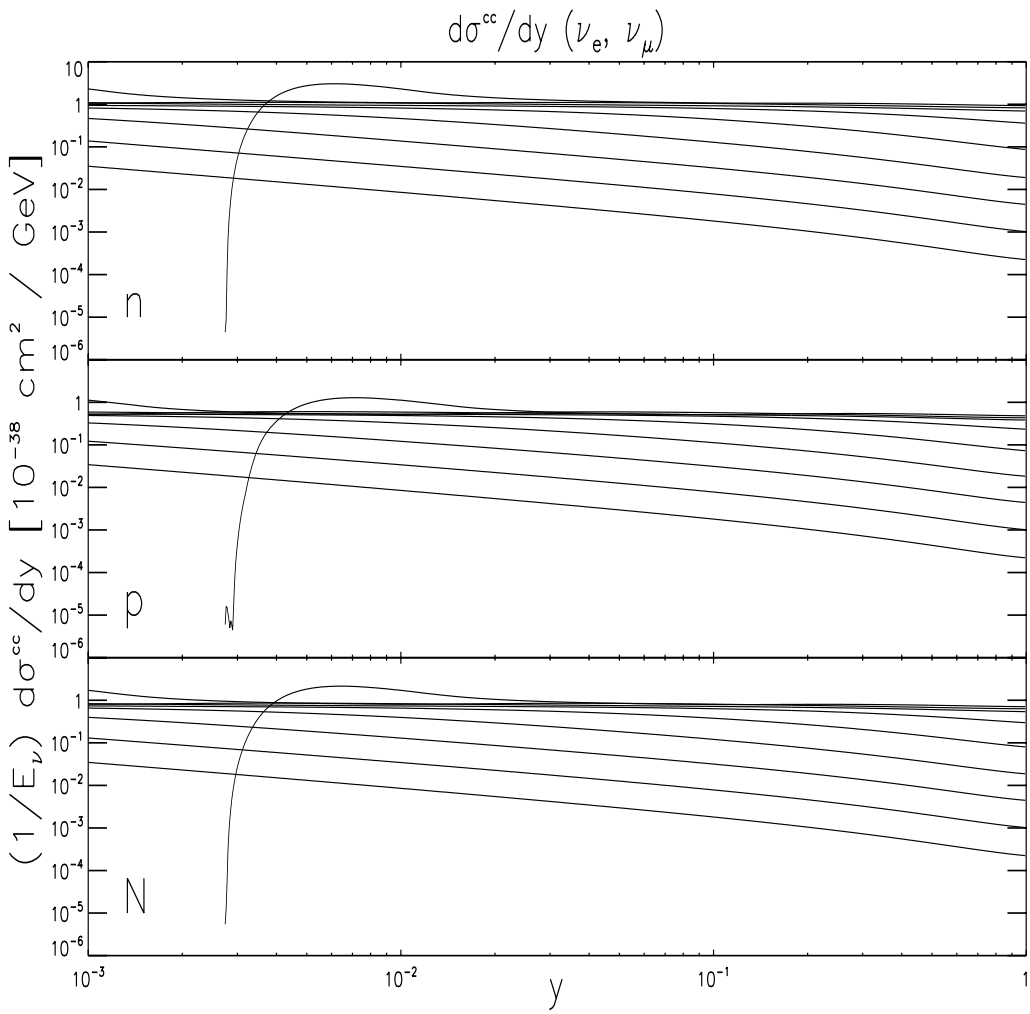

Figure 3.4 Differential cross sections for a charged current interaction between a ν_e or ν_μ and a neutron (n), proton (p), and isoscalar nucleon (N). From top to bottom at $y \approx 5 \times 10^{-3}$, the curves correspond to an initial neutrino energy of 10, 10^2, ..., 10^9 GeV. The 10^2 and 10^3 GeV curves are hard to distinguish on this scale. Note the sharp falloff in the 10 GeV curves at $y \approx 3 \times 10^{-3}$, which occurs because the momentum transfer at values of y below this is too small for the parton formalism used to calculate deep inelastic scattering to hold (essentially, the gauge boson cannot "resolve" the individual quarks). This is a general feature on all our $d\sigma/dy$ plots. Other scattering processes are dominant in this region; however, energies much below 100 GeV are not of interest to us.

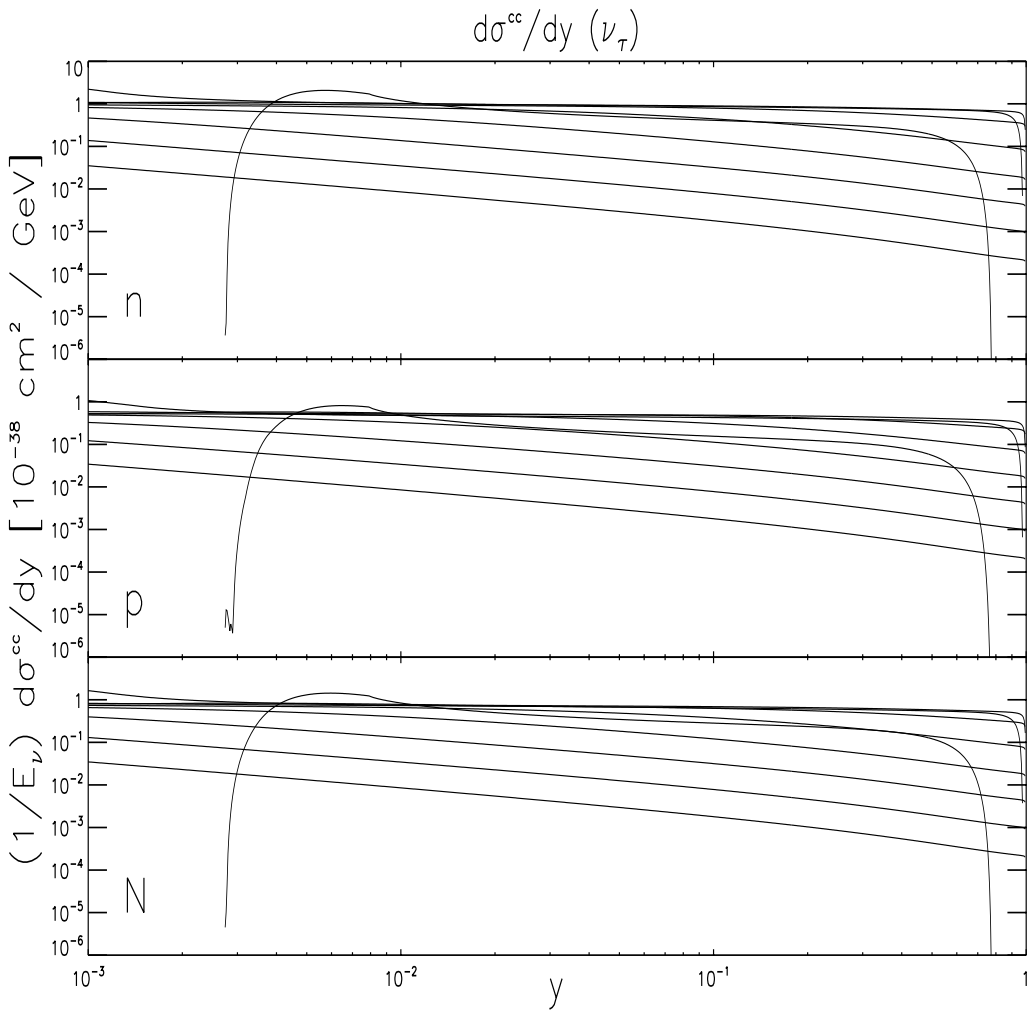

Figure 3.5 Differential cross sections for a charged current interaction between a ν_τ and a neutron (n), proton (p), and isoscalar nucleon (N). The 10 and (much less dramatically) 100 GeV curves are kinematically suppressed at large y by the τ mass.

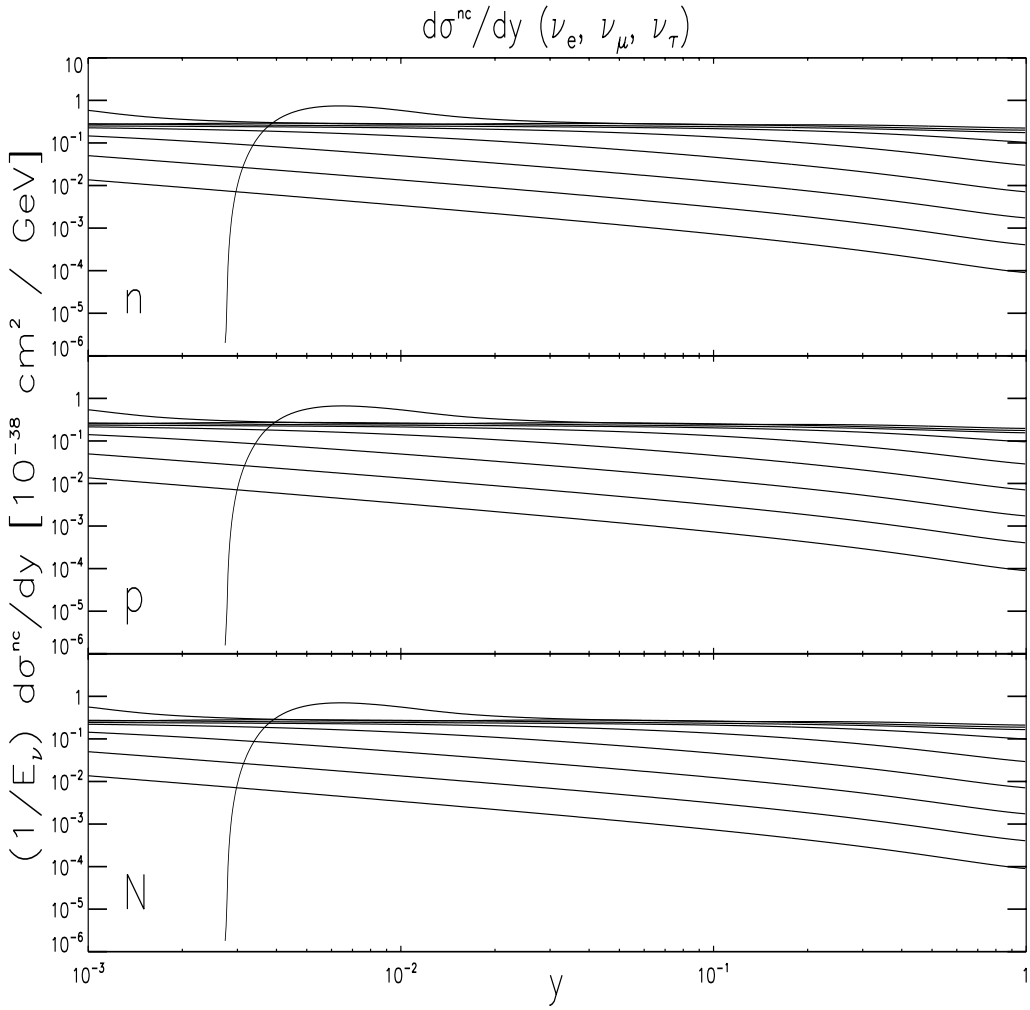

Figure 3.6 Differential cross sections for a neutral current interaction between ν_e, ν_μ, or ν_τ and a neutron (n), proton (p), and isoscalar nucleon (N).

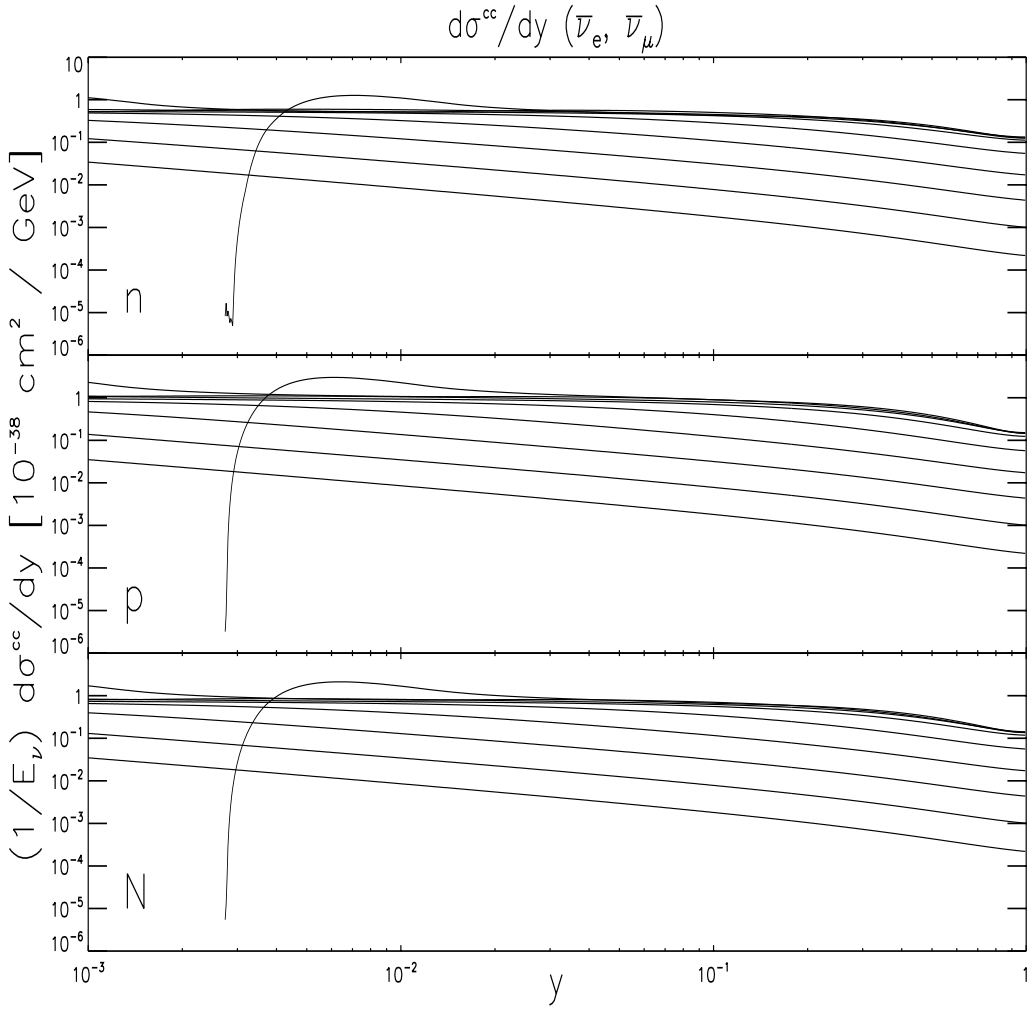

Figure 3.7 Differential cross sections for a charged current interaction between $\bar{\nu}_e$ or $\bar{\nu}_\mu$ and a neutron (n), proton (p), and isoscalar nucleon (N).

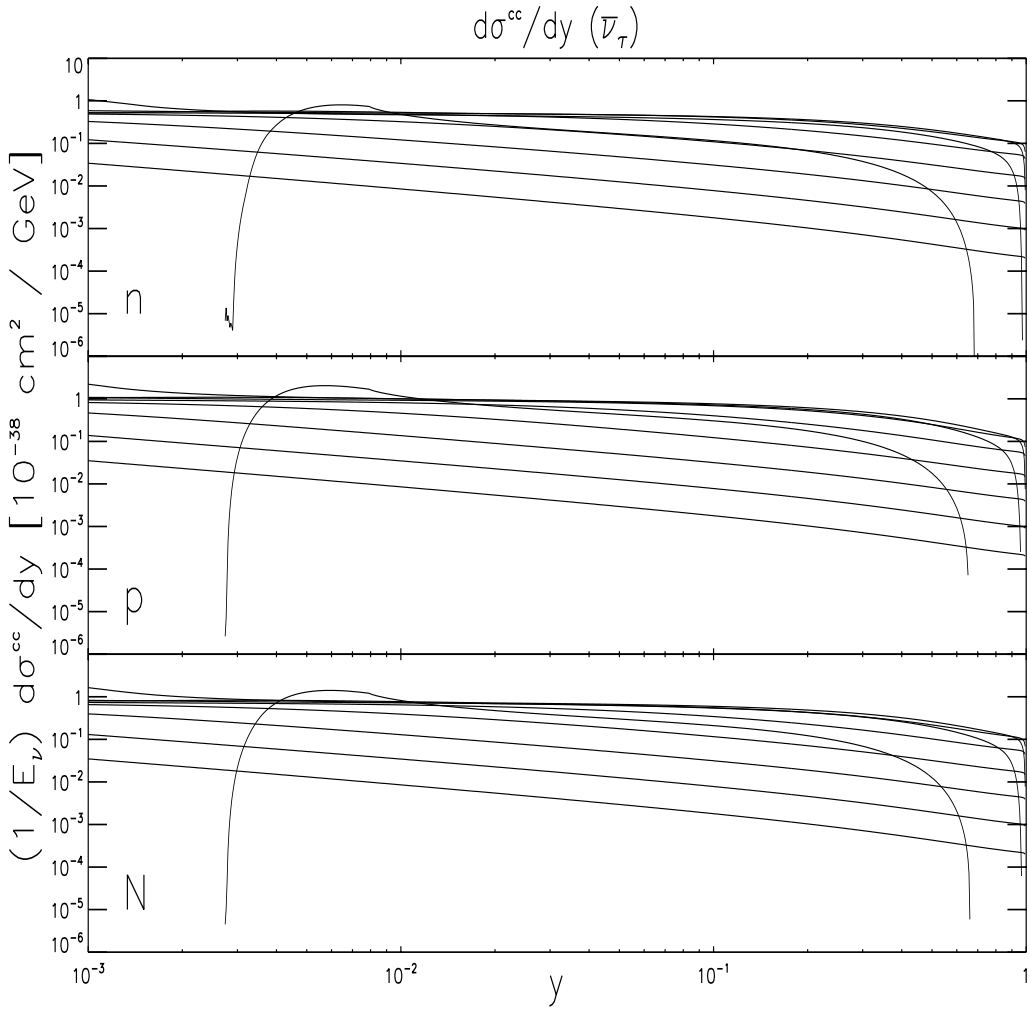

Figure 3.8 Differential cross sections for a charged current interaction between a $\bar{\nu}_\tau$ and a neutron (n), proton (p), and isoscalar nucleon (N). The 10 and 100 GeV curves are kinematically suppressed at large y by the τ mass.

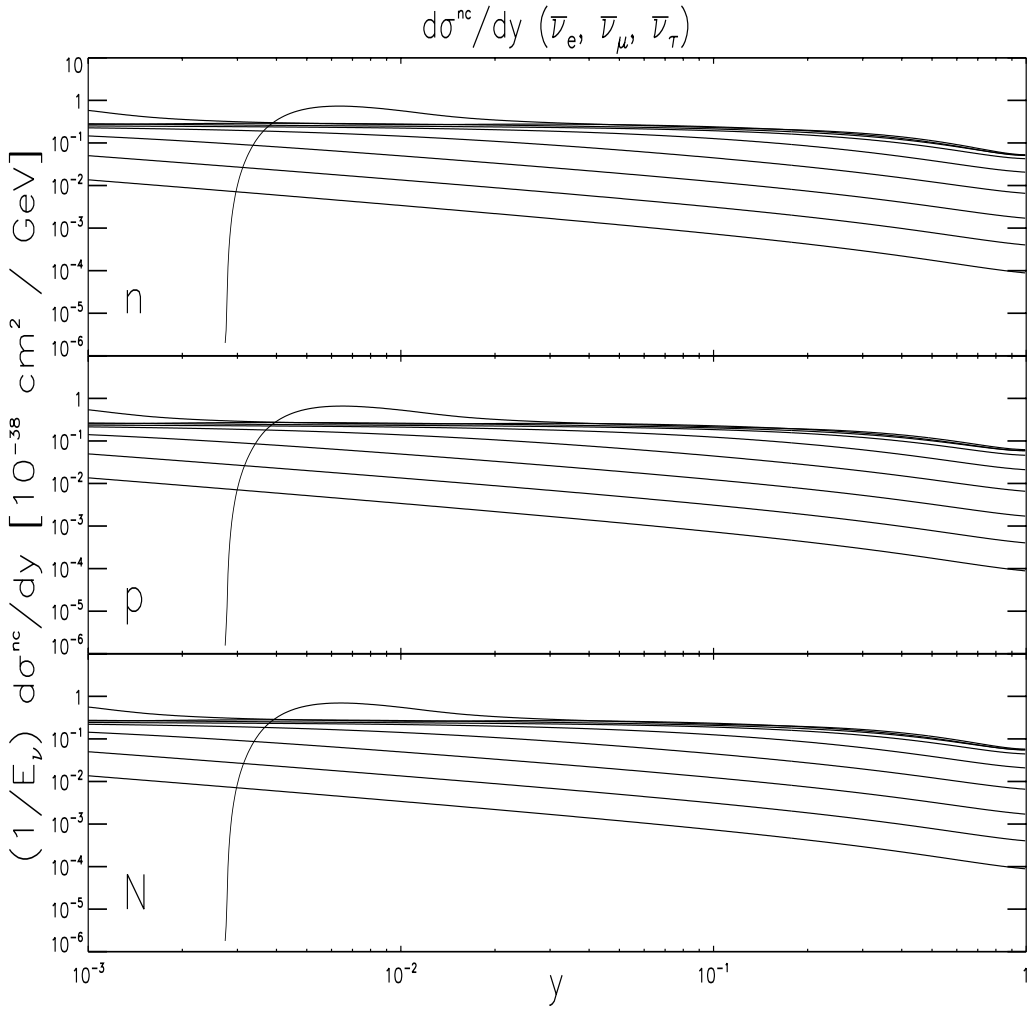

Figure 3.9 Differential cross sections for a neutral current interaction between $\bar{\nu}_e$, $\bar{\nu}_\mu$, or $\bar{\nu}_\tau$ and a neutron (n), proton (p), and isoscalar nucleon (N).

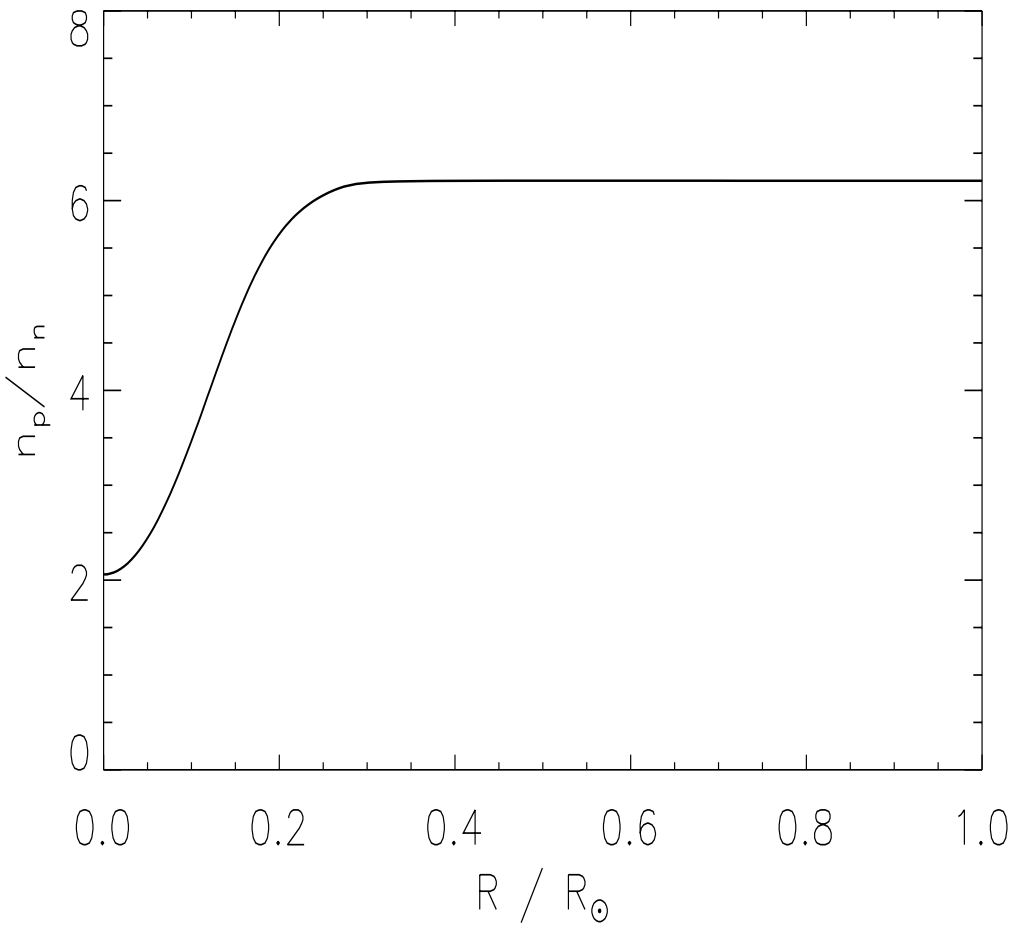

Figure 3.10 The ratio of the proton and neutron number densities in the Sun as a function of radius. The relative number density of neutrons is highest in the core, where more hydrogen has been processed into helium. We neglect isotopes other than ^{1}H and ^{4}He.

section exceeds the $\bar{\nu}_e$-A cross section by $1-2$ orders of magnitude. The W^- may in turn decay to any of the three antineutrinos and the associated charged leptons, or into hadronic channels.

However, we do not expect this to be significant for our results. Only $\sim 1\%$ of the initial simpzilla neutrino flux is in the range where the Glashow resonance is important, and of that only the $\bar{\nu}_e$ component is directly affected.

3.3 "Punch-through" neutrinos

Not all of the initial ν_μ and ν_e are absorbed by charged current interactions. Some propagate without experiencing any interactions at all, though the probability of this declines (roughly exponentially) with energy. Another fraction experience repeated neutral current scatterings until their energies are reduced to the point where the probability of further interactions in the Sun is small. They then emerge along with the down-scattered ν_τ. We discuss the characteristics of the emergent neutrinos further in Chapter 6.

This "punch-through" ν_μ and ν_e flux is currently the subject of a study by E. W. Kolb, J. F. Beacom, and the author. The Monte Carlo code we have written for the present calculation (see Chapter 6) takes it into account.

CHAPTER 4

HIGH-ENERGY NEUTRINOS: OSCILLATIONS

There has been a great deal of recent interest in neutrino flavor oscillations, largely because several experiments within the last few years have provided compelling evidence that they take place. The SuperKamiokande measurements of the atmospheric neutrino flux (Fukuda et al. 1998, 2000) indicate $\nu_\mu \leftrightarrow \nu_\tau$ oscillations, and rule out oscillations of ν_μ to sterile neutrinos[1] at the 99% confidence level.

Addtionally, it has long been known that there is a deficit of measured to predicted electron neutrino flux from thermonuclear reactions in the Sun (Bilenkii et al. 1999). The recent observations by the Sudbury Neutrino Observatory (Klein 2001; Ahmad et al. 2002b,a) of a significant non-ν_e component in the solar neutrino flux have given the best evidence yet for oscillations of ν_e to other active flavors.

The existence of oscillations, in turn, is evidence that neutrinos have masses – or more precisely, that they have nondegenerate mass eigenstates which are not aligned with the flavor eigenstates. This means that a given flavor eigenstate is a linear combination of two or more mass eigenstates. Since the mass eigenstates have different energies, they evolve in time with different phases, and hence the state to which they sum can evolve away from the original flavor eigenstate and pick up contributions from the other flavor eigenstates. There will thus be a probability, possibly substantial or even 1, that the neutrino will be measured to have a different flavor than the one it began with.

This effect can be enhanced when neutrinos are propagating through matter, in

[1] If there are more than three neutrino mass eigenstates, then there are some linear combinations of them which are orthogonal to the three known flavor eigenstates. These correspond to "sterile" neutrinos, which do not have weak interactions. We do not consider sterile neutrinos in this paper.

our case the Sun, because in certain energy ranges the different flavors have different weak interactions with the surrounding matter. The classic example, first pointed out by Mikheev, Smirnov, and Wolfenstein (Wolfenstein 1978; Mikheev & Smirnov 1985), is for solar neutrinos interacting with the electrons in the interior of the Sun. Electron neutrinos, in addition to the neutral current interactions with electrons and nucleons that all three flavors have, also have charged current interactions with them that allow for $\nu_e - e$ forward scattering and hence do not disrupt the coherent development of the neutrino beam. The effect of the latter is to add a term to one of the elements in the flavor-basis Hamiltonian; this in turn can enhance the ν_e oscillations (although, as we will see, it can also suppress them).

Our Monte Carlo takes both matter and vacuum oscillations into account, for all three flavors and including the effects of neutrino absorption. In this section, we review the physics of neutrino oscillations in vacuum and matter. We first go over the two-flavor case, which is somewhat more straightforward algebraically (although not conceptually different than the three-flavor case), and then present the extension of our results to three flavors.

4.1 Two-flavor oscillations

4.1.1 In vacuum

In this subsection, we loosely combine the discussions in Beacom & Balantekin (1997), Kayser (2001), and Mason & Sher (1994). Assume without loss of generality that neutrinos can be either ν_e or ν_μ. Let $\{|\nu_e\rangle, |\nu_\mu\rangle\}$ be the corresponding orthonormal flavor basis.

We also assume that there are two orthonormal mass eigenstates, $|\nu_1\rangle$ and $|\nu_2\rangle$,

with masses m_1 and m_2. An arbitrary neutrino state $|\nu\rangle$ can therefore be expressed as

$$|\nu\rangle = \psi_e |\nu_e\rangle + \psi_\mu |\nu_\mu\rangle = \psi_1 |\nu_1\rangle + \psi_2 |\nu_2\rangle \tag{4.1}$$

Because the flavor and mass bases are orthonormal, the ψ coefficients are related by a 2×2 unitary matrix U ($U^\dagger = U^{-1}$):

$$\Psi^F \equiv \begin{bmatrix} \psi_e \\ \psi_\mu \end{bmatrix} = U \begin{bmatrix} \psi_1 \\ \psi_2 \end{bmatrix} \equiv U\Psi^M \tag{4.2}$$

where

$$U \equiv \begin{bmatrix} \cos\theta & \sin\theta \\ -e^{i\phi}\sin\theta & e^{i\phi}\cos\theta \end{bmatrix} \tag{4.3}$$

We assume that the flavor and mass eigenkets are time-independent (and also position-independent, which is true in vacuum but not in matter of varying density), and the ψ coefficients are functions of time. As such, the initial state of the neutrino at $t = 0$ is

$$|\nu(0)\rangle = \psi_e(0) |\nu_e\rangle + \psi_\mu(0) |\nu_\mu\rangle \tag{4.4}$$

Typically, the neutrino will begin in a flavor eigenstate (e.g. if it is produced in a lepton weak interaction), so we will have $|\psi_e(0)| = 1$ and $\psi_\mu = 0$, or vica-versa.

The neutrino state at a subsequent time t is then

$$|\nu(t)\rangle = \exp\left(-iHt/\hbar\right) |\nu(0)\rangle \tag{4.5}$$

where H is the Hamiltonian operator. We keep $\hbar$ and c explicit in this section, rather than setting them to 1.

Thus, in the flavor basis representation, we have

$$\Psi^F(t) = \exp\left(-iH^F t/\hbar\right)\Psi_0^F \tag{4.6}$$

where H^F is the Hamiltonian matrix in the flavor basis, and $\Psi_0^F \equiv \Psi^F(0)$. This is the solution of the differential equation

$$\frac{d}{dt}\Psi^F(t) = -\frac{i}{\hbar}H^F\Psi^F(t) \tag{4.7}$$

H^F is related to the mass basis representation of the Hamilton, H^M, by

$$H^F = UH^MU^{-1} \tag{4.8}$$

Hence, we have

$$\Psi^F(t) = U\exp\left(-iH^M t/\hbar\right)U^{-1}\Psi_0^F \tag{4.9}$$

We assume that the neutrino is in a state of definite momentum k. The energy eigenvalues $E_{1,2}$ of $|\nu_{1,2}\rangle$ are therefore

$$E_{1,2} = \sqrt{k^2c^2 + m_{1,2}^2c^4} \approx \left[kc + \frac{(m_1^2 + m_2^2)c^3}{4k}\right] \mp \left[\frac{\Delta m^2 c^3}{4k}\right] \tag{4.10}$$

We define $\Delta m^2 \equiv m_2^2 - m_1^2$, assuming without loss of generality that $m_2 > m_1$. The expansion of the radical in (4.10) assumes that the neutrino is ultrarelativistic. For our purposes this is a good assumption, because the largest neutrino mass is thought to be under 25 MeV and we are studying energies above 50 GeV.

We define the first term in brackets in (4.10) as $f(k)$, and the second as $g(k)$. We then have

$$H^M = \begin{bmatrix} f(k) - g(k) & 0 \\ 0 & f(k) + g(k) \end{bmatrix} \tag{4.11}$$

and (dropping the k dependence of f and g for brevity)

$$\exp\left(-iH^M t/\hbar\right) = \exp\left(-ift/\hbar\right) \begin{bmatrix} \exp\left(igt/\hbar\right) & 0 \\ 0 & \exp\left(-igt/\hbar\right) \end{bmatrix} \tag{4.12}$$

The equivalent expressions in the flavor basis are then

$$H^F = UH^M U^{-1} = \begin{bmatrix} (f - g\cos 2\theta) & (e^{-i\phi} g \sin 2\theta) \\ (e^{i\phi} g \sin 2\theta) & (f + g\cos 2\theta) \end{bmatrix} \tag{4.13}$$

$$\begin{aligned} &\exp\left(-iH^F t/\hbar\right) = \exp\left(-ift/\hbar\right) \times \\ &\begin{bmatrix} \left(\cos\left(\frac{gt}{\hbar}\right) + i\sin\left(\frac{gt}{\hbar}\right)\cos 2\theta\right) & \left(-ie^{-i\phi}\sin\left(\frac{gt}{\hbar}\right)\sin 2\theta\right) \\ \left(-ie^{i\phi}\sin\left(\frac{gt}{\hbar}\right)\sin 2\theta\right) & \left(\cos\left(\frac{gt}{\hbar}\right) - i\sin\left(\frac{gt}{\hbar}\right)\sin 2\theta\right) \end{bmatrix} \end{aligned} \tag{4.14}$$

If we begin in a pure flavor eigenstate, say $|\nu_e\rangle$, then we will have (ignoring complex phases for simplicity)

$$\Psi_0^F = \begin{bmatrix} \psi_e(0) \\ \psi_\mu(0) \end{bmatrix} = \begin{bmatrix} 1 \\ 0 \end{bmatrix} \tag{4.15}$$

which, using (4.14), will at time t be

$$\Psi^F(t) = \begin{bmatrix} \psi_e(t) \\ \psi_\mu(t) \end{bmatrix} = \exp\left(-ift/\hbar\right) \begin{bmatrix} \left(\cos\left(\frac{gt}{\hbar}\right) + i\sin\left(\frac{gt}{\hbar}\right)\cos 2\theta\right) \\ \left(-ie^{i\phi}\sin\left(\frac{gt}{\hbar}\right)\sin 2\theta\right) \end{bmatrix} \tag{4.16}$$

The probability for the neutrino to have oscillated, that is to be measured as a ν_μ at time t, is

$$P_{e\mu}(t) = |\psi_\mu(t)|^2 = \sin^2\left(\frac{\Delta m^2 c^3 t}{4E\hbar}\right)\sin^2(2\theta) \tag{4.17}$$

where we have expanded $g(k)$ and used $k \approx E$.

The probability for it to have remained a ν_e is

$$\begin{aligned} P_{ee}(t) &= |\psi_e(t)|^2 = 1 - \sin^2\left(\frac{\Delta m^2 c^3 t}{4E\hbar}\right)\sin^2(2\theta) \\ &= 1 - P_{e\mu}(t) \end{aligned} \tag{4.18}$$

Note that we also have $P_{\mu e}(t) = P_{e\mu}$. This symmetry, in general, does *not* hold for the three-flavor case (de Gouvea 2001).

We may define the oscillation length L as

$$L = L(E) = \frac{4\pi E\hbar}{\Delta m^2 c^2} \tag{4.19}$$

L is the period (expressed as a distance) of $P_{e\mu}$, and thus oscillations are a maximum over $L/2$. If the size of the region we are considering is much smaller than L, then neutrino oscillations (for neutrinos produced in that region) are not significant. Conversely, if we are a considering a beam of neutrinos produced at many points inside a region of size $L/2$, then it is trivial to show that half of them have oscillated.

Note also that P_{ee} and $P_{e\mu}$, which are the observable quantities, do not depend on $f(k)$ or the complex phase ϕ in the unitary transformation matrix. This is a general feature of the two-flavor neutrino oscillation formalism: complex phases in U (and thus H^F) and terms in H^F which are proportional to the identity matrix do not have any physically observable consequences if the initial state is a pure flavor state, and so can be neglected. We can use these facts to simplify the math considerably; e.g. we can evolve the state using a reduced Hamiltonian matrix

$$\tilde{H}^F = g(k) \begin{bmatrix} -\cos 2\theta & \sin 2\theta \\ \sin 2\theta & \cos 2\theta \end{bmatrix} \tag{4.20}$$

The fundamental physical quantities, which can be deduced from the oscillation probabilities, are the mixing angle θ and the mass-squared difference Δm^2.

4.1.2 In matter

Normal matter consists of nucleons and electrons. All three flavors of neutrino can have neutral current interactions with nucleons and electrons that result in elastic forward scatterings, and contribute to a coherent development of the neutrino beam. However, electron neutrinos (and antineutrinos) may also forward-scatter via the charged current process $\nu_e + e^- \to e^- + \nu_e$. This channel is not available to the other two flavors, since the W exchange would change their flavors and disrupt the coherent development.

These coherent forward scatterings amplitudes give rise to an interaction potential energy for the neutrino. The neutral current scatterings apply equally to all flavors, and they contribute a term to the Hamiltonian which is proportional to the identity (and has no observable consequences). However, the elastic forward charged current

scattering only applies to ν_e, and so it contributes only to the electron neutrino part of the Hamiltonian. As we will see below, this can have the effect of enhancing or, at very high densities and energies, suppressing ν_e oscillations relative to what they are in vacuum. For a nice discussion of this "MSW Effect" (named after Mikheev, Smirnov, and Wolfenstein) as applied to solar electron neutrinos see Kayser (2001). We discuss the case of two active flavors below.

In this section, we neglect neutrino absorption. An analytical treatment of neutrino oscillations in the presence of absorbing matter is highly nontrivial and beyond the scope of this paper, although there has been some interesting recent work on the topic (Naumov 2002). Of course, we cannot neglect charged current interactions with nucleons in our code; indeed, they are the dominant process for neutrinos at high energies. We will discuss how we integrate the matter-enhanced oscillation formalism in our code in Chapter 6.

We consider once again the case of a beam of ν_e and/or ν_μ; the extension to three flavors is simple and is given in the next section. The elastic forward scattering amplitudes of the ν_e and ν_μ neutral current interactions are equal, and hence they contribute terms to H^F that are proportional to the identity. As discussed above, they have no effect on oscillation probabilities and can be neglected.

The $\nu_e(\bar{\nu}_e)-e$ charged current interaction contributes a term to the elastic forward scattering amplitude of $\nu_e(\bar{\nu}_e)$ (see e.g. de Gouvea (2001)),

$$A(x) = \pm\sqrt{2}G_F N_e(x) \tag{4.21}$$

where the $+$ sign holds for neutrinos, and the $-$ for antineutrinos, and where $N_e(x)$ is the number density of electrons at a point x in the medium. Using (4.20) for the flavor-basis Hamilton in vacuum, (4.7) becomes (where $g(k)$ is expanded)

$$\frac{d}{dt}\Psi^F(t) = -\frac{i}{\hbar}\left(\frac{\Delta m^2 c^4}{4E}\begin{bmatrix} -\cos 2\theta & \sin 2\theta \\ \sin 2\theta & \cos 2\theta \end{bmatrix} + \begin{bmatrix} A(x) & 0 \\ 0 & 0 \end{bmatrix}\right)\Psi^F(t) \tag{4.22}$$

We define (Beacom & Balantekin (1997)):

$$\zeta(t) \equiv \pm\frac{2\sqrt{2}N_e(x(t))E}{\Delta m^2 c^4} \tag{4.23}$$

using the same sign convention as with $A(x)$. (4.22) becomes

$$\frac{d}{dt}\Psi^F(t) = -\frac{i}{\hbar}\frac{\Delta m^2 c^4}{4E}\begin{bmatrix} [\zeta(t) - \cos 2\theta] & \sin 2\theta \\ \sin 2\theta & [-\zeta(t) + \cos 2\theta] \end{bmatrix}\Psi^F(t) \tag{4.24}$$

To obtain this, we added a term proportional to the identity matrix, which as discussed above does not have any physical effects and can be neglected.

Mixing is maximal when the diagonal elements are 0; that is, when $\zeta = \cos 2\theta$. Note that this in general is possible for neutrinos *or* antineutrinos, but not both, since θ is fixed while the sign of ζ is different.

Assuming that ζ is positive, we have

$$N_e(x)E = \frac{\Delta m^2 c^4 \cos 2\theta}{2\sqrt{2}G_F} \tag{4.25}$$

as the condition for resonance, that is, where the electron neutrino oscillations are maximal.

Conversely, if $\zeta \gg 1$ (all the other elements in H^F are of order 1), then the Hamiltonian is effectively diagonal, and oscillations minimal. Matter effects, at sufficiently

high electron number densities and/or neutrino energies, can *suppress* oscillations rather than enhance them.

4.2 Three-flavor oscillations

There are three known neutrino flavors, ν_e, ν_μ, and ν_τ, and if they have masses then there must also be at least three nondegenerate neutrino mass eigenstates $|\nu_1\rangle$, $|\nu_2\rangle$, and $|\nu_3\rangle$. We label them in increasing order of mass.

As in the two-flavor case, the flavor and mass eigenstates are related by a unitary matrix (de Gouvea 2001):

$$U = \begin{bmatrix} c_\omega c_\xi & s_\omega s_\omega c_\xi & s_\xi e^{i\phi} \\ (-s_\omega c_\theta - c_\omega s_\theta s_\xi e^{-i\phi}) & (c_\omega c_\theta - s_\omega s_\theta s_\xi e^{-i\phi}) & s_\theta c_\xi \\ (s_\omega s_\theta - c_\omega c_\theta s_\xi e^{-i\phi}) & (-c_\omega s_\theta - s_\omega c_\theta s_\xi e^{-i\phi}) & c_\theta c_\xi \end{bmatrix} \tag{4.26}$$

where for brevity we abbreviate $\cos x$ and $\sin x$ as c_x and s_x.

There are now three mixing angles θ, ξ, and ω. There is also a complex phase ϕ which, unlike in the two-flavor case, affects the final oscillation probabilities and introduces CP- violating effects. There is no experimental information on ϕ, and we set it to 0.

We also have two independent mass-squared differences, which with de Gouvea we take as Δm^2_{21} and Δm^2_{31} (the third is trivially derivable from the other two).

There is some uncertainty in the numerical values of these quantities, but the results from the SuperKamiokande atmospheric neutrino observations and the solar neutrino measurements of SNO and other groups suggest certain regions of parameter space (given e.g. in de Gouvea (2001)). The atmospheric neutrino results constrain 10^{-4} eV$^2 \lesssim |\Delta m^2_{31}| \lesssim 10^{-2}$ eV^2, $0.3 \lesssim \sin^2\theta \lesssim 0.7$, and $\sin^2\xi \lesssim 0.1$; we take $\Delta m^2_{31} =$

3×10^{-3} eV^2, $\sin^2\xi = 0.1$, and $\sin^2\theta = 0.5$. The other parameters, which influence solar neutrino oscillations, are constrained to a somewhat broader range. They can vary depending on whether the ν_e oscillations are due to vacuum oscillations outside the Sun or MSW oscillations within it, and even in the MSW case there are several different regions of parameter space consistent with the experimental data. However, the choice most currently favored by analysis of the solar neutrino data (Krastev & Smirnov 2002) is the "large mixing angle" (LMA) solution. We choose $\Delta m^2_{21} = 2 \times 10^{-5}$ eV^2 and $\sin^2\omega = 0.2$, which are characteristic of LMA. Our calculations assume the "normal" mass hierarchy, with $m_1 < m_2 < m_3$.

We may once again define a quantity ζ to characterize the matter effects. It is defined slightly differently than in the two-flavor case:

$$\zeta(t) \equiv \pm\frac{\sqrt{2}G_F N_e(x(t))E}{\Delta m^2_{31}c^4} \tag{4.27}$$

where, as before, the sign is negative for antineutrinos. We may write the differential equation for the flavor amplitudes as

$$\begin{aligned}\frac{d}{dt}\psi_\alpha(t) &= -\frac{i}{\hbar}\frac{\Delta m^2_{31}c^4}{2E}\sum_{\beta=1}^{3}\left[\left(\sum_{i=2}^{3}\frac{\Delta m^2_{i1}}{\Delta m^2_{31}}U^*_{\alpha i}U_{\beta i}\right)\right.\\ &+ \left.\zeta(t)\left(\delta_{\alpha1}\delta_{\beta1} - \delta_{\alpha2}\delta_{\beta2} - \delta_{\alpha3}\delta_{\beta3}\right)\right]\psi_\beta(t)\end{aligned} \tag{4.28}$$

This can be straightforwardly obtained from equation (3.4) of de Gouvea (2001). Once again, we have neglected terms proportional to the identity matrix.

Assuming that $\Delta m^2_{21} < \Delta m^2_{31}$, all of the terms in the vacuum part of the Hamiltonian are of order 1. If $\zeta \gg 1$, oscillations of ν_e to the other flavors are suppressed. ($\nu_\mu \leftrightarrow \nu_\tau$ oscillations are not suppressed for large ζ, because the additional large

terms have the same sign and can be removed by adding a term proportional to the identity.) The condition for suppression of ν_e oscillations is

$$E \gg \frac{\Delta m_{31}^2 c^4}{\sqrt{2} G_F N_e(x)} \tag{4.29}$$

4.3 Numerical simulation of neutrino oscillations

4.3.1 Analytical approximation

In theory, three-flavor oscillations can be simulated by numerically solving (4.28) as the neutrinos propagate. In practice, this tends to make the computation extremely slow. Our code therefore uses the analytical solution for the time-evolution operator $U_f(L)$ derived by Ohlsson and Snellman (Ohlsson & Snellman 2000):

$$U_f(L) = e^{-iL(E_1+E_2+E_3+A)/3} \sum_{a=1}^{3} e^{-iL\lambda_a} \frac{1}{3\lambda_a^2 + c_1} \left[\left(\lambda_a^2 + c_1\right) I_3 + \lambda_a \tilde{T} + \tilde{T}^2 \right] \tag{4.30}$$

Equation (4.30) is given in natural units with $\hbar = 1$ and $c = 1$. L is the distance the neutrino travels, A is from (4.21), and $\{E_i\}$ are the energies of the mass eigenstate neutrinos (of which the flavor eigenstate neutrino is a linear combination). I_3 is the 3×3 identity matrix, and $\tilde{T}$ is the flavor-basis representation of $H^M - tr(H^M)$, where H^M is the mass-basis Hamiltonian. $\{\lambda_a\}$ are the eigenvalues of T, the mass-basis representation of $\tilde{T}$, and $\{c_i\}$ are the coefficients in the characteristic equation for the eigenvalues. For brevity, we do not reproduce the lengthy formulas for these quantities here and refer the interested reader to the paper.

In Figures 4.1 and 4.2, we show the oscillation probabilities for 50 and 100 GeV neutrinos emitted from the core of the Sun and propagating without absorption.

These probabilities have been checked against those computed by integrating (4.28). To generate these graphs, we compute (4.30) over small enough steps so that the density at each step may be taken as constant, a technique we also use in our Monte Carlo code.

4.3.2 Other oscillation parameter choices

We have calculated the emergent flux only for the choice of oscillation parameters given above. We do not, however, expect that other choices for the parameters which are consistent with the observational data would cause large differences in the detection rates at Earth. Real detectors (as opposed to the idealized ones we model in Chapter 7, which detect all charged current events in their volumes) tend to preferably observe muons created in and around the detector by ν_μ and $\bar{\nu}_\mu$. The practical question, then, is how much a different choice of oscillation parameters would change the emergent $\nu_\mu + \bar{\nu}_\mu$ flux.

The two parameters which affect this the most (again, assuming that we restrict ourselves to ranges allowed by observation) are ξ and the sign of m_{31}^2. There is evidence from experiment that $m_{21}^2 > 0$ (de Gouvea 2001), but no such constraint exists for m_{31}^2. Our calculations assume that it is also positive. If it were negative, the effect would be to cause $\bar{\nu}_e$ rather than ν_e to have the resonant behavior shown in Figures 4.1 and 4.2 – the oscillation curves for neutrinos and antineutrinos in those graphs would essentially be interchanged by a change of sign in m_{31}^2. A change in ξ would modify the location and size of the resonance.

The worst-case scenario would be that either of the ν_μ or $\bar{\nu}_\mu$ fluxes was depleted completely by the $\nu_e/\bar{\nu}_e$ resonance. However, the other would be unaffected. The combined $\nu_\mu + \bar{\nu}_\mu$ flux, and hence the muon detection rate, would change at most

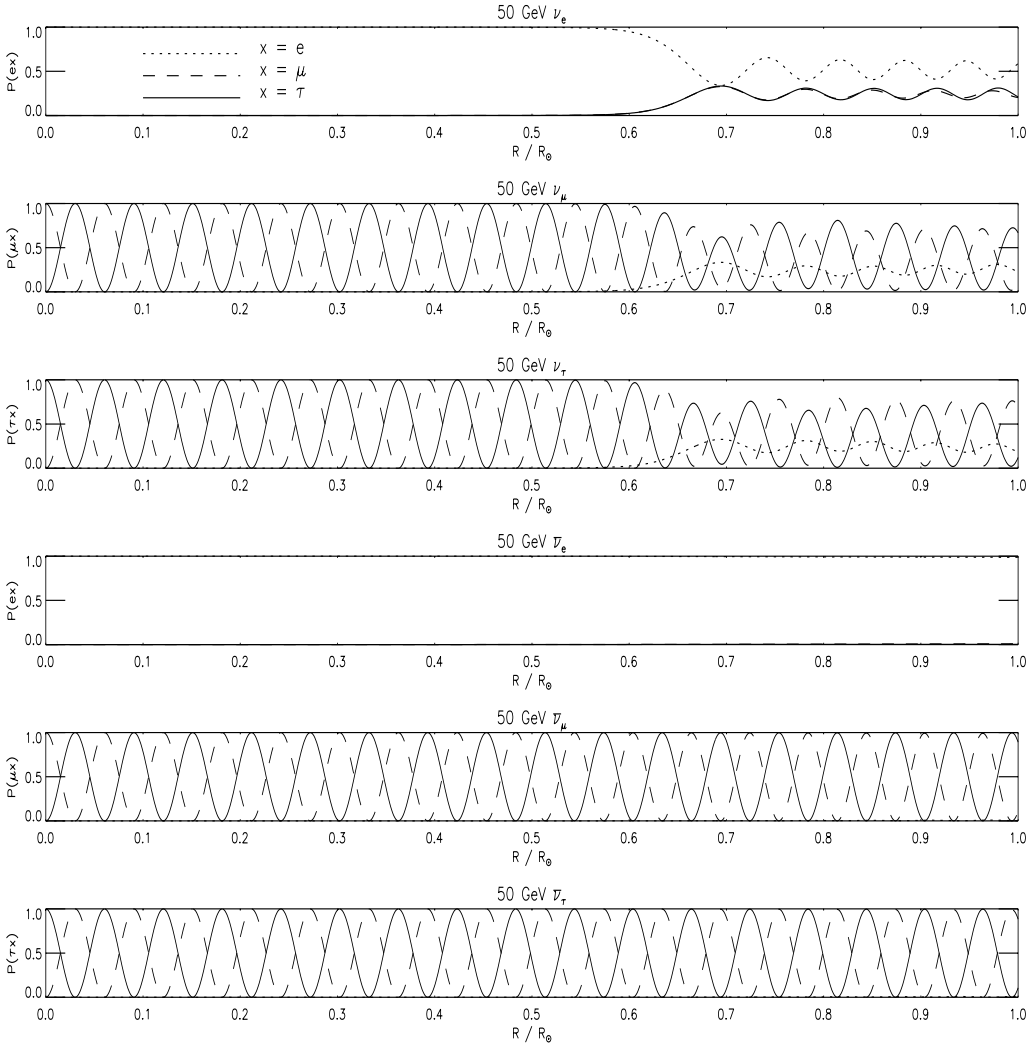

Figure 4.1 The oscillation probabilities of 50 GeV neutrinos in the Sun, assumed to begin in single-flavor states at the center. Note the MSW resonance at about $0.6R_\odot$. Below that, ν_e oscillations are almost completely suppressed by the large value of ζ. $\bar{\nu}_e$ oscillations, which do not have resonances, are also almost completely suppressed (the $\bar{\nu}_e$ probability is very close to 1 and hard to see on the fourth plot).

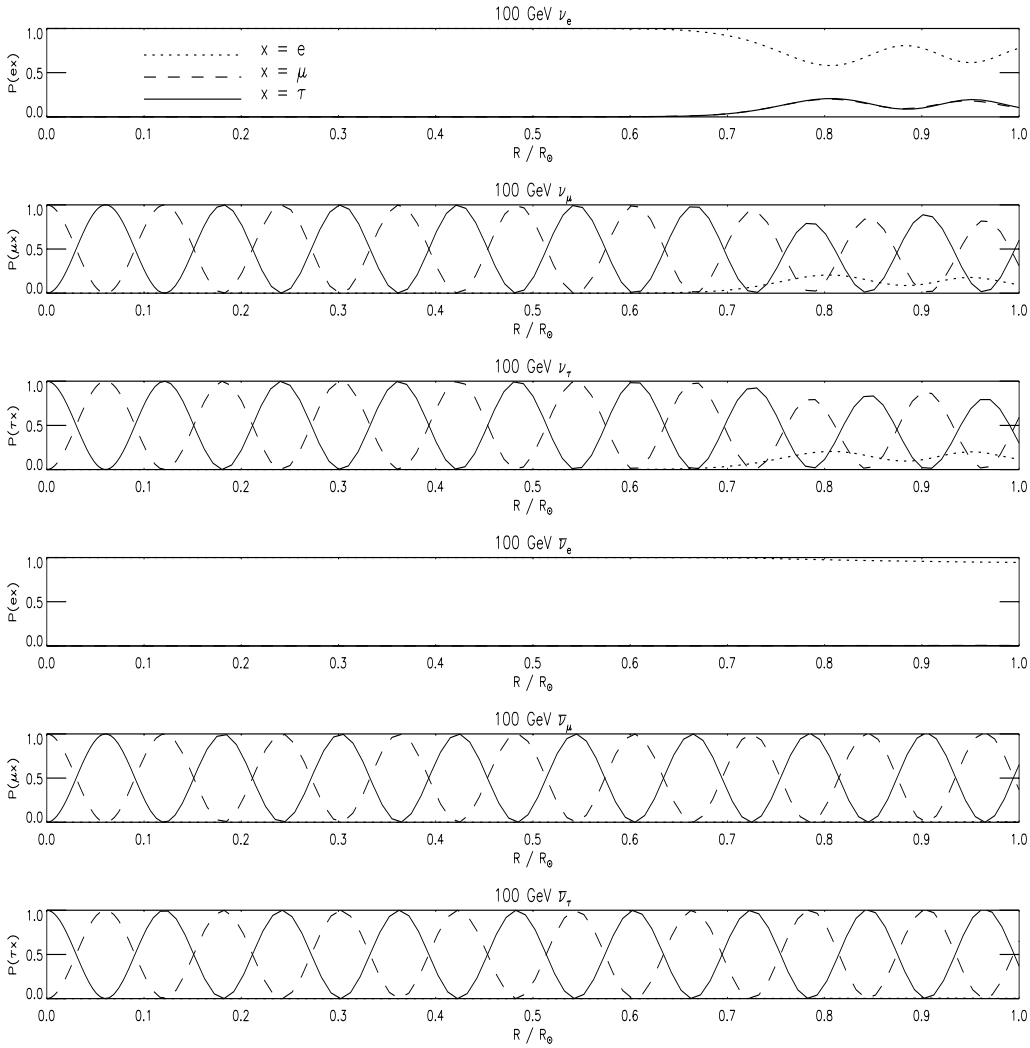

Figure 4.2 The oscillation probabilities of 100 GeV neutrinos in the Sun, assumed to begin in single-flavor states at the center. Note the MSW resonance at about $0.7R_\odot$. Below that, ν_e oscillations are almost completely suppressed by the large value of ζ.

only by roughly a factor of 2.

Therefore, we do not expect that different (reasonable) choices for the oscillation parameters would greatly alter the total simpzilla neutrino detection rates in a real-world detector observing μ.

CHAPTER 5

CHARGED LEPTON INTERACTIONS

The fate of the charged leptons produced in charged current neutrino-nucleon interactions is by far the most important factor in determining the energy distribution and flavor content of the emergent neutrino flux. While electrons and muons tend to be stopped by electromagnetic interactions, taus, with much shorter lifetimes, decay before losing a significant amount of energy. ν_τ are always among the decay products of τ, and hence they are regenerated, albeit at a slightly smaller energy determined by the inelasticity parameter in the original ν_τ-nucleon scattering and the decay distribution of τ. This downgrading of ν_τ energy continues until there is no longer a significant probability of interactions over the distance remaining to the surface of the Sun.

The survival of ν_τ versus that of ν_e and ν_μ was first noted by Ritz & Seckel (1988), in the context of a calculation of neutrino spectra from thermal wimp annihilations in the Sun. Kowalski (2001) has also studied tau neutrinos from wimps, including the effects of $\nu_\mu \leftrightarrow \nu_\tau$ oscillations. Halzen & Saltzberg (1998) have shown the ν_τ regeneration phenomenon to hold for high-energy extragalactic neutrinos propagating through the bulk of the Earth. Dutta et al. (2000) and Becattini & Bottai (2001) have calculated the effect of ν_τ regeneration and ν_e, ν_μ suppression in the Earth on high-energy extragalactic neutrino fluxes, which are generally expected to have equal ratios of ν_e, ν_μ, and ν_τ at the Earth due to oscillations over the long distances they travel. Both groups found that for fluxes which declined less steeply than E^{-2}, the ν_τ regeneration effect produces a substantial excess of ν_τ over ν_μ at the detector in the $10^3 - 10^6$ GeV range at low nadir angles (i.e., when the beam propagates through close to a full Earth diameter).

Another signal of ν_τ, which would appear in extragalactic neutrino beams from point sources, is the direction independence of the ν_τ number flux. Although the ν_τ energies are downgraded, essentially one ν_τ emerges at the detector for every one that enters the Earth. This is in contrast to the relative numbers of emergent ν_μ and ν_e, which are suppressed with decreasing nadir angle. In a detector which observes upward-going muons created just below it by neutrino charged current interactions, it would be possible to separate the μ due to ν_μ from those due to $\nu_\tau \to \tau \to \mu$ on a statistical basis.

Simpzilla neutrinos, however, have energies considerably below the Earth's transparency energy, so this direction independence is not of much use experimentally in their case.

5.1 Electromagnetic energy losses

As charged leptons move through matter, they interact with the surrounding electrons and nuclei and lose energy. Accurately treating the electronic and nuclear energy losses is of course critical to the ν_τ regeneration phenomenon. We discuss each briefly below, focusing on the heavy charged leptons. For the electronic energy losses, we follow, with some modifications, the discussion in Ritz & Seckel (1988). For the nuclear energy losses, we use the results of Dutta et al. (2001). (As mentioned below, we are not concerned with electrons/positrons produced by ν_e charged current interactions.)

5.1.1 Electronic

Interactions (classically, collisions) of μ and τ with e in the Sun are the dominant component of their energy losses up to around 10^4 GeV. To calculate these losses, we

use the energy loss rate for charged particles in plasma given in Ritz & Seckel (1988) to obtain the mean energy loss per unit column depth:

$$-\left\langle \frac{dE}{dx} \right\rangle = \left(9.2 \times 10^6\right) \left(\frac{Z}{A\beta^2 c}\right) \left[\ln\left(2m_e\gamma\beta^2\right) - \ln\left(\sqrt{\frac{4\pi\alpha n_e}{m_e}}\right)\right] \quad \left[\mathrm{GeV}/\left(\frac{\mathrm{g}}{\mathrm{cm}^2}\right)\right] \tag{5.1}$$

Z and A are the atomic number and weight of the nuclei in the medium; β and γ are the Lorentz parameters for the incident charged particle; c is the speed of light in cm/s; α is the fine structure constant; and m_e and n_e are the electron mass and number density, expressed in natural units (respectively, GeV and GeV^3). The argument of the second logarithm is ω_p, the plasma frequency, which in the core of the Sun is approximately 3×10^{-7} GeV.

5.1.2 Photonuclear scattering

The simplest electromagnetic interaction between a charged lepton and a nucleus is the exchange of a virtual photon. The differential cross section with respect to the inelasticity parameter is (Dutta et al. 2001)

$$\begin{aligned} \frac{d\sigma}{dy} &= \frac{\alpha}{2\pi} A\sigma_{\gamma N} y \left\{ \frac{3}{4} G(x) \left[\kappa \ln\left(1 + \frac{m_1^2}{t}\right) - \frac{\kappa m_1^2}{m_1^2 + t} - \frac{2m_\ell^2}{t}\right] \right. \\ &+ \frac{1}{4}\left[\kappa \ln\left(1 + \frac{m_2^2}{t}\right) - \frac{2m_\ell^2}{t}\right] \\ &+ \left. \frac{m_\ell^2}{2t}\left[\frac{3}{4} G(x) \frac{m_1^2}{m_1^2 + t} + \frac{1}{4}\frac{m_2^2}{t} \ln\left(1 + \frac{t}{m_2^2}\right)\right]\right\} \end{aligned} \tag{5.2}$$

with the parameters defined as

$$
\begin{aligned}
G(x) &= \frac{3}{x^3}\left(\frac{x^2}{2} - 1 + e^{-x}(1+x)\right) \\
x &= 0.00282 A^{1/3}[\sigma_{\gamma N}(E/\text{ GeV})/\mu\text{b}] \\
\sigma_{\gamma N}(E) &= 114.3 + 1.647 \ln^2(0.0213E/\text{ GeV})\ \mu\text{b} \\
t &= \frac{m_\ell^2 y^2}{1-y} \\
\kappa &= 1 - \frac{2}{y} + \frac{2}{y^2} \\
m_1^2 &= 0.54\ \text{GeV}^2 \\
m_2^2 &= 1.8\ \text{GeV}^2
\end{aligned} \tag{5.3}
$$

α is the fine structure constant, A is the atomic weight of the isotope, and m_ℓ is the mass of the charged lepton (m_μ or m_τ). E is the initial lepton energy.

5.1.3 Brehmsstrahlung

In brehmsstrahlung, a second, real photon is emitted. The differential cross section is (Dutta et al. 2001)

$$
\begin{aligned}
\frac{d\sigma}{dy} &= \alpha^3 \left(2Z\lambda_e \frac{m_e}{m_\ell}\right)^2 \frac{1}{y}\left(\frac{4}{3} - \frac{4}{3}y + y^2\right) \ln\left[\frac{\frac{189 m_\ell}{m_e} Z^{-1/3}}{1 + 189\frac{\sqrt{e}}{m_e}\delta Z^{-1/3}}\right] \\
\delta &\equiv \frac{m_\ell^2 y}{2E(1-y)} \\
0 \leq\ & y \leq 1 - \frac{3m_\ell}{4E}\sqrt{e} Z^{1/3}
\end{aligned} \tag{5.4}
$$

This form for $d\sigma/dy$ assumes $Z \leq 10$, where Z is the atomic number (1 for hydrogen,

2 for helium). λ_e is the Compton wavelength of the electron, 3.8616×10^{-11} cm. e is the number, not the electronic charge.

5.1.4 Pair production

In the pair production interaction between a charged lepton and a nucleus, a second photon is emitted as in brehmsstrahlung, which then becomes an electron-positron pair.

The differential cross section is (Dutta et al. 2001)

$$\frac{d^2\sigma}{dyd\rho} = \alpha^4 \frac{2}{3\pi}(Z\lambda_e)^2 \frac{1-y}{y}\left(\phi_e + \frac{m_e^2}{m_\ell^2}\phi_\ell\right) \tag{5.5}$$

The cross section is differentiated not only with respect to y, but also the "asymmetry parameter" ρ quantifying the difference in the energies of the final electron and positron:

$$\rho \equiv \frac{E(e^+) - E(e^-)}{E(e^+) + E(e^-)} \tag{5.6}$$

The limits on y and ρ are

$$\begin{aligned} \frac{4m_e}{E} \leq \quad y \quad &\leq 1 - \frac{3m_\ell}{4E}\sqrt{e}Z^{1/3} \\ 0 \leq \quad |\rho| \quad &\leq \left(1 - \frac{6m_\ell^2}{E^2(1-y)}\right)\sqrt{1 - \frac{4m_e}{Ey}} \end{aligned} \tag{5.7}$$

The other parameters in (5.5) are

$$
\begin{aligned}
\phi_e &= \left[[(2+\rho^2)(1+\beta)+\xi(3+\rho^2)]\ln\left(1+\frac{1}{\xi}\right)+\frac{1-\rho^2-\beta}{1+\xi}-(3+\rho^2)\right]L_e \\
\phi_\ell &= \left\{\left[(1+\rho^2)\left(1+\frac{3}{2}\beta\right)-\frac{1}{\xi}(1+2\beta)(1-\rho^2)\right]\ln(1+\xi)\right. \\
&+ \left.\frac{\xi(1-\rho^2-\beta)}{1+\xi}+(1+2\beta)(1-\rho^2)\right\}L_\ell \\
L_e &= \ln\left\{\frac{189Z^{-1/3}\sqrt{(1+\xi)(1+Y_e)}}{1+\frac{378m_e\sqrt{e}Z^{-1/3}(1+\xi)(1+Y_e)}{Ey(1-\rho^2)}}\right\}-\frac{1}{2}\ln\left[1+\left(\frac{3}{2}\frac{m_e}{m_\ell}Z^{1/3}\right)^2(1+\xi)(1+Y_e)\right] \\
L_\ell &= \ln\left\{\frac{189Z^{-2/3}\frac{2}{3}\frac{m_\ell}{m_e}}{1+\frac{378m_e\sqrt{e}Z^{-1/3}(1+\xi)(1+Y_\ell)}{Ey(1-\rho^2)}}\right\} \\
Y_e &= \frac{5-\rho^2+4\beta(1+\rho^2)}{2(1+3\beta)\ln(3+1/\xi)-\rho^2-2\beta(2-\rho^2)} \\
Y_\ell &= \frac{4+\rho^2+3\beta(1+\rho^2)}{(1+\rho^2)\left(\frac{3}{2}+2\beta\right)\ln(3+\xi)+1-\frac{3}{2}\rho^2} \\
\beta &= \frac{y^2}{2(1-y)} \\
\xi &= \left(\frac{m_\ell y}{2m_e}\right)^2\frac{1-\rho^2}{1-y}
\end{aligned}
\tag{5.8}
$$

β and ρ here should not, of course, be confused with the Lorentz parameter and density.

5.1.5 Total energy losses

We combine the above results into an expression for the total energy loss per unit column depth for a charged lepton in the Sun. We may consider the matter in the Sun to consist of two separate components: ^{1}H nuclei and their "associated" electrons; and ^{4}He nuclei and their "associated" electrons. The electrons are unbound, but from overall neutrality there is one for each hydrogen nucleus and two for each helium

nucleus.

To avoid notational confusion, define X and Y as the fractions by mass of ^{1}H and ^{4}He respectively at a given point in the Sun (we obtain these from Bahcall (1989)). Let distance be denoted by s, and the column depth in each isotope by $x_1 \equiv X\rho s$ and $x_4 \equiv Y\rho s$, where ρ is the total density of the Sun.

Let the index $i = \{1, 4\}$ refer to respectively ^{1}H or ^{4}He, and let j refer to a nuclear interaction (brehmsstrahlung, pair production or photonuclear scattering). The mean energy loss per unit column depth for a specific isotope is

$$-\left\langle \frac{dE}{dx_i} \right\rangle = \alpha_i + \sum_j \beta_i^j E \tag{5.9}$$

where α_i is the right hand side of (5.1) (using the appropriate Z and A for the isotope) and β_i^j is defined as

$$\beta_i^j(E) = \frac{N_0}{A_i} \int_{y_{min}}^{y_{max}} dy\, y \frac{d\sigma^j}{dy} \tag{5.10}$$

N_0 is Avogadro's number, and A_i is once again the atomic weight for the specific isotope. In practice, these integrals must be calculated numerically. (β^{pair} also requires an integration over the asymmetry parameter.)

It is straightforward to show that the energy loss per unit *total* column depth $x = \rho s$ is

$$\left\langle \frac{dE}{dx} \right\rangle = X \left\langle \frac{dE}{dx_1} \right\rangle + Y \left\langle \frac{dE}{dx_4} \right\rangle \tag{5.11}$$

5.2 Weak energy losses

Weak interactions, apart from decays, are not significant for the charged leptons created by simpzilla neutrinos. Their weak and electromagnetic energy losses in matter become comparable only at $E_{lepton} \approx 10^{16}$ GeV (Dutta et al. 2001), which is far above any lepton energies we are considering. We accordingly neglect weak energy losses in our code.

5.3 Decays

5.3.1 e

The electron or positron created by a ν_e charged current interaction, of course, never decays, and hence the ν_e can be considered to have been removed from the beam. The only possibility of regenerating a ν_e is for the e to undergo a charged current interaction of its own, but as discussed above the probability of this given the electromagnetic interactions is negligible. Our code does not follow the e produced in charged current interactions.

5.3.2 μ

Virtually all μ decays are in the channel $\mu \rightarrow \nu_\mu e \nu_e$. A fraction $\sim 1\%$ have an additional photon among the final products, and a fraction $\sim .003\%$ have an additional electron-positron pair (Groom et al. 2000), but we ignore these rare modes.

Almost all of the μ created in ν_μ charged current interactions lose their energy electromagnetically and essentially decay at rest. The resulting ν_μ are emitted in all directions and have energies below 50 MeV, and are of no interest to us.

To be internally consistent, our code includes both μ and τ decays above 50 GeV,

although in this energy range only the τ decays are significant. In the rare event that a μ decays in flight (i.e. at a high energy), the distribution of ν_μ energies is equal to that of the ν_τ energies in $\tau \to \nu_\tau \mu \nu_\mu$ and $\tau \to \nu_\tau e \nu_e$ decays, which is given below.

5.3.3 τ

The τ, unlike the μ, has several significant decay modes. These, along with their branching ratios, are (Dutta et al. 2000):

$$\begin{aligned} \tau &\longrightarrow \nu_\tau \mu \nu_\mu \quad (18\%) \\ &\longrightarrow \nu_\tau e \nu_e \quad (18\%) \\ &\longrightarrow \nu_\tau \pi \quad (12\%) \\ &\longrightarrow \nu_\tau \rho \quad (26\%) \\ &\longrightarrow \nu_\tau a_1 \quad (13\%) \\ &\longrightarrow \nu_\tau X \quad (13\%) \end{aligned} \tag{5.12}$$

where X indicates hadrons besides π, a_1, or ρ[1]. It is important to explicitly note that there is no difference for our purposes between τ^- and τ^+. The τ^- are produced in ν_τ charged current interactions, and exclusively have negative parity. Similarly, the τ^+ are produced in $\bar{\nu}_\tau$ charged current interactions and have positive parity. By CP invariance, the energy distributions of ν_τ, $\bar{\nu}_\mu$, and $\bar{\nu}_e$ from τ^- decays are equal to those of the corresponding (anti)neutrinos from τ^+ decays. (The same is true for the

[1]The hadrons in (5.12) are not a significant source of high-energy neutrinos. They and their charged decay products lose most of their energy before decaying into neutrinos, much like the muon.

distributions of ν_μ and $\bar{\nu}_\mu$ from $\mu^\mp$ decays.)

Defining $z \equiv E_\nu/E_\tau$ and $r_i \equiv m_i^2/m_\tau^2$, the distribution of ν_τ energies from τ decays (i.e., of ν_τ energies from τ^- decays and $\bar{\nu}_\tau$ energies from τ^+ decays) is (Dutta et al. 2000):

$$\begin{aligned}
\frac{dn}{dz}(\nu_\tau) &= 2 \times (0.18)\left[\frac{4}{3} - \frac{4}{3}z^3\right] + (0.12)\left[\left(\frac{1}{1-r_\pi} + \frac{2z-1+r_\pi}{(1-r_\pi)^2}\right)\Theta\left(1-r_\pi-z\right)\right] \\
&+ (0.26)\left[\left(\frac{1}{1-r_\rho} + \left(\frac{2z-1+r_\rho}{1-r_\rho}\right)\left(\frac{1-2r_\rho}{1+2r_\rho}\right)\right)\Theta\left(1-r_\rho-z\right)\right] \\
&+ (0.13)\left[\left(\frac{1}{1-r_{a_1}} + \left(\frac{2z-1+r_{a_1}}{1-r_{a_1}}\right)\left(\frac{1-2r_{a_1}}{1+2r_{a_1}}\right)\right)\Theta\left(1-r_{a_1}-z\right)\right] \\
&+ (0.13)\left[\frac{1}{0.3}\Theta\left(0.3-z\right)\right] \qquad (5.13)
\end{aligned}$$

Each term in brackets is the decay distribution for the respective channel in (5.12) (the $\tau \to \nu_\tau \mu \nu_\mu$ and $\tau \to \nu_\tau e \nu_e$ modes have the same distribution, hence the factor of 2 multiplying the first term). The numerical coefficients in parentheses are the branching ratios. $\Theta(x)$ is the usual step function and represents the kinematic cutoffs for the processes involving massive hadrons. We assume that the τ is ultrarelativistic, so its mass and those of the e and μ can be neglected.

In Figure 5.1, we show the τ decay distributions used by our code.

5.4 Secondary neutrinos from τ decays

Beacom et al. (2001) have noted that the τ decays which regenerate the ν_τ also produce a substantial flux of high-energy ν_e and ν_μ, and these secondary neutrinos must be taken into account when calculating the detected signal. Roughly 18% of τ decays are in the $\tau \to \nu_\tau \mu \nu_\mu$ channel, and another 18% are in the $\tau \to \nu_\tau e \nu_e$ channel.

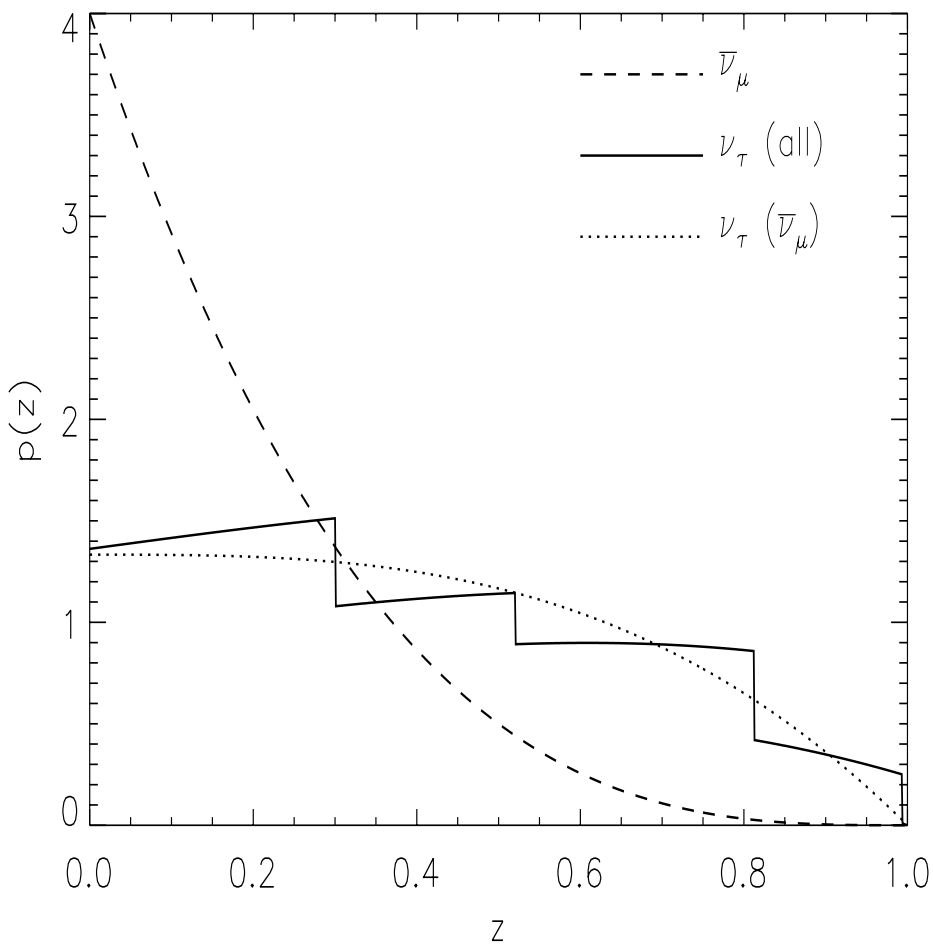

Figure 5.1 The normalized lab frame probability densities for the energies of ν_τ and $\bar{\nu}_\mu$ produced in τ^- decays, with $z \equiv E_\nu/E_\tau$. The τ^- is assumed to be ultrarelativistic. Solid curve: the combined probability density for the ν_τ energy, summing over all significant τ^- decay channels. The jagged appearence is due to some channels which produce massive hadrons becoming kinematically impossible above a certain neutrino energy. Dashed curve: the probability density for the $\bar{\nu}_\mu$ energy in the $\tau^- \to \nu_\tau \mu^- \bar{\nu}_\mu$ channel. Dotted curve: the probability density for the ν_τ energy in the $\bar{\nu}_\mu$-producing channel. The τ^- is assumed to have negative parity; hence these distributions also hold for $\bar{\nu}_\tau$ and ν_μ produced in the equivalent decay channels of postive-parity τ^+.

The kinematics of these decays are such that the secondary ν_μ or ν_e carries on the order of 1/8 of the ν_τ energy before the interaction. Although the earliest secondary neutrinos, which have the highest energies, tend to be absorbed, others are created farther out and at lower energies as the ν_τ propagates with repeated charged current interactions (and therefore loses energy itself in the regenerations).

Studying the case of high-energy neutrino beams propagating through the Earth[2], Beacom et al. (2001) found that the emergent secondary ν_e and ν_μ from τ decays each amount to roughly 20% (by number) of the emergent primary ν_τ beam. This is especially significant since the primary ν_e and ν_μ are almost completely absorbed.

Our Monte Carlo code includes secondary ν_e and ν_μ from τ decays. We are considering an initial flux rather than a monoenergetic beam, which falls over several orders of magnitude with increasing energy, and a large fraction of which is below the solar transparency energy of ~ 100 GeV (where ν_τ charged current interactions are infrequent). Thus, we do not expect, and indeed do not find, that secondaries have a dramatic effect on the emergent flux.

It is straightforward to calculate the energy distributions of the secondary ν_e and ν_μ, which are produced in the first two channels of (5.12). We boost the relevant lepton rest frame distributions obtained in Renton (1990) to obtain

$$\frac{dn}{dz}(\nu_e, \nu_\mu) = -4z^3 + 12z^2 - 12z + 4 \tag{5.14}$$

This distribution is also shown in Figure 5.1.

[2]The neutrinos were assumed to be of extragalactic origin and well above the Earth's transparency energy of ~ 100 TeV.

CHAPTER 6

CALCULATION OF THE EMERGENT NEUTRINO FLUX

To calculate the flux of simpzilla neutrinos from the Sun, we have written a Monte Carlo code to simulate their propagation from the solar core to the Earth, taking into account all the significant effects discussed in the previous three chapters.

Our code is in large part an adaptation of a previous Monte Carlo we wrote to simulate the propagation of high-energy neutrino beams from extragalactic point sources through the Earth (Beacom et al. 2001). That code was able to reproduce the results of a similar calculation by a different group (Halzen & Saltzberg 1998). The major modification we have made to our code is to include oscillations, which are not significant for neutrinos with energies above $\sim$ 100 TeV (the Earth's transparency energy) in the Earth.

6.1 Monte Carlo code

6.1.1 Without oscillations

We first discuss the case of when we are not following neutrino oscillations. All of the below is used in the neutrino oscillation case too, but for clarity we separate our discussion of how oscillations are simulated.

Our code follows the trajectories of individual neutrinos as they propagate through the Sun and to the Earth. At each point inside the Sun, we choose for our step size the smaller of $R_\odot/F$ and L_{int}/F, where $F = 100$ if we are not following oscillations. When we do follow oscillations, $F = 100$ for $E \geq 100$ GeV; for neutrino energies less than that, we use $F = 1000$ in order to have a step size small in comparison to the oscillation lengths (which decrease with energy).

L_{int} is the total interaction length for the neutrino or antineutrino (distance over which the mean number of interactions it experiences is 1), taking both charged and neutral current scatterings into account:

$$L_{int}(E) = \frac{1}{n_n\left(\sigma_n^{cc}(E) + \sigma_n^{nc}(E)\right) + n_p\left(\sigma_p^{cc}(E) + \sigma_p^{n}c(E)\right)} \tag{6.1}$$

n_n and n_p are the neutron and proton number densities, which as previously discussed vary within the Sun (although for the purposes of calculating L_{int} at each step, we consider them to be constant). The cross sections also depend somewhat on the neutrino flavor – for tau neutrinos, for example, the charged current cross section is kinematically suppressed at lower energies and hence its interaction length there is larger than the ν_e and ν_μ interaction lengths. (In practice, as we mentioned previously, this does not make a significant difference to our results, because most interactions happen at energies where the flavor differences among charged current cross sections are small.) For each flavor, the antineutrino has a smaller cross section on a given nucleon than the neutrino below about 10^4 GeV, and so their interaction lengths are larger too.

If the step length is λ, then the probability of the neutrino experiencing an interaction over that length is $P_{int} = 1 - e^{-\lambda/L_{int}}$. (This is technically the probability of the neutrino experiencing *at least* one interaction, but the step size is small enough so that multiple interactions may be neglected.) The code uses a pseudorandom number generator to determine whether an interaction took place over the step, and then to determine whether it was on a neutron or proton and whether it was charged or neutral current. The interaction is assumed to have taken place at the end of the step.

In the event of a neutral current interaction, the new neutrino energy is determined

by randomly choosing the inelasticity parameter from the appropriate y distribution for that interaction and energy ($y = 1 - E'/E_\nu$).

If a charged current interaction takes place, we consider the neutrino to have been "converted" into the corresponding charged lepton. Electrons, as we have discussed, are not followed and so ν_e which have charged current interactions are considered absorbed. For muons and taus, we choose the step size to be the smallest of $h_d/100$, $h_E/100$, and $R_\odot/100$, where h_d is the (boosted) decay length of the lepton and $h_E \equiv E/\left(\left\langle \frac{dE}{dx} \right\rangle \rho\right)$ is the distance over which the lepton would lose all its energy if the energy loss rate were constant. (It isn't, but h_E is of the same order as the total range of the lepton in the absence of decays.) We determine the initial lepton energy similarly to the case of the neutrino in a neutral current scattering, by using the y distribution.

When we follow a μ or τ, the probability of a decay is calculated over each step and then randomly determined whether or not to have occurred. If no decay takes place, then the lepton's energy is reduced according to $\left\langle \frac{dE}{dx} \right\rangle$.

If a decay takes place, the lepton is considered "converted" back into a neutrino. The neutrino energy is randomly chosen using the appropriate decay distribution. When we are following secondary neutrinos from τ decay, we first randomly determine (using the branching ratio for the production of secondary ν_μ) whether a decay into the ν_μ-producing mode has taken place; and if so, we use the distribution for that mode only to obtain both the ν_τ and secondary ν_μ energies. If not, then we use the τ decay distribution summed over all modes *except* the ν_μ-producing mode. When we are not following secondaries, we sum over all τ decay modes.

When we are not following oscillations, we do not separately calculate the secondary ν_e flux from τ decays; we assume this to be equal to the secondary ν_μ flux.

The branching ratios into the two modes are virtually identical, and ν_e and ν_μ have the same cross sections at these energies. The only potential differences would come from the decays of muons in flight, but this is not significant.

The code propagates N_0^ℓ neutrinos through the Sun and then (if they are not absorbed) to the Earth, recording their initial energies, final energies, and final flavors, and total number of emergent neutrinos N_f^ℓ, where ℓ specifies the flavor. This data can be used to construct the probability distribution of final neutrino energies $n_f^\ell(E)$, which is related to the flux by

$$\frac{1}{\sqrt{M_{12}}\Gamma_A}\frac{d\Phi^\ell}{dAdEdt} = \frac{10^4\kappa_\ell}{4\pi R_{es}^2}\left(\frac{N_f^\ell}{N_0^\ell}\right)n_f^\ell(E) \tag{6.2}$$

As before, $M_{12} = m_X/10^{12}$ GeV; Γ_A is the simpzilla annihilation rate; and $\kappa_\ell = 1$ for ν_τ and $\frac{1}{2}$ for ν_e and ν_μ. R_{es} is the Earth-Sun distance (1 Au).

Typical neutrino propagation

We describe briefly the interactions experienced by a (non-oscillating) typical neutrino on its way from the Sun's center to the surface. If the neutrino has an energy much below about 100 GeV – or, in the case of an antineutrino, about 200 GeV – interactions are not very probable and it passes through the Sun unaffected.

If the energy is above this range, the neutrino (from now on, we use the "generic" terminology) can have charged or neutral current interactions. The charged current cross section is around three times the neutral current cross section at the same energy, and so the charged current interactions are considerably more likely. The large majority of interactions take place in the first tenth of the distance to the surface.

A ν_e or ν_μ is almost always absorbed by the *first* charged current interaction

it experiences. The higher its energy, the deeper inside the core this interaction takes place. The interaction creates an e or μ; either subsequently loses energy in electromagnetic interactions with the solar medium and is brought to rest. The e never decays, and the ν_μ from the eventual μ decay are at very low energies and are not of interest to us. The high-energy ν_e and ν_μ which emerge, then, are the ones which have not experienced any interactions at all (we neglect the small number which have had only neutral current scatterings). The probability of emerging without interactions declines roughly exponentially with energy, and therefore the emergent ν_e and ν_μ flux is exponentially attenuated from the intial flux.

A ν_τ, however, is not absorbed in charged current interations due to the short lifetime of the τ, which has negligible energy losses and quickly decays back into a ν_τ. Each regeneration reduces the ν_τ energy by a factor of about 1/4. A typical high-energy ν_τ coming from the core thus experiences repeated charged current scatterings, along with the occasional neutral current scattering, until its energy is reduced to below about 100 GeV and the probability of further interactions is small. The total number of charged current scatterings is roughly $N = \log(E_0/E_k)/\log 4$ (Beacom et al. 2001), where E_k is the transparency energy (discussed below). The highest initial energy we consider is $E_0 = 2 \times 10^4$ GeV, where $N \approx 4$. Like the ν_e and ν_μ, ν_τ generally experience all their interactions during the first tenth or so of the way through the Sun. There are also some ν_τ which emerge without experiencing any interactions, although the probability declines exponentially with energy just as for the other flavors. However, the crucial difference is that the scattered ν_τ are not absorbed.

6.1.2 With oscillations

To simulate oscillations, our code uses the analytical expression for the time-evolution operator in (4.30) to evolve the probability amplitudes over the step. As mentioned, we choose a small enough step size so that the oscillation probabilities do not change significantly over each step.

Each neutrino is considered to begin at the Sun's core in a pure flavor state. Over each step, as in the non-oscillation case, we test for an interaction. In this, we take advantage of the fact that the cross sections do not differ substantially among the flavors in the energy range ($E \gtrsim 100$ GeV) where interactions are significant, and so the oscillations should not significantly affect the probability of an interaction at a given energy.

In a charged current interaction, a charged lepton of a certain flavor is emitted – this, unlike a neutral current interaction, amounts to a measurement of the neutrino flavor. As such, when a charged current interaction is determined to have occurred, we randomly sample using the present oscillation probabilities to determine a new neutrino flavor, and assign the outcoming charged lepton that flavor. When (and if) the lepton decays, the emergent neutrino begins in a pure flavor state just as the initial one did, and the process repeats.

In the case of secondary neutrinos from τ decays, ν_e and ν_μ (and their antineutrinos) have significantly different oscillation behaviors as is evident from Figures 4.1 and 4.2. We thus, in contrast to the case with no oscillations, follow secondary ν_e and ν_μ separately when they are oscillating.

We also calculate the oscillations in the vacuum between the Sun and the Earth. When calculating the final neutrino flux at the Earth, we assume a 10% energy resolution in the detector. This means that if the detector is set to measure neutrinos

of energy E, it will actually measure neutrinos with energies from $E - \delta E$ to $E + \delta E$, where $\delta E = \frac{1}{20}E$. The mean probability measured is

$$\langle P \rangle = \frac{1}{2\delta E} \int_{-\delta E}^{\delta E} d\epsilon K \sin^2 \left(\alpha \frac{x}{(E+\epsilon)} \right) \tag{6.3}$$

where α and K are constants, and x is the distance from the Earth to the Sun. We assume the range of E is small enough so that the events are uniformly distributed in it, a fairly good assumption for our fluxes. Since ϵ in (6.3) is by assumption much smaller than E, it can be shown that this is equivalent to holding the energy constant and averaging over 10% of the *distance*; that is,

$$\frac{1}{2\delta E} \int_{-\delta E}^{\delta E} d\epsilon K \sin^2 \left(\alpha \frac{x}{(E+\epsilon)} \right) \approx \frac{1}{2\delta x} \int_{x-\delta x}^{x+\delta x} dx' K \sin^2 \left(\alpha \frac{x'}{E} \right) \tag{6.4}$$

where $\delta x = \frac{1}{20}x$. We therefore average the oscillation probabilities over a tenth of the Earth-Sun distance.

6.2 Numerical results

We present our numerical results for the simpzilla neutrino flux at the Earth in Figures 6.1 through 6.4. We consider four cases: the simplest, with no secondaries from τ decays or oscillations; including secondaries; including oscillations; and including both.

These fluxes are normalized by m_X and Γ_A (the latter depends on m_X and the simpzilla-nucleon interaction cross section σ). Including the secondaries has a fairly small effect. The oscillations, however, have the effect of enhancing the emergent ν_μ flux and depleting that of the ν_τ. For neutrinos, the ν_e flux is increased as well. For antineutrinos, the $\bar{\nu}_e$ flux is less affected by oscillations because, as is evident from

Figures 4.1 and 4.2, high-energy $\bar{\nu}_e$ never encounter a resonance in the Sun. The subsequent oscillations of $\bar{\nu}_e$ are much smaller than are those of ν_e.

6.3 Analytical approximation

The reason we have used a computational approach to this problem is that it would be exceedingly difficult, if not impossible, to analytically solve for the emergent flux in terms of the decay distributions, total and differential cross sections, oscillation parameters, etc. However, it possible to gain some analytical understanding by making simplifying assumptions about the emergent fluxes. We do so here in the simplest case, neglecting oscillations and secondary neutrinos from τ decays.

ν_e and ν_μ

The emergent flux of ν_e and ν_μ consists primarily of neutrinos which have not experienced any interactions on their way from the Sun's core to its surface. Charged current interactions, as we have noted, are generally equivalent to absorption of ν_e and ν_μ. There is a small "punch-through" component consisting of neutrinos which have had only neutral current scatterings, but we neglect that here.

Given an initial flux $d\Phi_0/dEdt$, the emergent *unscattered* flux of ν_e or ν_μ is (Albuquerque et al. 2001a)

$$\frac{d\Phi_f}{dEdt} = \frac{d\Phi_0}{dEdt} \exp\left(-\int_0^{R_\odot} dr\,[n_p(r)\sigma_p(E) + n_n(r)\sigma_n(E)]\right) \tag{6.5}$$

n_p and n_n are the proton and neutron number densities as a function of position, and σ_p and σ_n are the total (charged + neutral current) cross sections. The exponential factor is the probability that a neutrino of energy E propagates through the Sun

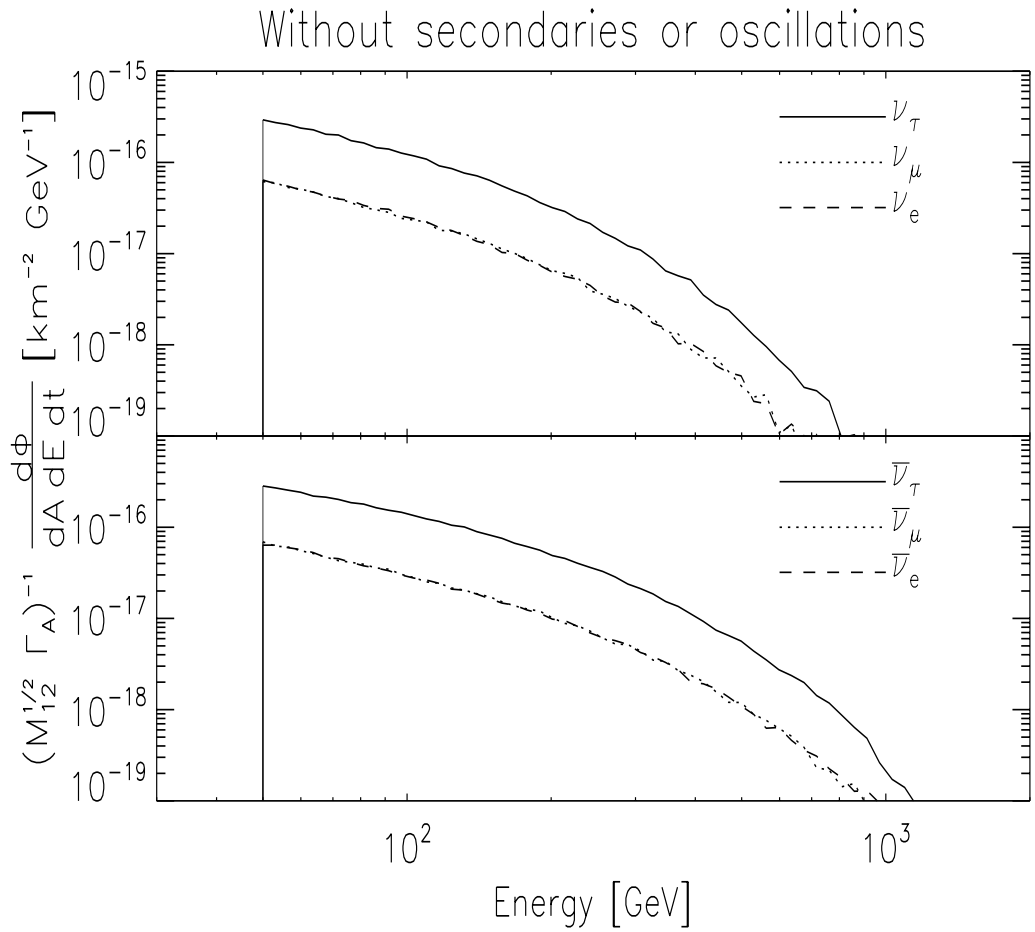

Figure 6.1 The simpzilla neutrino fluxes at the Earth, without taking secondaries or oscillations into account. M_{12} is the simpzilla mass in units of 10^{12} GeV and Γ_A is the simpzilla annihilation rate in the Sun's core. Note that the initial flux of ν_τ from simpzilla annihilations is twice that of ν_e and ν_μ, and similarly for the antineutrinos.

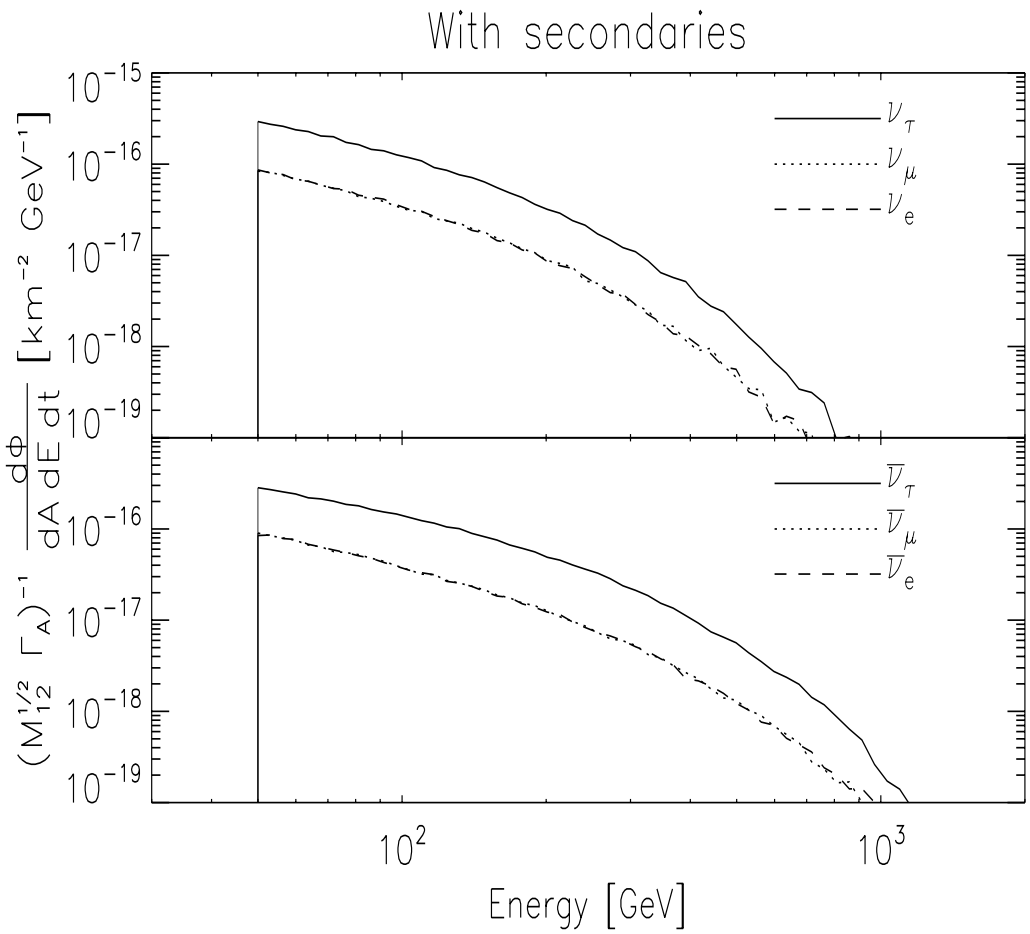

Figure 6.2 The simpzilla neutrino fluxes at the Earth, neglecting oscillations but taking secondary neutrinos from τ decays into account.

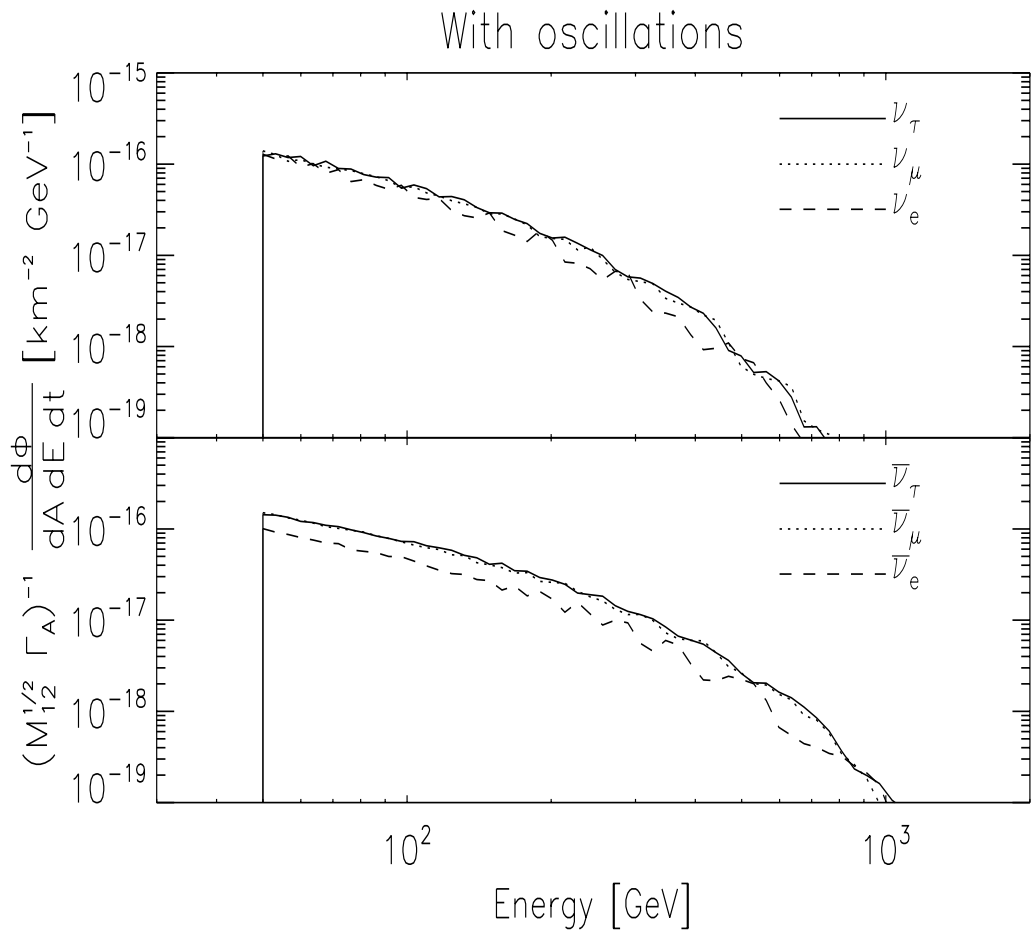

Figure 6.3 The simpzilla neutrino fluxes at the Earth, neglecting secondaries but taking oscillations into account.

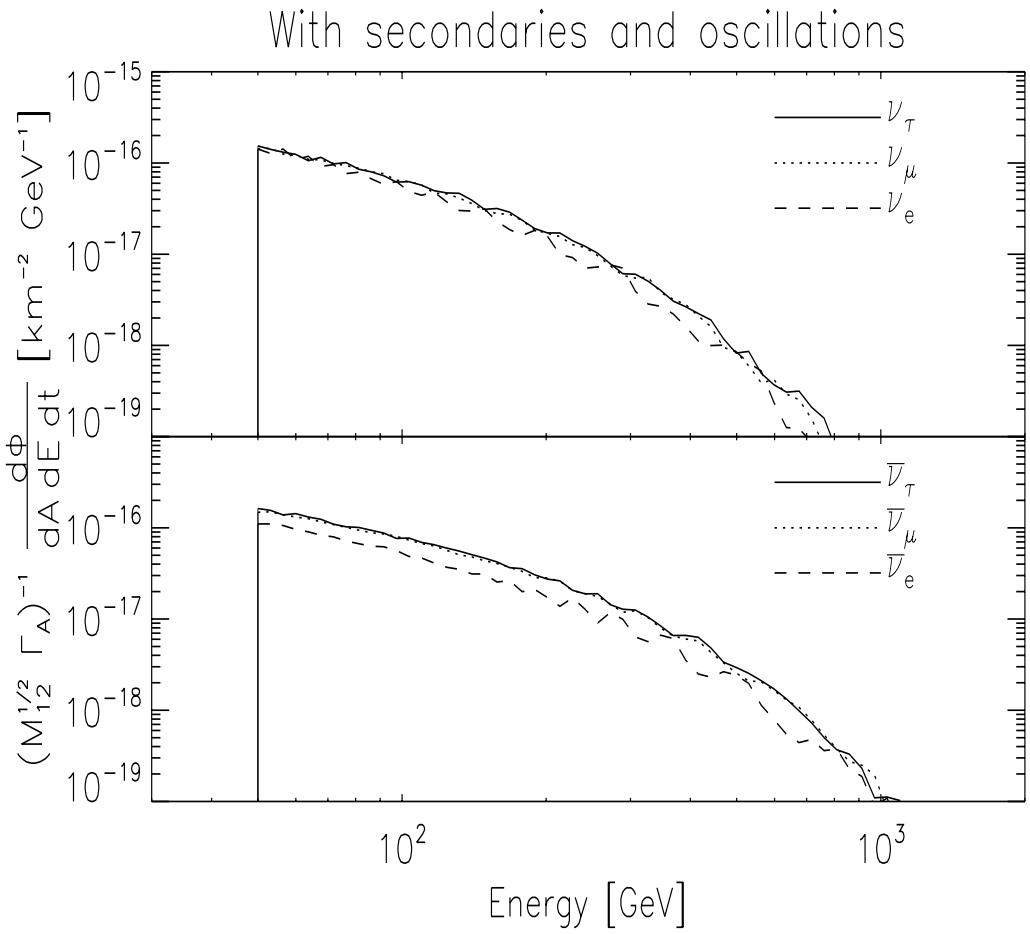

Figure 6.4 The simpzilla neutrino fluxes at the Earth, taking both secondaries and oscillations into account.

without having any interactions; it generalizes the interaction length to a varying density.

In the neutrino energy range we are considering, the cross sections are approximately proportional to energy (see Chapter 3). We may make use of this fact to write

$$\frac{d\Phi_f}{dEdt} = \frac{d\Phi_0}{dEdt}\, e^{-E/E_k} \tag{6.6}$$

where E_k is defined as the energy such that

$$\int_0^{R_\odot} dr\, [n_p(r)\sigma_p(E_k) + n_n(r)\sigma_n(E_k)] = 1 \tag{6.7}$$

E_k is called the transparency energy. The Sun is of course not completely transparent to neutrinos at this energy; indeed, about $\frac{2}{3}$ of them are still absorbed. But it is a useful concept for delineating where interactions are significant[1].

We find numerically that $E_k \approx 133$ GeV for ν_e and ν_μ, and 205 GeV for $\bar{\nu}_e$ and $\bar{\nu}_\mu$ (the larger transparency energies of the antineutrinos are due to their smaller cross sections). We therefore approximate the emergent electron and muon neutrino and antineutrino fluxes by using these values in (6.6), with (2.12) used for the initial flux. Our results are shown in Figure 6.7. They are in qualitative agreement with the numerical results shown in Figure 6.1.

ν_τ

The ν_τ, as we have discussed, are not absorbed by charged current interactions but instead are moderated down to lower energies, until the probability of an interaction

[1] In astrophysics, E_k is sometimes defined as the energy where half, rather than two thirds, of the flux is absorbed.

is no longer significant. Of course, there are still a number of them which, like the ν_e and ν_μ, do not experience any interactions at all.

We therefore approximate the emergent ν_τ flux as consisting of two components: an unscattered component similar to the ν_e and ν_μ emergent fluxes, and a scattered component. For the unscattered component, we numerically find that $E_k \approx 157$ GeV for ν_τ and 230 GeV for $\bar{\nu}_\tau$.

To model the scattered component, we use the observation of ourselves and other groups that the scattered tau neutrinos and antineutrinos tend to emerge in roughly log-normal distributions near their transparency energies. The log-normal distribution is defined as

$$\frac{dn}{dE} = \frac{1}{\sqrt{2\pi}\ln 10\,\sigma E} \exp\left[-\frac{1}{2\sigma^2}\log\left(\frac{E}{E_t}\right)\right] \tag{6.8}$$

i.e., when transformed to a distribution in $\log E$, it is a Gaussian centered about $\log E_t$ with standard deviation σ (whose "units" are decades of energy). The factor of $\ln 10$ comes from the Jacobian term relating dn/dE and $dn/d(\log E)$.

It is plausible that the scattered ν_τ would emerge in this way. The central limit theorem of statistics states that if x is the sum of a large number of independent random variables r_i, each of which has the same (though unspecified) probability distribution, then x is itself distributed as a Gaussian (Limpert et al. 2001). A corollary states that if x is the *product* of many such r_i, with the further restriction that $r_i > 0$ for all i, then x has a log-normal distribution.

In our case, $x = E/E_0$, where E_0 and E are the initial and final energies of the ν_τ. We have $E \approx E_0 r_1 r_2 ... r_n$. Each r_i is the fraction of the ν_τ energy before a charged current interaction carried away by the ν_τ after the interaction and τ decay. (We ignore neutral current scatterings, which is why this relation is only approximate).

The r_i are random variables; indeed, their probability distributions are the products of τ decay distributions and inelasticity parameter distributions. The latter are not independent of energy, however, and therefore the r_i do not all have exactly the same distributions. We also have $n \lesssim 4$ in the range of neutrino energy we are considering, another factor which could cause the distribution in E to differ from a log-normal.

However, we do find numerically that E obeys an approximately log-normal distribution, as shown in Figures 6.5 and 6.6. We plot the emergent ν_τ and $\bar{\nu}_\tau$ energy distributions for an initially monoenergetic beam at the center of the Sun with $E_0 = 10^3$ GeV. We also show log-normal fits to the emergent energy distributions. As expected, these are not exact, and in both cases somewhat underestimate the low-energy neutrinos while overestimating the high-energy ones.

We have used different values for E_0 and found the log-normal curves to peak around the same energies; accordingly, we make the assumption that the scattered simpzilla ν_τ and $\bar{\nu}_\tau$ emerge as log-normal distributions with the given values of σ and E_t. Numerically, we find that about 80% of the simpzilla ν_τ and $\bar{\nu}_\tau$ are scattered, and we weight the scattered and unscattered components accordingly.

We show the sums of the scattered and unscattered ν_τ and $\bar{\nu}_\tau$ fluxes in Figure 6.7. The under- (over-) estimation of the low- (high-) energy emergent fluxes is apparent, but qualitatively the curves do not greatly disagree with the numerical results in Figure 6.7. The pileup of scattered ν_τ and $\bar{\nu}_\tau$ is also the reason that their fluxes exceed those of the other flavors by more than the initial factor of 2.

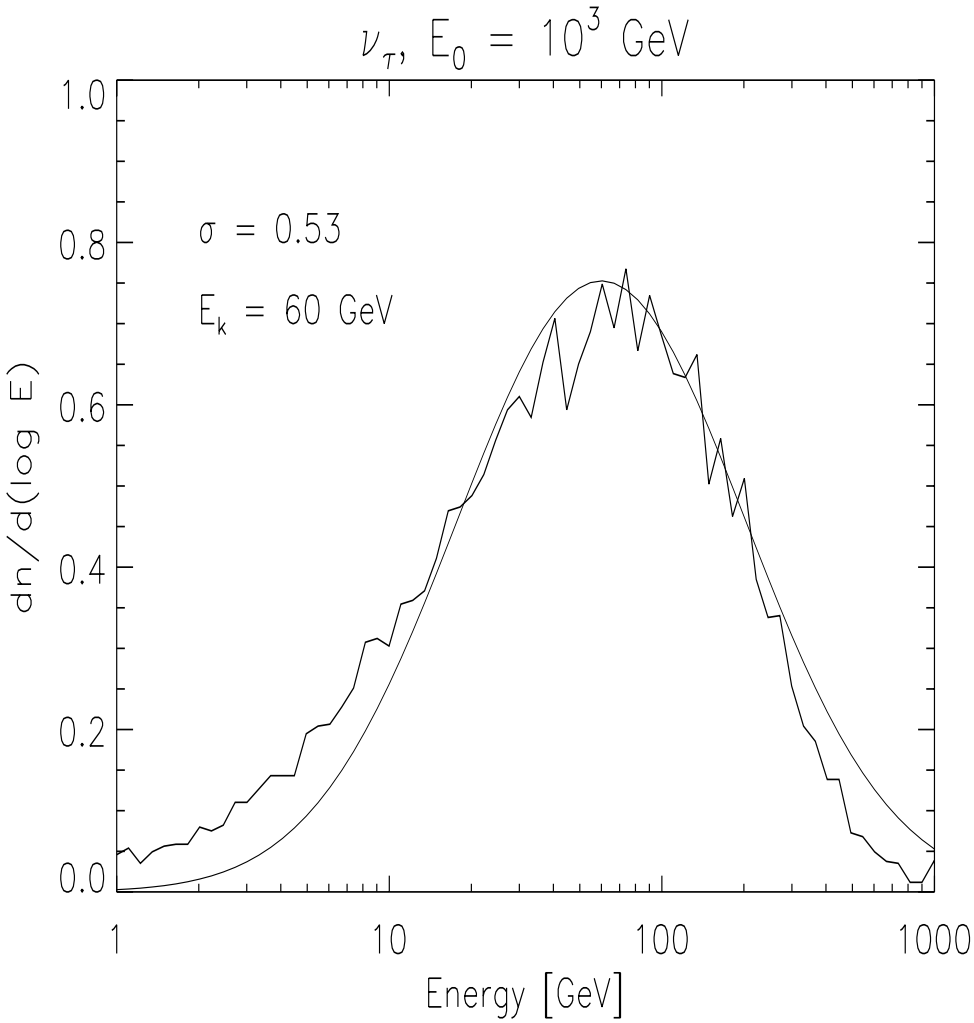

Figure 6.5 Distribution of emergent ν_τ energies for a monoenergetic beam with initial energy $E_0 = 10^3$ GeV. We plot as a distribution in $\log E$ rather than E. Oscillations are neglected. The distribution corresponds approximately (although obviously not exactly) to a log-normal distribution with the parameters shown.

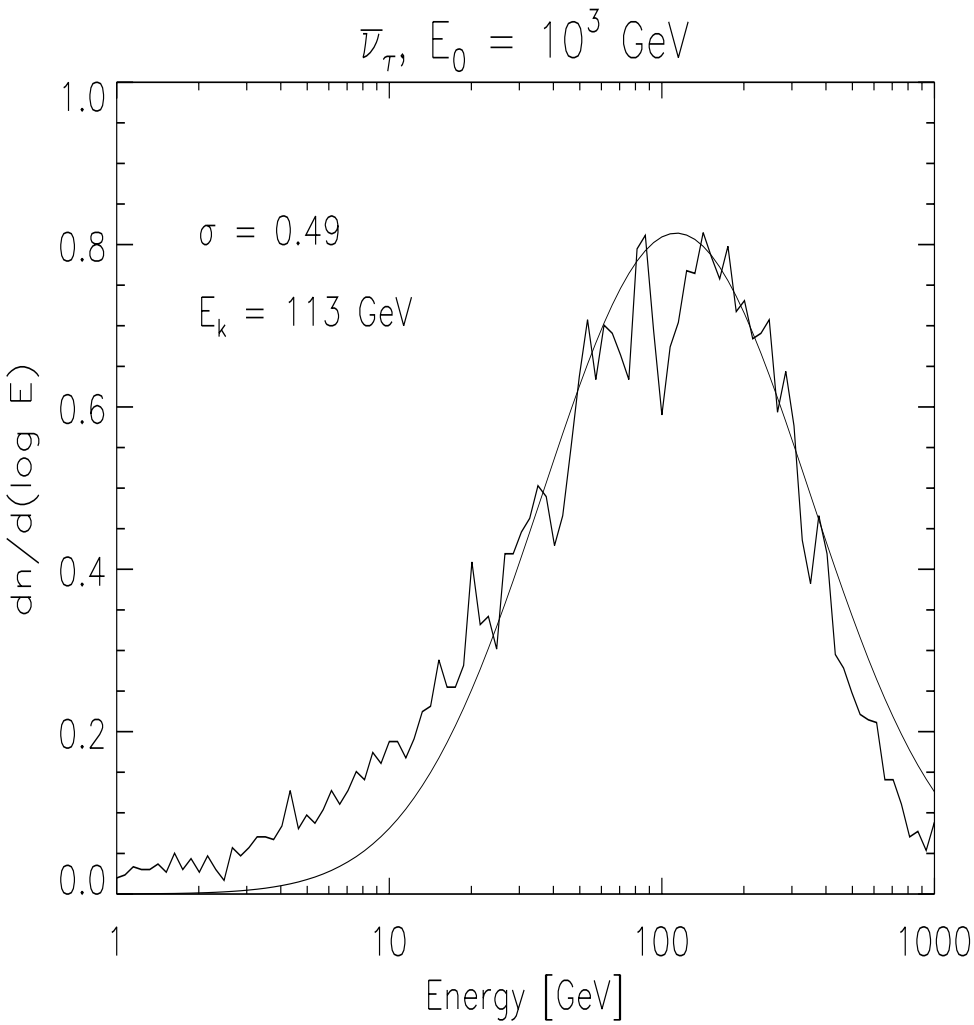

Figure 6.6 Distribution of emergent $\bar{\nu}_\tau$ energies for a monoenergetic beam with initial energy $E_0 = 10^3$ GeV, and a log-normal fit. The centroids are higher than they are in the ν_τ case because the antineutrino cross sections are lower.

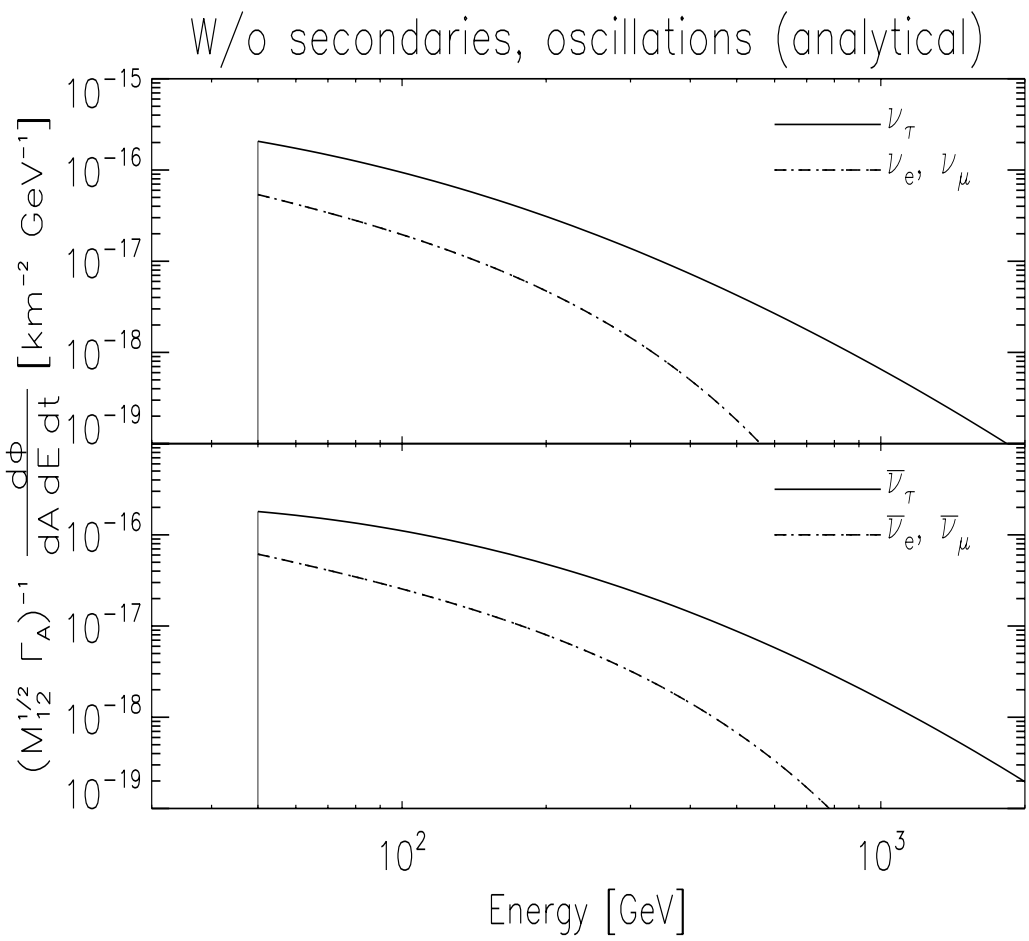

Figure 6.7 Analytical approximation for the emergent simpzilla neutrinos fluxes at the Earth, neglecting secondaries and oscillations. We assume the ν_e and ν_μ fluxes to consist entirely of the remaining unscattered neutrinos, and the ν_τ flux to be the sum of an unscattered component and a scattered component obeying a log-normal distribution. We make similar assumptions about the antineutrino fluxes, using higher transparency and log-normal mean energies.

CHAPTER 7

DETECTION OF SIMPZILLA NEUTRINOS

To calculate the event rate from a simpzilla neutrino flux, we assume an idealized water-ice detector of size 1 km^3. By "idealized," we mean that every neutrino charged current interaction taking place inside the detector above 50 GeV can be detected. Real detectors will of course be far more complicated than this, and may also be able to detect muons produced in the rock or ice surrounding the detector, thus increasing the effective detection volume. One must also take energy and direction resolutions, etc., into account to a far greater degree than we have done. A sophisticated calculation of the event rate would require a detector Monte Carlo, which we leave to others.

The probability of a single neutrino of energy E experiencing a charged current interaction inside the detector is

$$P_{cc}(E) = 1 - e^{-\lambda/L_{int}(E)} \tag{7.1}$$

where $\lambda = 1$ km is the size of the detector, and

$$L_{int}(E) = \frac{1}{n_p \sigma_p^{cc}(E) + n_n \sigma_n^{cc}(E)} \tag{7.2}$$

is the interaction length. Here, n_p and n_n are the proton and neutron number densities in ice of density $\rho_{ice} = 0.917$ g/cm^3. The cross sections (and hence L_{int} and the event rate) are of course depend on neutrino flavor too.

Given an incident neutrino flux $d\Phi/dAdEdt$, the event rate is

$$\frac{dN}{dt} = \lambda^2 \int dE \frac{d\Phi(E)}{dAdEdt} P_{cc}(E) \tag{7.3}$$

In terms of the energy distribution $n_f^\ell(E)$, this can be rewritten as

$$\frac{1}{\sqrt{M_{12}}\Gamma_A}\frac{dN^\ell}{dt} = \lambda^2 \frac{\kappa_\ell}{4\pi R_{es}^2}\frac{N_f^\ell}{N_0^\ell}\int_{E_{min}}^{E_{max}} dE n_f^\ell(E) P_{cc}^\ell(E) \tag{7.4}$$

where ℓ again denotes the flavor, and $\kappa_\ell = 1$ for $\ell = \tau$ and $\frac{1}{2}$ for the other flavors.

In Figures 7.1 through 7.4, we show the event rate spectrum $dN/dEdt$ (whose integral over E is (7.4)) for each neutrino and antineutrino flavor. In Figures 7.5 through 7.8, we integrate these to show the total event rates as a function of m_X and σ (we choose values of σ consistent with the strong interaction).

We note that we are assuming the detector has sufficient angular resolution to measure the directions of the simpzilla neutrinos and identify them as coming from the Sun. The Sun subtends about 1° on the sky, and IceCube is expected to have an angular resolution of that order, so our assumption is probably not unrealistic.

Atmospheric Background

The background from atmospheric neutrinos is approximately (Albuquerque et al. 2001b)

$$\frac{d\Phi_{atm}}{dE\, dA\, dt\, d\omega} = (1.1 \times 10^{12}) E^{-3.2} \ \left[\mathrm{km}^{-2}\ \mathrm{yr}^{-1}\ \mathrm{deg}^{-2}\ \mathrm{GeV}^{-1}\right] \tag{7.5}$$

between 50 and 2×10^4 GeV, our energy range of interest. The atmospheric neutrino flux is a function of zenith angle, though the variation is fairly minor above 50 GeV; (7.5) is the vertical flux, since a realistic ice detector would look only at upward-coming neutrinos.

Atmospheric neutrinos come from the interactions of cosmic rays with the Earth's atmosphere. In this energy range, and for the upward-coming flux, they consist almost entirely of ν_μ and $\bar{\nu}_\mu$. Tau neutrinos are not produced in significant quantities, and

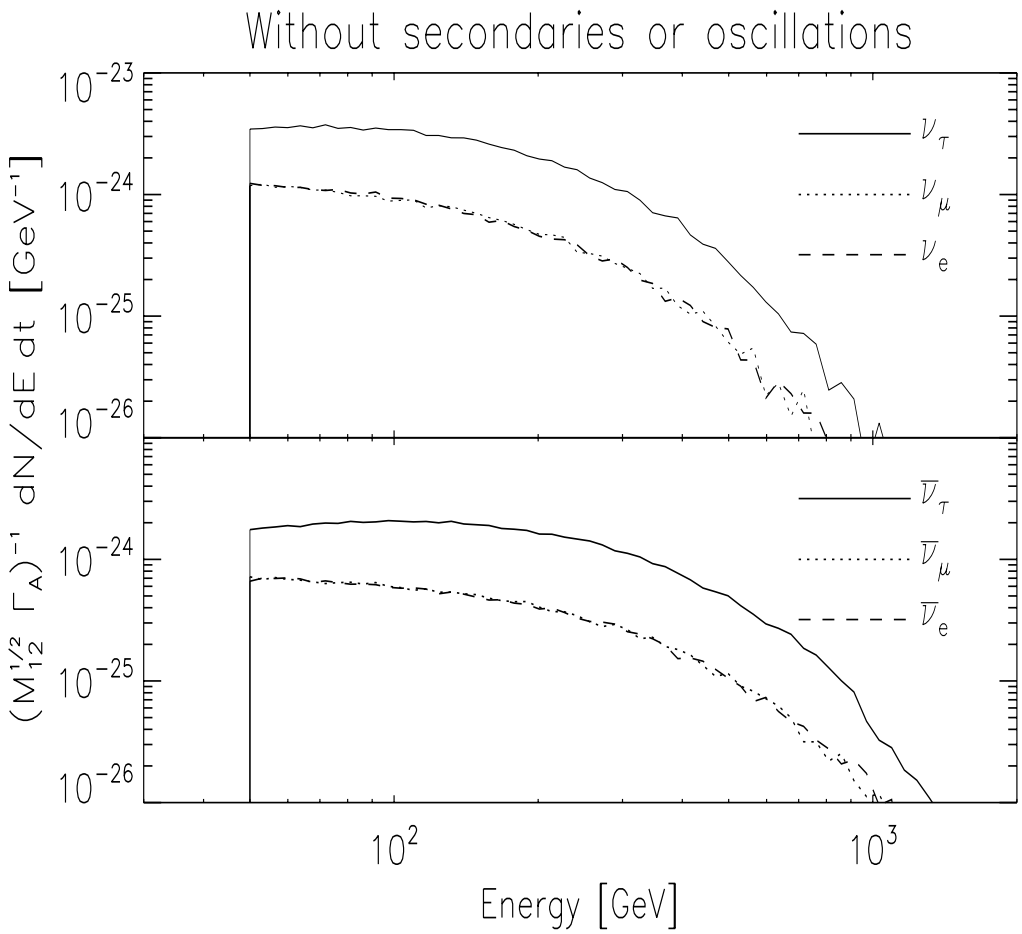

Figure 7.1 Simpzilla neutrino event rate spectrum in a km^3 ice detector on Earth, without taking oscillations or secondary neutrinos from τ decays into account.

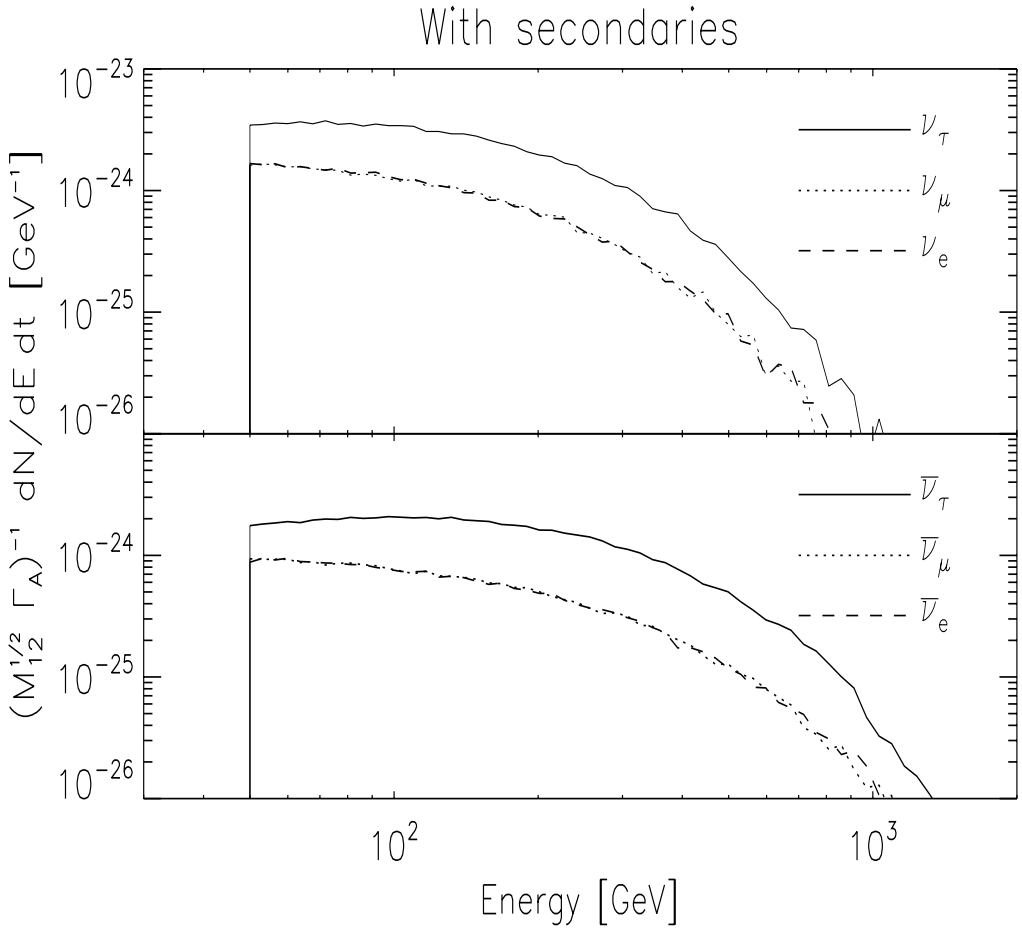

Figure 7.2 Simpzilla neutrino event rate spectrum in a km^3 ice detector on Earth, including secondary neutrinos produced in τ decays in the Sun.

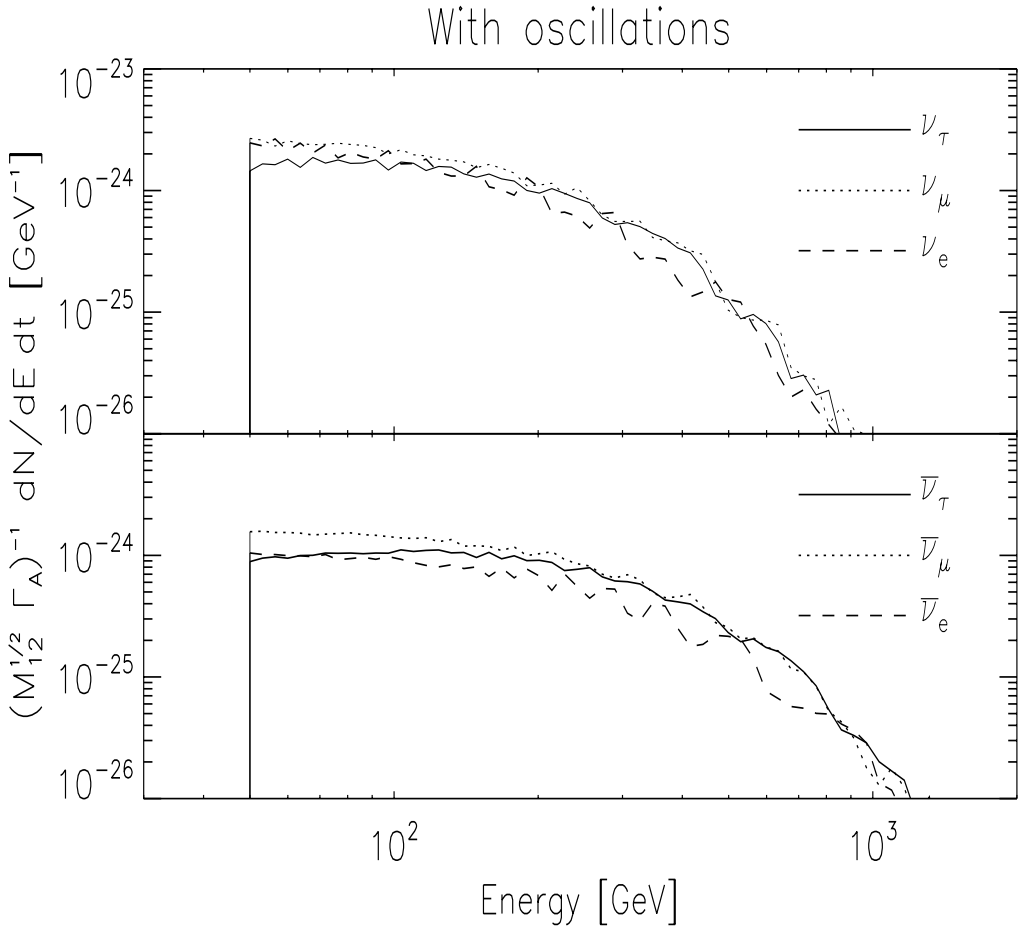

Figure 7.3 Simpzilla neutrino event rate spectrum in a km^3 ice detector on Earth, including neutrino oscillations in the Sun and vacuum.

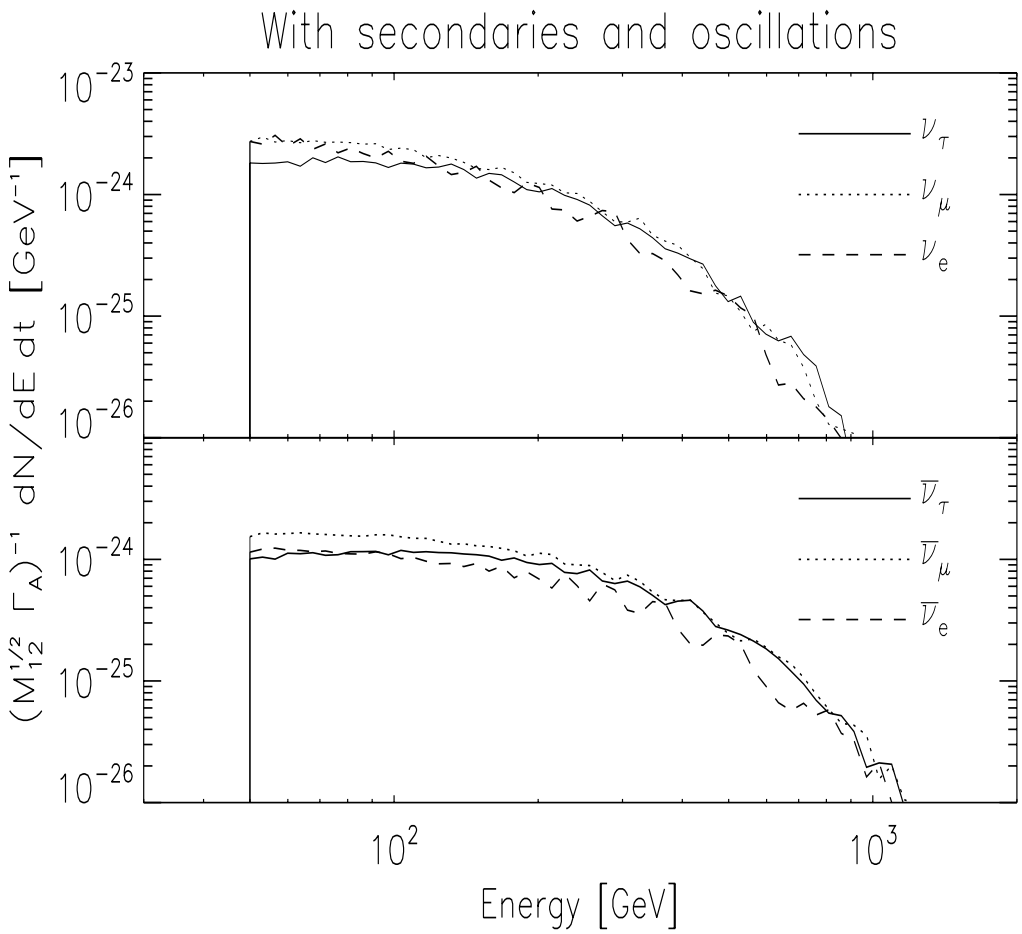

Figure 7.4 Simpzilla neutrino event rate spectrum in a km^3 ice detector on Earth, including both oscillations and secondaries.

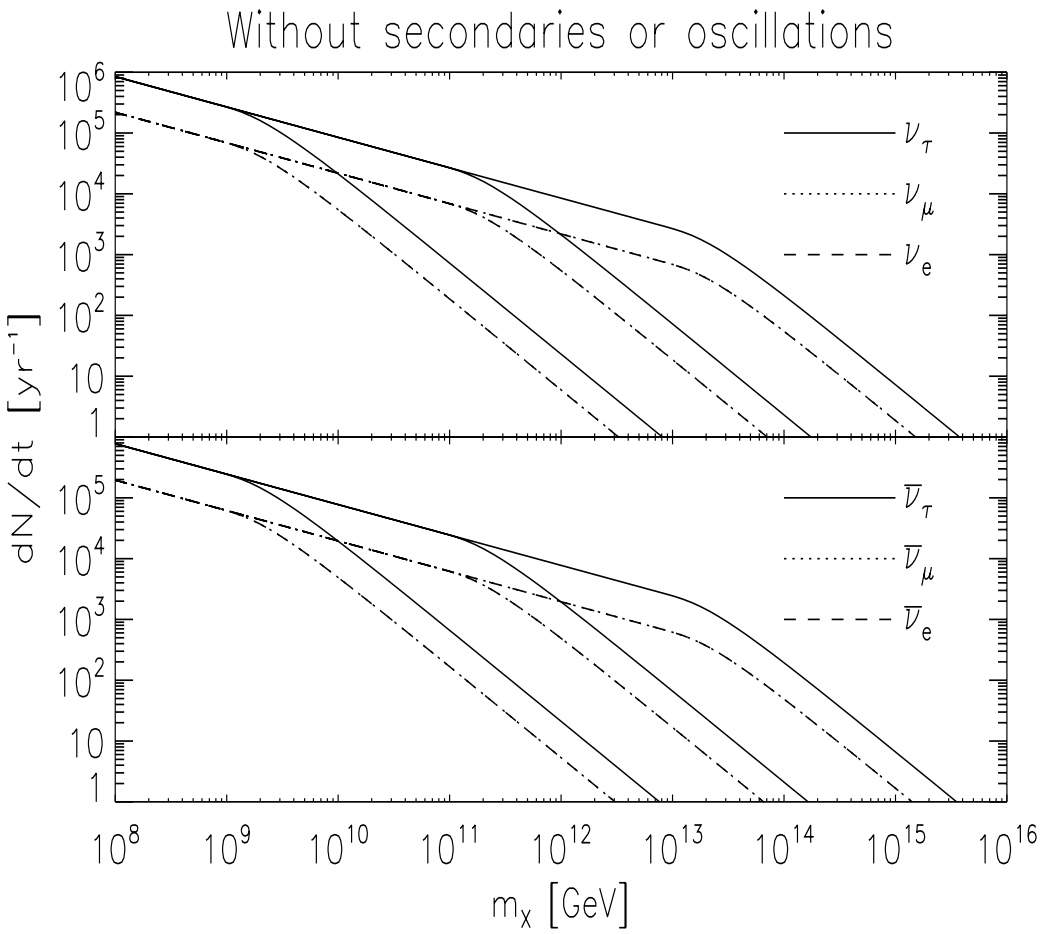

Figure 7.5 The total event rate in a km^3 ice detector, without taking oscillations or secondary neutrinos from τ decays into account. We plot the rate as a function of simpzilla mass m_X and for three different choices of the simpzilla interaction cross section σ. From left to right, these are: $\sigma = 10^{-26}$, 10^{-24}, and 10^{-22} cm^2.

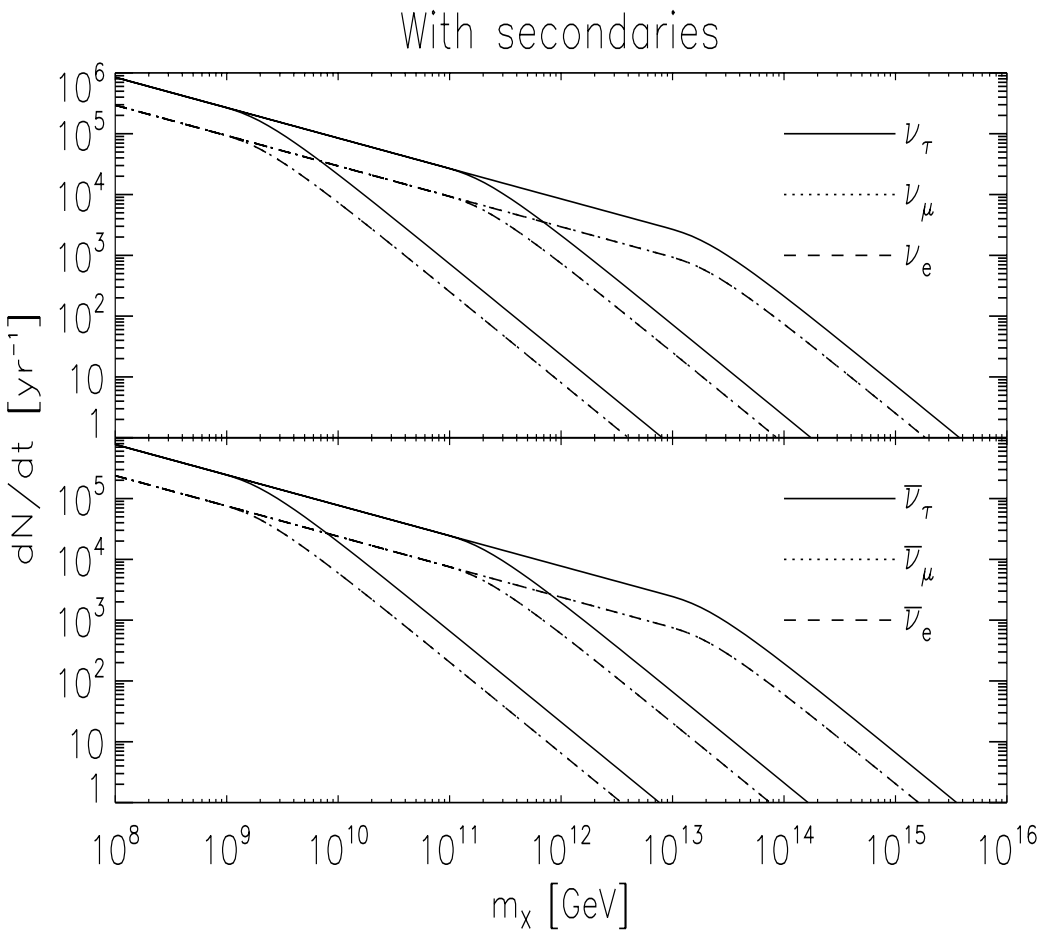

Figure 7.6 The total event rate in a km^3 ice detector, taking secondary neutrinos from τ decays into account.

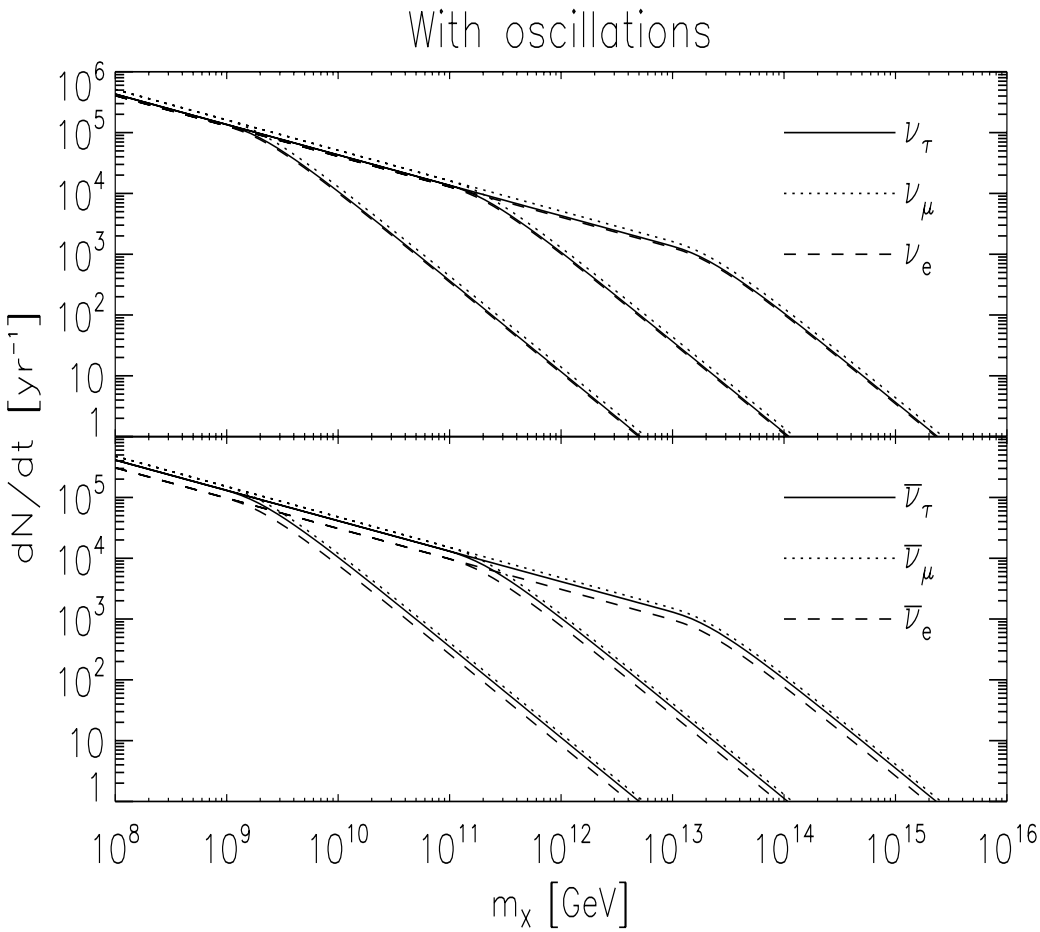

Figure 7.7 The total event rate in a km^3 ice detector, taking neutrino oscillations into account.

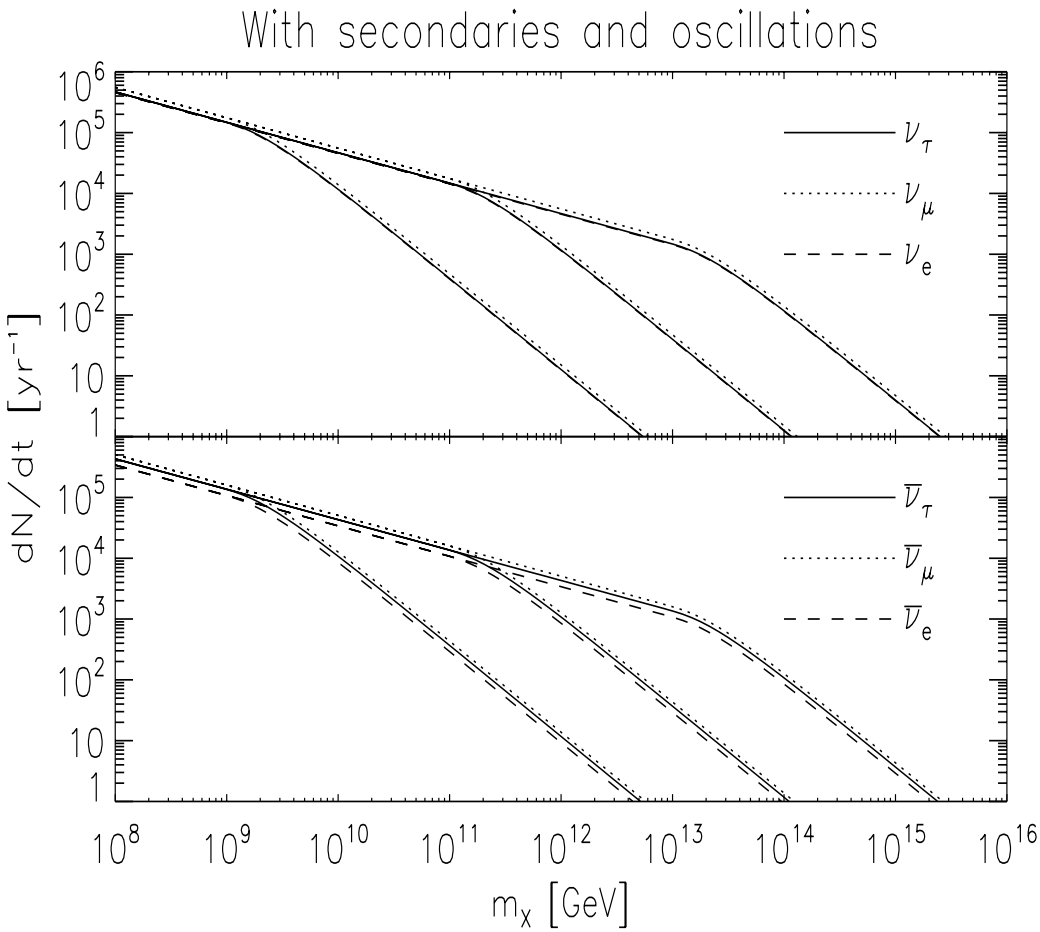

Figure 7.8 The total event rate in a km^3 ice detector, taking both secondaries and oscillations into account.

the electron neutrinos come largely from the decays of μ produced in the interactions – at 50 GeV and above, the latter reach the ground and lose their energy before decaying.

The angular size of the Sun is approximately one square degree (which is also about the smallest resolvable angular region by IceCube), and the area of the detector is 1 km^2. By integrating the product of (7.5) and the charged current interaction probability $P_{cc}(E)$ over E, as we did in (7.4), we obtain an atmospheric neutrino event rate of approximately 2 events per year coming from the portion of the sky occupied by the Sun.

The simpzilla neutrino event rates plotted in Figures 7.5 through 7.8 are generally higher than this by several orders of magnitude. Hence, unless the simpzilla mass m_X is very high and/or its interaction cross section σ is very low, we expect any simpzilla neutrino signal to be easily observable by a km^3 ice detector.

CHAPTER 8

CONCLUSION

We have shown that the annihilations of supermassive, strongly interacting dark matter particles in the Sun should in general produce a large flux of high-energy neutrinos easily observable by km^3 scale detectors.

Our flux calculation includes all significant processes affecting neutrino propagation and oscillation. We have used a set of oscillation parameters in agreement with current observational data. The effect of oscillations on the flux is to approximately equalize the fluxes of the different flavors.

Our event rates are based on several simplifying assumptions about the detector, and a more realistic calculation of these taking the actual detector response characteristics into account would be necessary to predict the event rate with a high degree of accuracy. We would not, however, expect a more sophisticated treatment in this regard to alter our general conclusion that the high-energy neutrino signal from simzpilla annihilations would be conspicuous.

We also note that even if a large high-energy neutrino signal from the Sun were observed, further analysis would be necessary to rule out other possible candidate sources such as thermal wimps, and to constrain m_X and σ.

The next generation of neutrino detectors should be able to either rule out simpzillas as a significant component of the non-baryonic dark matter, or provide unambiguous evidence for them.

REFERENCES

Ahmad, Q. R. et al. 2002a, nucl-ex/0204008

—. 2002b, nucl-ex/0204009

Ahrens, J. et al. 2001, IceCube Preliminary Design Document (ver. 1.20)

Albuquerque, I. F. M., Hui, L., & Kolb, E. W. 2001a, Phys. Rev., D64, 083504, hep-ph/0009017

Albuquerque, I. F. M., Lamoureux, J., & Smoot, G. F. 2001b, hep-ph/0109177

Bahcall, J. N. 1989, Neutrino Astrophysics (Cambridge Univ. Pr.)

Beacom, J. F. & Balantekin, A. B. 1997, hep-th/9709117

Beacom, J. F., Crotty, P., & Kolb, E. W. 2001, astro-ph/0111482

Becattini, F. & Bottai, S. 2001, Astropart. Phys., 15, 323, astro-ph/0003179

Bilenkii, S. M., Giunti, C., & Grimus, W. 1999, Prog. Part. Nucl. Phys., 43, 1, hep-ph/9812360

Chung, D. J. H. 1998, hep-ph/9809489

Chung, D. J. H., Crotty, P., Kolb, E. W., & Riotto, A. 2001, Phys. Rev., D64, 043503, hep-ph/0104100

Chung, D. J. H., Kolb, E. W., & Riotto, A. 1998, Phys. Rev. Lett., 81, 4048, hep-ph/9805473

—. 1999, Phys. Rev., D59, 023501, hep-ph/9802238

de Gouvea, A. 2001, Nucl. Phys. Proc. Suppl., 95, 141

Dutta, S. I., Reno, M. H., & Sarcevic, I. 2000, Phys. Rev., D62, 123001, hep-ph/0005310

Dutta, S. I., Reno, M. H., Sarcevic, I., & Seckel, D. 2001, Phys. Rev., D63, 094020, hep-ph/0012350

Ellis, J. R., Flores, R. A., & Masood, S. S. 1992, Phys. Lett., B294, 229

Fornengo, N. 1999, hep-ph/9904351

Fukuda, S. et al. 2000, Phys. Rev. Lett., 85, 3999, hep-ex/0009001

Fukuda, Y. et al. 1998, Phys. Rev. Lett., 81, 1562, hep-ex/9807003

Gandhi, R., Quigg, C., Reno, M. H., & Sarcevic, I. 1996, Astropart. Phys., 5, 81, hep-ph/9512364

—. 1998, Phys. Rev., D58, 093009, hep-ph/9807264

Goldman, I. & Nussinov, S. 1989, Phys. Rev., D40, 3221

Gould, A. 1987, Astrophys. J., 321, 571

Gould, A., Draine, B. T., Romani, R. W., & Nussinov, S. 1990, Phys. Lett., B238, 337

Griest, K. & Seckel, D. 1987, Nucl. Phys., B283, 681

Groom, D. E., Mokhov, N. V., & Striganov, S. I. 2001, Atom. Data Nucl. Data Tabl., 78, 183

Groom, D. E. et al. 2000, Eur. Phys. J., C15, 1

Halzen, F. 2001, astro-ph/0111059

Halzen, F. & Martin, A. D. 1984, Quarks and Leptons (Wiley)

Halzen, F. & Saltzberg, D. 1998, Phys. Rev. Lett., 81, 4305, hep-ph/9804354

Hill, C. T. 1983, Nucl. Phys., B224, 469

Kayser, B. 2001, hep-ph/0104147

Klein, J. R. 2001, hep-ex/0111040

Kowalski, M. 2001, Phys. Lett., B511, 119, hep-ph/0009183

Krastev, P. I. & Smirnov, A. Y. 2002, Phys. Rev., D65, 073022, hep-ph/0108177

Kuzmin, V. & Tkachev, I. 1999, Phys. Rev., D59, 123006, hep-ph/9809547

Limpert, E., Stahel, W. A., & Abbt, M. 2001, BioScience, 51, 341

Linde, A. D. 1994, Phys. Rev., D49, 748, astro-ph/9307002

Maartens, R., Wands, D., Bassett, B. A., & Heard, I. 2000, Phys. Rev., D62, 041301, hep-ph/9912464

Mason, B. & Sher, M. 1994, hep-ph/9409400

Mikheev, S. P. & Smirnov, A. Y. 1985, Sov. J. Nucl. Phys., 42, 913

Nardi, E. & Roulet, E. 1990, Phys. Lett., B245, 105

Naumov, V. A. 2002, Phys. Lett., B529, 199, hep-ph/0112249

Ohlsson, T. & Snellman, H. 2000, J. Math. Phys., 41, 2768, hep-ph/9910546

Paschos, E. A. & Yu, J. Y. 2002, Phys. Rev., D65, 033002, hep-ph/0107261

Peacock, J. A. 1999, Cosmological Physics (Cambridge Univ. Pr.)

Press, W. H. & Spergel, D. N. 1985, Astrophys. J., 296, 679

Pumplin, J. et al. 2002, hep-ph/0201195, see also the CTEQ web site at http://www.phys.psu.edu/ cteq/

Renton, P. 1990, Electroweak Interactions (Cambridge Univ. Pr.)

Ritz, S. & Seckel, D. 1988, Nucl. Phys., B304, 877

Wolfenstein, L. 1978, Phys. Rev., D17, 2369